Anthropogenic and natural alterations of shallow groundwater temperatures

Zur Erlangung des akademischen Grades einer

DOKTORIN DER NATURWISSENSCHAFTEN

von der Fakultät für

Bauingenieur-, Geo- und Umweltwissenschaften

des Karlsruher Instituts für Technologie (KIT)

genehmigte

DISSERTATION

von

Dipl.-Geol. Kathrin Menberg

aus Kassel

Tag der mündlichen

Prüfung: 12.02.2014

Referent: Jun.-Prof. Dr. habil. Philipp Blum

Korreferent: Prof. Dr. Nico Goldscheider

Karlsruhe 2014

Abstract

The thermal regime of the shallow subsurface is mainly governed by the heat flow from the Earth's interior and the temperature at the surface. Thermal signals from temperature variations at the surface penetrate through the unsaturated zone mainly by heat conduction and can perturb the temperature distribution in the deeper subsurface. Thus, shallow subsurface temperatures are prone to be influenced by various processes, which alter the ground surface temperature. In particular, the thermal environment under urban areas is profoundly changed by anthropogenic activities and under several cities an increase in groundwater temperatures is observed. However, little is known about the spatial extension and intensity of these thermal anomalies in the urban subsurface, and the individual influencing factors and driving forces are not yet comprehensively understood. Moreover, also in rural areas atmospheric temperatures exhibit an increasing trend due to climatic changes. Yet, the direct implications of increasing air temperatures, and consequently ground surface temperatures, for the long-term temperature development in shallow aquifers are still unclear.

The first part of this study deals with the thermal conductivity of unconsolidated sedimentary rocks as an important parameter for conductive heat transport. Different methods for the determination of the thermal conductivity are applied on samples obtained from a borehole or on a pilot borehole heat exchanger, which is installed in the borehole. Thermal conductivity is measured on core samples in the laboratory and a Thermal Response Test is carried out to determine a corresponding value in the field. Furthermore, the thermal conductivity is calculated with different theoretical models under consideration of several ground parameters that are determined by laboratory tests. The best agreement between measured and calculated thermal conductivity values is obtained using the geometric mean model. The accuracy of the thermal conductivity calculation is lower than the accuracy of the laboratory and field measurements, but it nevertheless represents a more accurate method than, for instance, parameter estimation based on published values.

Furthermore, a detailed spatial analysis of groundwater temperatures under several German cities is conducted. It reveals that extensive positive thermal anomalies exist under each of the studied cities, with the highest temperatures usually occurring under the densely urbanized city centers. Yet, often many local hot spots are found, which result in a very heter-

ogeneous temperature distribution. A comparison with the magnitude of atmospheric urban warming shows that the groundwater warming is more pronounced, which reflects the long-term accumulation of heat in the subsurface. The spatial correlation of the subsurface thermal anomalies with the atmospheric urban heat island and the population density indicates that increased ground surface temperatures and heat loss from subsurface infrastructure, such as basements of buildings, may act as dominant heat sources.

Based on the identified heat sources an analytical heat flux model is developed in order to quantify the individual heat flux processes, such as increased ground surface temperatures and heat loss from basements and other subsurface structures. By modeling the heat fluxes into the subsurface of the city of Karlsruhe for the years 1977 and 2011, the long-term trend of the heat flux processes can be assessed. The highest heat flux densities in both years occur from the increased ground surface temperatures and the basements. Although the magnitude of the individual heat flux densities changed significantly over the last decades. However, the total annual heat input into the shallow urban aquifer originating from the considered heat sources accounts up to around 1.5×10^{15} J in 1977 and 2011.

Finally, the coupling of air and groundwater temperature development is evaluated by statistically analyzing time-series of several decades with special regard to abrupt shifts in the long-term mean temperature. The observed positive shifts in the aquifer temperature are linked to preceding abrupt increases in regional air temperatures, which can be in turn associated with changes in the global mean air temperature. The increase in groundwater temperatures is generally found to be more gradual than atmospheric warming, as the thermal signals from the surface are attenuated and delayed by conductive and advective heat transport in the subsurface. However, it is revealed that these signals can have a pronounced impact on the development of groundwater temperatures in economically important aquifers.

Thus, it is shown that anthropogenic alterations at and beneath the ground surface as well as increasing air temperatures can significantly and permanently elevate groundwater temperatures in shallow aquifers. These temperatures changes may have a negative impact on groundwater quality and thus implications for drinking water supply. On the other hand, the extensive heat anomalies in the urban groundwater contain a vast amount of stored thermal energy that is continuously recharged from above. Therefore, the understanding of the thermal processes in the urban subsurface provides a useful basis for a sustainable management of this attractive geothermal reservoir.

Kurzfassung

Das thermische Regime im oberflächennahen Untergrund wird hauptsächlich durch den Wärmestrom aus dem Erdinneren und der Temperatur an der Erdoberfläche bestimmt. Thermische Signale durch Temperaturveränderungen an der Oberfläche dringen hauptsächlich mittels konduktiven Wärmetransports durch die ungesättigte Zone und können auch die Temperaturen im tieferen Untergrund beeinflussen. Somit sind auch die Grundwassertemperaturen in oberflächennahen Aquiferen anfällig für Beeinflussungen durch verschiedene Prozesse, die die Temperatur an der Oberfläche verändern. Insbesondere das thermische Umfeld unter urbanen Gebieten ist tiefgreifenden Veränderungen durch anthropogene Aktivitäten unterworfen und unter einigen Städten wurden bereits erhöhte Grundwassertemperaturen beobachtet. Jedoch ist nur wenig bekannt über die räumliche Ausdehnung und die Intensität dieser thermischen Anomalien im städtischen Untergrund, und auch die einzelnen Einflussfaktoren und treibenden Prozesse sind noch nicht umfassend verstanden. Darüber hinaus zeigen auch die Atmosphärentemperaturen in ländlichen Gebieten einen ansteigenden Trend aufgrund klimatischer Veränderungen. Die unmittelbaren Auswirkungen der ansteigenden Lufttemperaturen, und folglich auch Oberflächentempertaturen, auf die langfristige Temperaturentwicklung in oberflächennahen Aquiferen sind noch ungeklärt.

Der erste Teil der vorliegenden Arbeit befasst sich mit der Wärmeleitfähigkeit von sedimentärem Lockergestein als wichtige Bestimmungsgröße für den konduktiven Wärmetransport. Dabei werden verschiedene Methoden für die Bestimmung der Wärmeleitfähigkeit an einer Bohrung für eine Erdwärmesondenanlage angewendet. Die thermische Leitfähigkeit wird an den gewonnenen Kernproben im Labor bestimmt, außerdem wird ein Thermal Response Test durchgeführt. Weiterhin wird die Wärmeleitfähigkeit mit mehreren theoretischen Modellansätzen unter Berücksichtigung einiger im Labor bestimmter Gesteinsparameter berechnet. Die beste Übereinstimmung zwischen gemessenen und berechneten Werten der Wärmeleitfähigkeit ergibt sich mit der Berechnung des geometrischen Mittels. Zwar ist die Genauigkeit der Berechnung der Wärmeleitfähigkeit geringer als die einer Messung im Labor oder im Feld, dennoch lassen sich auf diese Weise genauere Ergebnisse erzielen, als beispielsweise durch eine Abschätzung anhand von Literaturwerten.

Außerdem wird eine detaillierte räumliche Untersuchung der Grundwassertemperaturen unter mehreren deutschen Städten durchgeführt. Diese zeigt, dass unter allen betrachteten Städten ausgedehnte positive thermische Anomalien existieren, wobei die höchsten Temperaturen meist unter den dicht bebauten Stadtzentren gemessen werden. Jedoch existieren auch oft lokal stark erwärmte Bereiche, die zu einer insgesamt sehr heterogenen Temperaturverteilung im Untergrund führen. Ein Vergleich mit der atmosphärischen, urbanen Erwärmung zeigt, dass die Erwärmung im Untergrund deutlich ausgeprägter ist, wodurch die langfristige Anreicherung von thermischer Energie im Untergrund widergespiegelt wird. Die räumliche Korrelation der thermischen Anomalien im Untergrund mit den atmosphärischen Wärmeinseln und der Einwohnerdichte lässt darauf schließen, dass erhöhte Oberflächentemperaturen und Wärmeabgabe von unterirdischen Bauwerken, wie z.B. Gebäudekellern, wichtige Wärmequellen darstellen.

Auf Grundlage der zuvor identifizierten Wärmequellen wird ein analytisches Wärmetransportmodell entwickelt, um die einzelnen Wärmeeinträge, z.B. durch erhöhte Oberflächentemperaturen, aus Gebäudekellern und anderen unterirdischen Strukturen, zu quantifizieren. Durch eine Analyse der Wärmeströme in den Karlsruher Untergrund für die Jahre 1977 und 2011 können auch Aussagen über die langfristige Entwicklung der einzelnen Wärmeeintragsprozesse gemacht werden. Die dominierenden Wärmeeinträge in beiden Jahren werden von den erhöhten Oberflächentemperaturen und Gebäudekellern verursacht, während sich die absoluten Werte der einzelnen Wärmeeinträge über die Jahrzehnte teilweise erheblich verändern. Der Gesamtenergieeintrag der betrachteten Wärmequellen in den oberflächennahen Aquifer ist jedoch mit rund $1,5 \times 10^{15}$ J in beiden Jahre ungefähr gleich groß.

Schließlich wird die Kopplung der Temperaturentwicklung in der Atmosphäre und im Grundwasser über die ungesättigte Zone mit Hilfe von statistischen Zeitreihenanalysen, unter besonderer Berücksichtigung von abrupten Änderungen der langjährigen Durchschnittstemperatur, untersucht. Die verzeichneten abrupten Anstiege der Grundwassertemperatur stehen in einem eindeutigen Zusammenhang mit vorausgehenden Änderungen im langjährigen Mittel der regionalen Lufttemperatur, die wiederum an Veränderungen der globalen Durchschnittstemperatur gekoppelt sind. Die Erwärmung des Grundwassers verläuft jedoch generell gradueller als der Anstieg der Lufttemperaturen, da die thermischen Signale von der Oberfläche durch konduktiven und advektiven Wärmetransport im Untergrund abgeschwächt und verzögert werden. Dennoch zeigen diese Beobachtungen, dass die thermischen Signale einen aus-

geprägten Einfluss auf die Grundwassertemperaturen in wirtschaftlich bedeutsamen Aquiferen haben können.

Insgesamt konnte somit gezeigt werden, dass anthropogene Veränderungen an der Oberfläche und im Untergrund, sowie ansteigende Lufttemperaturen einen erheblichen und andauernden Einfluss auf die Grundwassertemperaturen in oberflächennahen Aquiferen haben können. Diese Temperaturveränderungen können einen negativen Einfluss auf die Grundwasserqualität haben und damit möglicherweise auch auf die Verwendung zur Trinkwasserversorgung. Auf der anderen Seite enthalten die ausgedehnten Wärmeanomalien im urbanen Grundwasser eine beträchtliche Menge an gespeicherter thermischer Energie, die kontinuierlich von oben gespeist wird. Das Verständnis der thermischen Prozesse im urbanen Untergrund stellt daher eine wertvolle Grundlage für ein nachhaltiges Management dieses attraktiven geothermischen Reservoirs dar.

Contents

Contents

Abbreviations

AHF	anthropogenic heat flux
AHF_s	anthropogenic heat flux into the subsurface
AO	arctic oscillation
CRS	climate regime shift
GST	ground surface temperature
GWT	groundwater temperature
LST	land surface temperature
PDO	pacific decadal oscillation
SAT	surface air temperature
SST	subsurface temperature
SUHI	surface urban heat island
SUHII	surface urban heat island intensity
TRT	thermal response test
UHI	urban heat island
UHII	urban heat island intensity
$UHII_s$	subsurface urban heat island intensity

1 Introduction

1.1 Subsurface temperature and heat transport

The temperature distribution in the shallow subsurface is mainly governed by the heat flow from the Earth's interior and by the temperature at the Earth's surface (*Turcotte & Schubert*, 2002). Typical values for the near surface continental geothermal heat flow range between 40–90 mWm^{-2}. In addition, temperature variations at the surface influence the temperature in the subsurface down to a certain depth. While annual variations in air and ground temperatures cause temperature perturbations in depths up to 10-15 m, long-term climate variations can influence the subsurface temperature down to several hundred meters (*Turcotte & Schubert*, 2002).

Therefore, *Anderson* (2005) defines two different thermal zones in the subsurface: a surficial zone of around 10 m, which is strongly influenced by seasonal temperature variations at the surface, and a geothermal zone, with an increasing temperature according to the geothermal gradient. This increase of temperature with depth is usually in the order of 1 K per 20 to 40 m (*Anderson,* 2005). The temperature in the shallow subsurface at around 10 to 20 m depth is usually found to be 1-2 K warmer than the local mean annual air temperature (*Domenico & Schwartz*, 1990). Assuming a thermal equilibrium between the solid and liquid phase, groundwater temperatures are commonly considered representative for subsurface temperatures (*Domenico & Schwartz*, 1990). Therefore, the conventional method for measuring subsurface temperatures is to measure groundwater temperatures.

Heat transport in a porous medium is dominated by heat conduction in the solid and liquid phase due to thermal gradients and advective heat transport in a moving fluid. Conductive heat transport is described by Fourier's Law, in which the heat flux and the temperature gradient are related to each other by a proportionality factor, namely the thermal conductivity (*Domenico & Schwartz*, 1990).

When dealing with porous media, the thermal conductivity depends on the phase mixture, i.e. the percentage of solid, fluid and gaseous phases, and the thermal conductivities of the individual components. In addition to laboratory and field methods for the determination of the thermal conductivity, several theoretical models exist to estimate the thermal conductivity of a multi-phase medium based on different assumption how the individual phases are

spatially arranged (*Woodside & Messmer*, 1961). The thermal conductivity of the solid phase itself, for instance of sedimentary deposits, is a mixture of different mineralogical components with individual thermal conductivities.

In systems with fluid movement due to external forces, e.g. groundwater flow in a porous aquifer due to a pressure gradient, additional heat transfer by advection occurs in the fluid phase (*Domenico & Schwartz*, 1990). In the presence of groundwater flow, an advective effect referred to as thermal dispersion occurs due to differential groundwater flow paths at pore scale and heterogeneous permeability fields. In this case the effective thermal conductivity of a porous medium consists of the bulk thermal conductivity and an additional component caused by the linear relationship of the groundwater flow velocity dispersivity (*Domenico & Schwartz*, 1990).

1.2   Soil and groundwater temperatures

Temperature at the ground surface is generally influenced by atmospheric parameters, such as solar irradiation and air temperature, and surface properties, for instance the albedo. Surface temperatures are often determined as land surface temperatures (LST) with thermal sensors by airborne or satellite remote sensing. The heat transfer from the surface into the ground, commonly termed ground heat flux, as a part of the surface energy balance depends on many factors, including surface properties, soil properties and atmospheric conditions (*Oke,* 1982). The temperature at or directly beneath the surface is commonly referred to as ground surface temperature (GST) (*Taylor & Stefan*, 2009). Seasonal variations in GST penetrate into the subsurface mainly by heat conduction and influence the soil temperatures in the surficial subsurface (*Smerdon et al.*, 2003).

Aside from the temporal variations due to seasonal temperature fluctuations at the surface, permanent changes in GST also have a persistent impact on shallow subsurface and groundwater temperature. Changes of GST and according alteration of subsurface temperature are often observed in connection with land-use or surface cover changes. For example, *Taniguchi et al.* (1999a) and *Nitoui & Beltrami* (2005) found an increase of several degrees in GST and shallow subsurface temperatures after deforestation. Likewise, *Gunawardhana & Kazama* (2012) detected a positive correlation between aquifer warming and the degree of impervious surfaces in urban areas.

In addition to thermal signals from the surface, groundwater temperatures in shallow aquifers can also be significantly influenced by advective effects, such as interactions with surface waters (*Molina-Giraldo et al.,* 2011b) or due to the regional distribution of groundwater recharge and discharge areas (*Taniguchi,* 1993). Accordingly, heat carried by groundwater can serve as a tracer and spatiotemporal variations in groundwater temperature may be used for hydrogeological interpretations (*Anderson,* 2005). *Saar* (2011) provides a review on the application of geothermal measurements to determine groundwater flow velocities and permeability fields.

In the following paragraphs two scenarios for the alteration of shallow groundwater temperature are discussed in more detail. First, profound land-use changes and additional anthropogenic subsurface processes in urban areas and secondly, recent climate warming that causes an increase in surface air temperatures as wells as GST in rural areas.

1.2.1   Groundwater temperatures under urban areas

In the urban environment the thermal regime is more complex than in rural, less disturbed environments. Surface air temperatures (SAT) in urban areas are often considerably higher than in rural areas. This microclimatic phenomenon is known as urban heat island (UHI) effect and has been a focus of atmospheric research for several decades (e.g. *Landsberg,* 1956; *Kanda,* 2007). The important drivers for this atmospheric warming, such as heat loss from buildings, reduction of the potential evaporation due to urbanization and impervious surfaces, and the according impacts on the urban energy balance are quite well understood (e.g. *Oke,* 1988; *Arnfield,* 2003). Artificial soil covers, such as pavements or streets, strongly alter the surface energy budget and lead to an increase of GST in urban areas, which is often referred to as surface urban heat island (SUHI) (*Peng et al.,* 2012).

Similar to the urban warming in the atmosphere and at the surface, an increase in subsurface temperatures can be observed under urban areas (e.g. *Changnon,* 1999; *Ferguson & Woodbury*, 2007; *Yalcin & Yetemen*, 2009). So far, this phenomenon was mainly studied in fast-growing Asian megacities, where temperature deviations from the geothermal gradient were detected in up to 140 m depth (*Taniguchi et al.,* 2007; *Taniguchi et al.*, 2009). Thus, the anthropogenic subsurface warming is prone to affect large volumes of urban groundwater. A study by *Zhu et al.* (2010) revealed that the shallow GWTs in the cities of Cologne and Win-

nipeg are up to 5 K higher than in the rural background. However, detailed spatial analyses of groundwater temperatures under urban areas are rare.

The processes and factors that cause this extensive subsurface warming are not yet completely understood. Different surface covers in urban environments were found to influence the groundwater temperature significantly (*Taylor & Stefan*, 2009), causing differences between urban and rural groundwater temperatures of up to 3 K. By analyzing the relationship between subsurface temperatures and air temperatures *Taniguchi et al.* (2007) found that the subsurface warming cannot be explained by the increase in air temperatures alone. The impact of the heat loss from basements on the groundwater temperature was investigated by *Ferguson & Woodbury* (2004). But the effect is only significant within a distance of few tens of meters from the building and thus it cannot explain the vast spatial increase in GWT. However, the urban subsurface environment is influenced by a large number of anthropogenic structures and processes, such as sewage networks or injections of thermal waste water, which should also be considered when discussing urban GWT.

The extensive warming of urban aquifers has positive as well as negative implications for groundwater use. Significant temperature changes modify the chemical properties of groundwater and affect microbiological and fauna diversity that play an important role for water quality (*Brielmann et al.,* 2009; *Hähnlein et al.,* 2013).

On the other hand, these subsurface temperature anomalies contain an enormous amount of stored thermal energy. Consequently, the warm urban aquifers represent attractive reservoirs of thermal energy for geothermal use such as space heating. *Zhu et al.* (2010) estimated the geothermal potential of urban heat islands and found that the potential heat content in an urban aquifer, for instance in Cologne, could cover the residential space heating demand for at least several years. Furthermore, the elevated temperatures improve the efficiency of ground water and ground source heat pumps systems. However, at the same time, high groundwater temperatures restrict the use of groundwater for cooling purposes. Hence, a profound knowledge of the evolution of GWT and the involved processes is important for an efficient and sustainable management of this enhanced geothermal resource.

1.2.2   Impacts of climate change on groundwater temperature

A significant alteration of shallow subsurface temperatures can not solely be observed in urban areas, but also in rural areas variations of the air and ground surface temperatures generate changes in the subsurface thermal regime. Thus, deep borehole temperature profiles can be used for palaeoclimate studies that cover up to several hundreds of years (*Kohl*, 1998; *Pollack et al.,* 1998; *Huang et al.,* 2000). Under the consideration of conductive heat transport in the subsurface temperature-depth profiles can be inverted to yield an estimate of the site-specific GST history that is assumed to be closely coupled to SAT development over long time scale (e.g. *Beltrami et al.*, 1997; *Beltrami*, 2002a).

The short-term coupling of SAT, GST and soil temperatures in different depths over several years is intensively examined by observational and modeling studies (e.g. *Smerdon et al.,* 2004; *Smerdon et al.,* 2006). The propagation of temperature signals in the first meters of the subsurface in the absence of groundwater flow is found to be dominated by heat conduction that causes an attenuation of the temperatures signal with depth (*Smerdon et al.,* 2003). However, solar irradiation on the surface can perturb the surface energy balance in a manner contrary to that assumed in the purely conductive model approaches (*Beltrami & Kellman*, 2003). Hence, depending on the site-specific surface properties the offset between GST and SAT may vary with time, so that the relationship between SAT and GST over several years may be irregular (*Beltrami & Kellman*, 2003).

Furthermore, *Lesperance et al.* (2010) show that the relationship between air temperature and subsurface temperature development over intervals of several years to decades is also strongly impacted by the annual variability of SAT. Based on observational data and modelling results, they conclude that similar or equivalent trends in SAT and shallow subsurface temperatures are not sufficient to characterize their long-term relationship. Hence, other statistical approaches than trend comparison may prove useful for examining the coupling of atmospheric and subsurface temperature development. Moreover, in the presence of groundwater flow, the development of GWT is likely to be influenced by advective heat transport and thermal dispersion in the aquifer (*Saar*, 2011), which are not being accounted for in the aforementioned approaches.

The general impact of climate change on the hydrological cycle is expected to be quite significant (*Bates et al.*, 2008). Many studies scrutinized the possible consequences on hydrological processes above the surface, such as spatial and temporal changes in precipitation or

river flow (*Bates et al.,* 2008; *Kundzewicz,* 2008). Yet, equivalent studies evaluating the influence on groundwater systems, such as groundwater recharge mechanisms or storage capacities, are rather limited as relevant long-term data are rare (*Green et al.,* 2011; *Taylor et al.,* 2013).

In particular, the consequences for shallow GWT as an important driver for water quality (*Hähnlein et al.,* 2013), and therefore crucial parameter for groundwater resource management, are poorly understood (*Green et al.,* 2011). *Figura et al.* (2011) demonstrated that atmospheric temperatures changes directly influence stream water temperatures and consequently groundwater temperatures in aquifers that are recharged by bank infiltration. However, it remains uncertain if increasing air temperatures also have a detectable impact on the long-term development of groundwater temperatures in aquifers that are not connected to infiltrating surface water bodies. As pointed out by *Treidel et al.* (2012) it is not yet fully understood how climate change signals are transferred into shallow aquifers through the unsaturated zone.

1.3 Objectives

According to the discussion of conductive heat transport and the thermal conductivity of porous media, one aim of this study is to investigate which ground parameters, such as water or carbonate content, have a significant impact on the bulk thermal conductivity of a porous medium. In addition, the question, which soil parameters are needed to estimate the thermal conductivity based on theoretical models within a reasonable range compared to field and laboratory measurements, is addressed.

Further aims of this study are related to the above mentioned profound alterations of shallow GWT in urban areas. One focus is set on the detailed spatial analysis of urban groundwater temperatures in different cities, in order to identify the dominant drivers and influencing factors for the subsurface warming. Subsequent to the identification of the main heat sources, another aim is to quantify the anthropogenic heat fluxes in urban areas and to find out how they develop temporally in a changing urban environment.

Finally, this study aims to answer the question whether the increase in GWT in rural aquifers, which are not influenced by surface water, can be directly linked to the atmospheric warming of the last decades.

1.4 Thesis structure

The present work is a cumulative dissertation and consists of four independent studies (chapter 2, 3, 4 and 5) and a section with summarized conclusions (chapter 6). The studies in the chapters 2, 3, and 4 are published in ISI-listed journals and the manuscript in chapter 5 is currently under review.

The first publication in chapter 2 focuses on the thermal conductivity of the shallow subsurface and its determination with field and laboratory tests, as well as with theoretical models for the estimation of the thermal conductivity of sedimentary rocks. Core samples for the laboratory test are obtained from a geothermal test site, consisting of four boreholes that were later equipped with borehole heat exchangers. For the determination of the effective thermal conductivity a Thermal Response Test (TRT) is carried out and evaluated using the Kelvin's line source theory. In addition, several ground parameters, such as water content and carbonate content, are determined by laboratory tests. With these parameters the thermal conductivity is calculated using different theoretical models. Furthermore, the influence of these ground parameters on the thermal conductivity is examined by a correlation analysis.

In the second study in chapter 3 the spatial distribution of shallow GWT in several German cities is investigated. The interpolated isotherm maps are analyzed qualitatively with special regard to possible heat sources and influencing factors, by comparing them to land-use plans, positions of district heating networks, underground railway systems and locations of thermal wastewater injections. Furthermore, the spatial correlation between GWT and population density, as a simple surrogate for building density, and between GWT and SAT is examined. The magnitude of urban warming in the atmosphere is usually described by the urban heat island intensity (UHII) as temperature difference between rural and urban sites. In order to enable a comparison of atmospheric and subsurface urban warming, a quantitative indicator for large-scale subsurface UHI intensity, the 10–90%-quantile range $UHII_{10-90}$ of the temperature distribution, is introduced.

In chapter 4 the dominant heat sources discussed in the previous study are evaluated quantitatively. Therefore, a novel approach using an analytical heat flux model is developed for the city of Karlsruhe. The spatial heterogeneity and the uncertainties of the input parameters are taken into account by performing a Monte Carlo simulation with assigned parameter ranges. To identify the most relevant parameters a sensitivity analysis is conducted. By using a data set from 1977 and recent data from 2011 the evolution of the heat fluxes in Karlsruhe

over the last decades can be assessed. Furthermore, the heat flux from basements into the groundwater is resolved spatially for both years to investigate the spatial heat flux distribution.

While the previous chapters scrutinize the anthropogenic impacts on GWT in urban areas, chapter 5 focuses on the alteration of shallow GWT in rural areas due to increasing SAT in the last decades. A statistical analysis for the detection of abrupt changes in time-series is applied to long term measurements of GWT as well as SAT. Furthermore, different spatially averaged time-series of air temperature change are evaluated to discuss the regional temperature increase in the context of global warming. The magnitudes of the abrupt shifts and the time lags between the individual shifts in the investigated time-series are evaluated under consideration of the different thermal processes in the subsurface and the site-specific hydrogeological settings.

2 Bestimmung der Wärmeleitfähigkeit im Untergrund durch Labor- und Feldversuche und anhand theoretischer Modelle

Kurzfassung

Für die Auslegung und Planung von Erdwärmesondenanlagen ist die Kenntnis der thermischen Untergrundparameter, besonders der Wärmeleitfähigkeit, von großer Bedeutung. In dieser Studie wurden an einer Bohrung für eine Erdwärmesonde verschiedene Verfahren für die Bestimmung der thermischen Leitfähigkeit des Untergrundes angewendet. An den durch die Kernbohrung gewonnenen Proben wurden im Labor Wärmeleitfähigkeiten gemessen. Außerdem wurde nach dem Einbau der Erdwärmesonde (EWS) ein Thermal Response Test (TRT) durchgeführt. Zusätzlich wurden im Labor wichtige Gesteinsparameter, wie beispielsweise Wassergehalt und Kalkgehalt, bestimmt, mit deren Hilfe die Wärmeleitfähigkeit mit verschiedenen theoretischen Modellansätzen berechnet wurde. Die beste Übereinstimmung zwischen den berechneten und den im Labor gemessenen Wärmeleitfähigkeiten ergibt sich mit einer durchschnittlichen Genauigkeit von ca. 12% für Berechnungen der Wärmeleitfähigkeit des porösen Mediums mit der Gewichtung der Festphase und des gesättigten Porenraumes über das geometrische Mittel. Zwar ist die Berechnung der Wärmeleitfähigkeit unzuverlässiger als eine aufwendige Laborbestimmung oder ein TRT, auf diese Weise lassen sich jedoch deutlich genauere Ergebnisse erzielen als zum Beispiel durch Abschätzung anhand von Literaturwerten.

Abkürzungsverzeichnis

γ	Euler'sche Konstante [-]
g_i	geometrische Parameter nach de Vries (1963) [-]
F_1	Korrekturfaktor nach deVries (1963) [-]
κ	thermische Diffusivität [$m^2 s^{-1}$]
λ_{eff}	effektive Wärmeleitfähigkeit [$Wm^{-1}K^{-1}$]
λ_m	Wärmeleitfähigkeit des porösen Mediums [$Wm^{-1}K^{-1}$]
λ_i	Wärmeleitfähigkeiten der mineralogischen Komponenten [$Wm^{-1}K^{-1}$]
λ_s	Wärmeleitfähigkeit des Feststoffes [$Wm^{-1}K^{-1}$]
λ_w	Wärmeleitfähigkeit von Wasser [$Wm^{-1}K^{-1}$]
Φ	Porosität [-]
q	Wärmeleistung pro Meter [Wm^{-1}]
R_b	thermischer Bohrlochwiderstand [mKW^{-1}]
r_b	Radius der Bohrung [m]
T_0	ungestörte Untergrundtemperatur [K]
$T(r_b, t)$	Temperatur an der Bohrlochwand [K]
x_i	Anteile der mineralogischen Komponenten

2.1 Einleitung

Für die kostenoptimierte und nachhaltige Nutzung der oberflächennahen Geothermie durch Erdwärmesonden (EWS) spielt die Auslegung dieser Anlagen eine große Rolle (*Blum et al.,* 2010; *Blum et al.,* 2011). Für die Auslegung wiederum ist die Kenntnis der thermischen Untergrundparameter notwendig, wobei die effektive Wärmeleitfähigkeit des Untergrundes entscheidend ist. Die effektive Wärmeleitfähigkeit an einem Standort setzt sich zusammen aus einem konduktiven Anteil, der durch die Wärmeleitfähigkeit der Gesteine bestimmt wird, und einem möglichen konvektiven (bzw. advektiven) Anteil durch Grundwasserströmung (*de Marsily,* 1986; *Treidel et al.,* 2012). Die Wärmeleitfähigkeit des Gesteins ist abhängig von den Gesteinseigenschaften, wie dem Gefüge, der Mineralogie, der Porosität und dem Wassergehalt (*Woodside & Messmer*, 1961; *Brigaud & Vasseur*, 1989).

Zur rechnerischen Bestimmung der Wärmeleitfähigkeit bietet sich eine Reihe alternativer Verfahren an. *Woodside & Messmer* (1961) geben einen Überblick über mathematisch-statistische Ansätze, wie z. B. die geometrische und harmonische Mittelung der Wärmeleitfähigkeit der Einzelkomponenten des Materials. Das empirische Modell von *Johansen* (1975) beruht auf der Interpolation zwischen den angenommen Wärmeleitfähigkeiten für trockenes und gesättigtes Material. Andere Modelle wie die von *de Vries* (1963) oder *Campbell* (1994) verfolgen einen Ansatz analog zum Maxwell'schen Modell für die elektrische Leitfähigkeit eines Mediums mit einer zufälligen Verteilung von festen Sphären in einer homogenen Phase. Vergleichende Studien zur Bestimmung der Wärmeleitfähigkeit von Sedimentmaterial mit diesen unterschiedlichen Modellen sind unter anderem von *Brigaud & Vasseur* (1989), *Troschke & Burkhardt* (1998) und *Markle et al.* (2006) durchgeführt worden.

Für die experimentelle Bestimmung der Wärmeleitfähigkeit an Proben im Labor gibt es verschiedene stationäre und instationäre Messverfahren. Der Nachteil stationärer Verfahren wie der „divided bar"-Methode sind lange Messzeiten von bis zu 25 Minuten, die benötigt werden, um ein thermisches Gleichgewicht zu erreichen (*Sass et al.,* 1984). Daher werden oft instationäre Messverfahren bevorzugt, die wesentlich kürzere Versuchslaufzeiten erlauben, sodass damit auch eine größere Anzahl an Proben in einer überschaubaren Zeit analysiert werden kann. Dabei werden Messsonden bestehend aus einem Heizdraht und einem Thermometer (*Woodside & Messmer*, 1961; *Nakshabandi & Kohnke*, 1965) in das Probenmaterial eingebracht oder in Form von Oberflächensonden auf die präparierte Oberfläche des Probenkörpers gelegt (z. B. *Pribnow & Sass*, 1995; *Davis et al.,* 2007). Die Auswertung im instatio-

nären Fall beruht auf der Linienquellentheorie (*Carslaw & Jaeger*, 1959). Ein weiteres Verfahren zur Bestimmung der Wärmeleitfähigkeit im Labor ist das Optical-Scanning, bei dem die Wärmeleitfähigkeit kontaktlos mit Hilfe einer Laser-induzierten Aufheizung mit nachgeschalteter Temperaturmessung ermittelt wird (*Popov et al.*, 1999).

Durchteuft eine EWS einen Aquifer mit fließendem Grundwasser, so weicht die effektive Wärmeleitfähigkeit von der rein konduktiv bestimmten Wärmeleitfähigkeit ab. Bei der in-situ Bestimmung der thermischen Eigenschaften des Untergrundes hat sich daher der Thermal Response Test (TRT) etabliert (*Eklöf & Gehlin*, 1996; *Austin et al.*, 2000). Beim TRT wird dem Untergrund durch das in der EWS zirkulierende Fluid eine spezifische Heizleistung zugeführt oder entzogen und die Temperaturänderung im Fluid am Sondenkopf gemessen. Die Auswertung des Versuches erfolgt meist über einen Linienquellen-Ansatz (*Carslaw & Jaeger*, 1959), ist aber auch über den Zylinderquellenansatz möglich (*Sass & Lehr*, 1979). Es werden auch numerische Modelle zur Hilfe genommen (z. B. *Gehlin & Hellström*, 2003; *Raymond et al.*, 2011; *Wagner et al.*, 2011), mit denen durch die Berücksichtigung zusätzlicher Randbedingungen und Parameter, z. B. der Wärmekapazität, die Messergebnisse oft genauer reproduziert werden können (z. B. *Shonder & Beck*, 2000; *Spitler et al.*, 2000; *Witte et al.*, 2002).

Während die standardisierte Durchführung eines TRTs einen integralen Wert der standortspezifischen effektiven Wärmeleitfähigkeit liefert, ermöglichen Weiterentwicklungen des TRT eine tiefenabhängige Bestimmung, wodurch auch Bereiche mit hohem konvektivem Wärmefluss identifiziert werden können. Eine Möglichkeit ist die Bestimmung aus tiefenaufgelösten Temperaturmessungen im Untergrund, wobei jedoch der lokale Wärmefluss ebenfalls tiefenaufgelöst bekannt sein muss. Tiefenaufgelöste Temperaturmessungen können zum einen mit Hilfe von Temperatur-Tiefen-Messsonden, die in die EWS eingebracht werden, durchgeführt werden (*Homuth et al.*, 2008; *Forrer et al.*, 2008). Bei einer anderen Weiterentwicklung des TRTs, dem sog. „Enhanced Geothermal Response Test" (EGRT) wird die tiefenaufgelöste Temperaturmessung über ein mit in das Bohrloch eingebautes Glasfaserkabel ermöglicht (*Dornstädter et al.*, 2008).

Das Ziel der vorliegenden Studie ist es, durch detaillierte Laboruntersuchungen an Bohrkernproben einer EWS-Bohrung den Einfluss der verschiedenen Gesteinsparameter (mineralogische Zusammensetzung, Porosität, Wassergehalt, etc.) auf die Wärmeleitfähigkeit der Gesteine zu bestimmen und mögliche Korrelationen zwischen den einzelnen Parametern zu untersuchen. Die Wärmeleitfähigkeiten des Probenmaterials werden zunächst mit verschiede-

nen theoretischen Modellen (harmonisches, arithmetisches und harmonisches Mittel, Modell nach de Vries) berechnet, um zu klären, ob jene Berechnungen auch ohne Kenntnis des genauen Mineralbestandes durchgeführt werden können. Danach werden die Wärmeleitfähigkeiten mit der gleichen Methode, jedoch mit im Labor bestimmten mineralogischen Zusammensetzungen der Proben, berechnet und die Ergebnisse gegenübergestellt. Weiterhin werden die Ergebnisse der Wärmeleitfähigkeiten aus dem Labor mit den Ergebnissen eines konventionellen TRTs an einer EWS verglichen, um eine mögliche Übertragbarkeit der Laborergebnisse ins Feld zu prüfen. Entscheidend ist hierbei vor allem die mögliche Beeinflussung der thermischen Gesteinseigenschaften durch die lokalen Grundwasserverhältnisse.

2.2 Grundlagen

2.2.1 Wärmeleitfähigkeit von porösen Medien

Die Wärmeleitfähigkeit oder thermische Leitfähigkeit, λ [Wm^{-1}K^{-1}], beschreibt die Fähigkeit eines Materials zum Energietransport durch Wärmeleitung. Bei einem porösen Material hängt die Wärmeleitfähigkeit (λ_m) von der Wärmeleitfähigkeit des Feststoffes (λ_s), der Porosität (Φ) und dem Sättigungsgrad (S_r) ab (*Woodside & Messmer*, 1961). Im flachen Untergrund ist das Porenfluid das Wasser im Boden oder das Grundwasser, das bei einer Temperatur von 10°C eine Wärmeleitfähigkeit (λ_w) von 0,58 Wm^{-1}K^{-1} aufweist. Da Luft hingegen nur eine geringe Wärmeleitfähigkeit von 0,026 Wm^{-1}K^{-1} besitzt, ist die Abhängigkeit von λ von der Porosität und dem Wassergehalt entsprechend groß (*Clauser,* 2006).

Statistische Ansätze zur Berechnung von λ_m in heterogenen gesättigten Medien orientieren sich wie bei der hydraulischen Leitfähigkeit an der Anordnung der einzelnen Materialkomponenten (*Woodside & Messmer*, 1961). Eine parallele Anordnung entspricht der Vorstellung, dass die Richtung des Wärmeflusses parallel zu der Schichtung eines Mediums, bestehend aus Feststoff und Fluid, gerichtet ist. Mathematisch wird dies durch das arithmetische Mittel (Gl. 2−1) ausgedrückt. Eine Anordnung der Phasen in Reihe entspricht der Vorstellung, dass der Wärmefluss senkrecht zur Schichtung des Mediums gerichtet ist und durch das harmonische Mittel berechnet werden kann (Gl. 2−2). Die dritte mögliche Verteilung ist eine zufällige Verteilung der Komponenten, quantifiziert durch das geometrische Mittel (Gl. 2−3).

$$\lambda_m = \phi \lambda_w + (1-\phi)\lambda_s \qquad\qquad\qquad \text{arithmetisches Mittel (Gl. 2−1)}$$

$$1/\lambda_m = \phi/\lambda_w + (1-\phi)/\lambda_s \qquad\qquad \text{harmonisches Mittel (Gl. 2–2)}$$

$$\lambda_m = \lambda_w^\phi \cdot \lambda_s^{(1-\phi)} \qquad\qquad \text{geometrisches Mittel (Gl. 2–3)}$$

Das ebenfalls häufig angewandte Modell von *de Vries* (1963), das analog zum Max-wellschen Modell für elektrische Leitfähigkeit formuliert wurde, nimmt eine zufällige Vertei-lung von festen Sphären in einem Fluid an (Gl. 2–4). F_1 beschreibt das Verhältnis der durch-schnittlichen Temperaturgradienten der beiden Phasen (Gl. 2–5).

$$\lambda_m = \frac{\phi\lambda_w + (1-\phi)F_1\lambda_s}{\phi + (1-\phi)F_1} \qquad\qquad \text{(Gl. 2–4)}$$

$$F_1 = \frac{1}{3}\sum_{i=3}^{3}\left[1 + (\lambda_s/\lambda_w - 1)g_i\right]^{-1} \qquad\qquad \text{(Gl. 2–5)}$$

Die geometrischen Parameter g_1, g_2 und g_3 definieren die Form der festen Partikel. Für die Annahme von kugelförmigen Partikeln ($g_1 = g_2 = g_3$) reduziert sich Gl. 2–4 zur ursprüng-lichen Maxwell-Gleichung (*Woodside & Messmer*, 1961). Die meisten Bodenpartikel haben jedoch eine sphäroide Form mit $g_1 = g_2 = n{\cdot}g_3$, wobei n zwischen 0,1 und 100 variiert. In die-ser Arbeit werden die ursprünglich von *de Vries* (1963) benutzten Werte von $g_1 = g_2 = 1/8$ und $g_3 = 3/4$ verwendet.

2.2.2 Thermal-Response-Test

Der Thermal-Response-Test (TRT) ist eine Feldmethode, mit der die effektive Wärme-leitfähigkeit des Untergrundes vor Ort in einer fertig eingebauten EWS bestimmt werden kann. Dadurch werden auch die Bohrlochverfüllung, die ungestörten Untergrundverhältnisse, sowie ein eventuell vorhandener Grundwasserfluss mit einbezogen. Bei einem TRT wird eine definierte Wärmeleistung an die EWS angelegt, und der sich dabei ergebende Verlauf der Ein- und Austrittstemperaturen des Wärmeträgerfluides an der EWS aufgezeichnet (*Reuß & Sanner*, 2001). Die standardisierte Berechnung der durchschnittlichen (bzw. integralen) effek-tiven Wärmeleitfähigkeit des Untergrundes erfolgt über die Auswertung der gemessenen Flu-idtemperaturen (*Eklöf & Gehlin*, 1996):

$$T_{(r_b,t)} = \frac{q}{4\pi\lambda_{eff}} \cdot \left[\ln\left(\frac{4\kappa t}{r_b^2}\right) - \gamma \right] + qR_b + T_0 \qquad \text{(Gl. 2–6)}$$

Gleichung 2–6 stellt eine Näherungslösung der Linienquellengleichung für lange Messzeiten dar. Für die Temperatur an der Bohrlochwand $T_{(rb,\,t)}$ gilt daher folgende Beziehung:

$$T(t) = a\ln(t) + b \qquad \text{(Gl. 2–7)}$$

$$\text{mit } a = \frac{q}{4\pi\lambda_{eff}} \text{ und } b = q\left(R_b + \frac{\ln\left(\dfrac{4\kappa}{r_b^2}\right) - \gamma}{4\pi\lambda_{eff}} \right).$$

Die effektive Wärmeleitfähigkeit λ_{eff} kann so aus der Steigung der linearen Regression der Temperatur T gegen den natürlichen Logarithmus der Zeit abgelesen werden. Ist neben λ_{eff} auch die thermische Diffusivität κ bekannt, kann daraus der Bohrlochwiderstand R_b ermittelt werden.

2.3 Standort

Nördlich von Freising wurde ein geothermisches Testfeld mit vier im Rechteck angeordneten, 80 m tiefen Bohrungen (ZAEB1–4) eingerichtet. Die Bohrung ZAEB1 wurde für die Probennahme als Kernbohrung durchgeführt, während bei den anderen drei Bohrungen das Imlochhammer-Verfahren zur Anwendung kam. Bei dem Bohrverfahren für die Kernbohrung handelt es sich um ein Einfach-Kernrohr-Bohrverfahren. Dabei wurde in tieferen Bereichen mit rolligem Lockermaterial teilweise mit einer Bohrspülung gearbeitet. Detaillierte Angaben zum Ausbau der einzelnen Bohrungen finden sich in Tabelle 2-1.

Tabelle 2-1: Ausbaudaten der vier Bohrungen ZAEB1 - 4 des geothermischen Testfeldes.

Bohrung	ZAEB1	ZAEB2	ZAEB3	ZAEB4
Endteufe	80 m	80 m	80 m	80 m
Sonde	Doppel U-Rohr, 32mm	Doppel U-Rohr, 32mm	Doppel U-Rohr, 32mm	Einfach U-Rohr, 40mm
Sondenmaterial	PE-Xa	PE-Xa	PE-Xa	HD-PE
Sondenhersteller	REHAU AG	REHAU AG	REHAU AG	MuoviTech
Hinterfüllung	ThermoCem plus	ThermoCem plus	ThermoCem	ThermoCem plus
Anzahl der Abstandshalter	31	31	31	31
Anzahl der PT-100 Temperaturfühler	9	9	9	9
Bohrverfahren	Einfach-Kernrohr	Imlochhammer	Imlochhammer	Imlochhammer
Teufe und Bohrdurchmesser	0-10 m: 220 mm 10-80 m: 178 mm	0-80 m: 131 mm	0-80 m: 131 mm	0-80 m: 131 mm

Das Testfeld liegt im Bereich des alpinen Molassebeckens. Die im Testfeld erbohrten Gesteine zählen zur oberen Süßwassermolasse (osm), die sich nach Ablagerungsbedingungen faziell weiter untergliedern lässt. Die erbohrten Sedimente (bzw. Sedimentgesteine) bis 26 m u. GOK gehören zu den Ablagerungen der Oberen Serie. Es handelt sich dabei hauptsächlich um blaugraue, halbfeste, schluffige Tone und Mergel, in denen sich dünne Zwischenlagen aus rotbraunem Feinsand und in den obersten Bohrmetern auch aus Feinkies befinden. Ab 26 m u. GOK stehen die groben rolligen Sedimente der Mittleren Serie an. Diese bestehen aus mächtigen hellen, wenig verfestigten Sand- und Kieslagen, zwischen denen graue, steife Schluffe und Tone lagern. Auch diese Schluffe und Tone verfügen teilweise über hohe Kalkgehalte. Bei der Bohrkernansprache wurden 110 Probennahmepunkte festgelegt, um eine detaillierte boden- und thermophysikalische Charakterisierung des Bohrprofils vornehmen zu können. In Abbildung 2-1 ist daher nur ein vereinfachtes Bohrprofil der Bohrung ZAE B1 dargestellt.
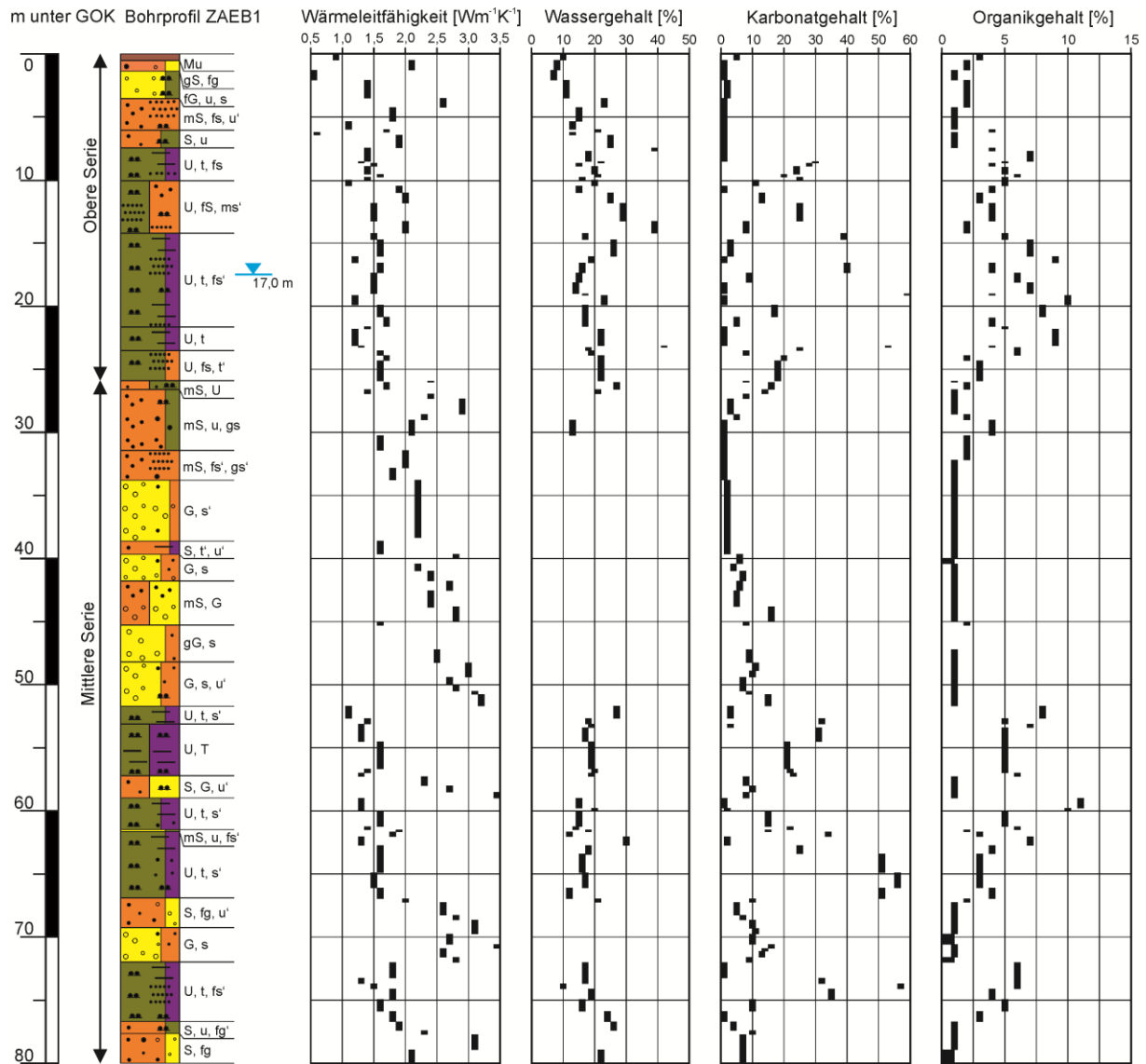
Abbildung 2-1: Bohrprofil der Kernbohrung ZAEB1 mit Darstellung der Ergebnisse der Laboruntersuchung.

Grundwasser im oberflächennahen Bereich kommt im Testgebiet vor allem in den Sand- und Kieslagen der Mittleren Serie vor. Durch die häufige Wechsellagerung von groben und feinkörnigen Sedimenten bzw. Sedimentgesteinen sind in diesem Bereich meist mehrere Grundwasserstockwerke ausgebildet. Aufgrund der ausgeprägten lateralen und vertikalen Heterogenität der Sedimentablagerungen schwanken die Mächtigkeiten und Durchlässigkeiten der Aquifere stark. *Rauert et al.* (1992) geben für die sandig-kiesigen Aquifere der Oberen Süßwassermolasse eine durchschnittliche hydraulische Durchlässigkeit von 2×10^{-5} ms^{-1} an. Die Grundwasserfließrichtung in der Umgebung des Testgebietes ist nach Süden gerichtet, wo

die Amper den lokalen Vorfluter darstellt. Das Grundwassergefälle und damit die Fließgeschwindigkeit sind in diesem Bereich sehr gering.

2.4 Methode

2.4.1 Laboruntersuchungen

Insgesamt lagen für die Laboruntersuchungen 105 Proben der Kernbohrung ZAEB1 vor, davon 54 überwiegend schluffige und tonige Proben als Kernproben, und 51 überwiegend sandige und kiesige Proben als Lockermaterial. An 5 Probennahmepunkten bestand das gewonnene Material nur aus einigen wenigen groben Kiesstücken, sodass nicht genügend repräsentatives Probenmaterial für die Untersuchungen zur Verfügung stand. Zur Konservierung des natürlichen Wassergehaltes wurden die Proben direkt nach der Gewinnung möglichst luftdicht in Plastik verpackt und danach kühl und dunkel gelagert. Die Laboruntersuchungen wurden auf Grundlage der entsprechenden DIN-Normen durchgeführt. Zur lithologischen Charakterisierung wurden von allen Proben der Wassergehalt (*DIN 18121-1*, 1998), der Karbonatgehalt (*DIN 18129*, 2011), der Gehalt an organischem Material (*DIN 18128*, 2002), die Korndichte (*DIN 18124*, 2011), sowie die Korngrößenverteilung durch Siebung und Schlämmung (*DIN 18123*, 2011) bestimmt. Die mineralogische Zusammensetzung wurde für alle Proben über semi-quantitative Röntgendiffraktometrie an Pulverpräparaten ermittelt (*Brigaud & Vasseur*, 1989).

Die Wärmeleitfähigkeiten der einzelnen Proben wurden instationär mithilfe des Messgerätes Isomet 2104 der Firma Applied Precision Ltd. gemessen. Für das Messgerät inklusive der Messsonden wird von Herstellerseite eine Messgenauigkeit von ±10 % angegeben. Bei der Messung wird das Material durch eine Linienquelle mit einem Wärmeimpuls erhitzt und die Temperaturänderung in unmittelbarer Nähe der Heizquelle in Abhängigkeit von der Zeit gemessen. Bei einem sehr geringen Abstand zwischen der Wärmequelle und dem Ort der Temperaturmessung, sowie bei ausreichend langen Zeitintervallen, kann so die Wärmeleitfähigkeit nach der Linienquellen-Theorie ermittelt werden. Die Messsonden, auf deren Unterseite sich das Heizelement und die Temperatursensoren befinden, müssen hierfür auf eine möglichst ebene Oberfläche des Probenmaterials gelegt werden. Bei den bindigen Lockergesteinsproben wurden Querschnittflächen der Bohrkerne planar abgeschliffen und so die Wärmeleitfähigkeit bei natürlichem Wassergehalt bestimmt.

Bei den rolligen Lockergesteinsproben wurde das Material in ein zylindrisches Gefäß gefüllt, verdichtet und die Oberfläche geglättet. Da aufgrund der Standortbedingungen davon ausgegangen werden kann, dass die Schichten aus groben Sand-Kies-Gemischen im tieferen Untergrund Grundwasser führen, wurden die rolligen Lockergesteinsproben vor der Messung der Wärmeleitfähigkeit mit Wasser gesättigt. Die rolligen Proben oberhalb des Wasserspiegels in 17 m Tiefe wurden ohne vorherige Sättigung gemessen. Da sich bei manchen kieshaltigen Proben keine glatten Oberflächen herstellen ließen, wurden hier auch Messungen mit einer Nadelsonde, die in den Probenkörper hineingesteckt wird, durchgeführt. So wurden an jeder Probe mindestens 3 Messungen durchgeführt und der Durchschnittswert berechnet. Waren die Streuungen größer als $0,05 \mathrm{Wm^{-1}K^{-1}}$, wurden Wiederholungsmessungen durchgeführt. Für den Vergleich mit den anderen Methoden wurde jeweils der Mittelwert der Messungen verwendet.

2.4.2 Berechnung der Wärmeleitfähigkeit mit theoretischen Modellen

Um mit den Gleichungen 2−1 bis 2−4 die Wärmeleitfähigkeit eines Materials (λ_m) zu berechnen, muss die Porosität (Φ) und die Wärmeleitfähigkeit des reinen Feststoffes (λ_s) bekannt sein. Aufgrund der stark schwankenden Konsistenz der Sedimente konnten nur 13 Schichten mithilfe von Ausstechzylindern beprobt werden. Über Trocknung wurde von diesen Proben die Porosität bestimmt. Von den anderen Schichten wurden die Porositäten anhand der ermittelten Korngrößenverteilungen über Literaturwerte abgeschätzt (Tabelle 2-2). Die Wärmeleitfähigkeit des Feststoffes (λ_s) wurde über die Anteile x_i der mineralogischen Komponenten i und deren jeweiliger Wärmeleitfähigkeit λ_i bestimmt (*Markle et al.,* 2006):

$$\lambda_s = \prod_{i=1}^{n} \lambda_i^{x_i} \qquad \text{(Gl. 2−8)}$$

Tabelle 2-2: Literaturwerte für die Porosität verschiedener Sedimente (nach *Prinz & Strauß*, 2006).

Material	Porosität (min. – max.)	Porosität (Durchschnitt)
Ton, schluffig	0,45 – 0,65	0,55
Schluff, tonig	0,40 – 0,55	0,48
Schluff	0,35 – 0,55	0,45
Schluff, sandig	0,35 – 0,45	0,40
Mittelsand	0,30 – 0,40	0,35
Sand, kiesig	0,30 – 0,35	0,33
Kies, sandig	0,25 – 0,35	0,30

Die Wärmeleitfähigkeiten der gesteinsbildenden Minerale in Sedimenten sind hinreichend bekannt (z. B. *Clauser,* 2006; *Brigaud & Vasseur*, 1989; vgl. Tabelle 2-3). Da eine Bestimmung der mineralogischen Bestandteile mithilfe von Röntgendiffraktometrie (XRD) aufwändig ist, wurden die mineralogischen Zusammensetzungen für die Berechnung im ersten Schritt nur abgeschätzt. Die Ergebnisse der Röntgendiffraktometrie dienten zur Validierung des Schätzverfahrens.

Tabelle 2-3: Wärmeleitfähigkeiten von gesteinsbildenden Mineralen in Sedimenten.

Material/Mineral	Wärmeleitfähigkeit [$Wm^{-1}K^{-1}$]	Quelle
Quarz	7,9	*Clauser* (2006)
Feldspat (Plagioklas)	2,5	*Clauser* (2006)
Calcit	3,3	*Clauser* (2006)
Dolomit	5,1	*Clauser* (2006)
Illit	1,9	*Brigaud & Vasseur* (1989)
Smectit	1,9	*Brigaud & Vasseur* (1989)
Kaolinit	2,6	*Brigaud & Vasseur* (1989)
Org. Material	0,4	*VDI 4640* (2010)

Aus der ermittelten Korngrößenverteilung sind die prozentualen Anteile an Kies, Sand, Schluff und Ton im Probenmaterial bekannt. Um von diesen Werten auf die mineralogische Zusammensetzung zu schließen, wurde für jede Korngrößenfraktion eine spezifische minera-

logische Zusammensetzung angenommen. Auf Grundlage der sedimentpetrographischen Untersuchungen im Bereich der osm von *Lemcke* (1953) wurde für die Kiesfraktion eine Zusammensetzung von 90 % Quarzkörnern und 10 % Karbonatanteil definiert. Für die Körner im Sandbereich wurde eine Zusammensetzung von 75 % Quarz und 25 % Feldspat angenommen. Für die Schlufffraktion wurde eine Zusammensetzung von 40 % Quarz, 40 % Feldspat und 20 % Tonminerale geschätzt, während für die Tonfraktion von 80 % Tonmineralen, 10 % Feldspat und 10 % Quarz ausgegangen wurde. Die in der Berechnung verwendeten Wärmeleitfähigkeiten der Minerale sind in Tabelle 2-3 aufgeführt. Für die Tonfraktion wurde mit einem Mittelwert der Wärmeleitfähigkeiten der sehr häufig vorkommenden Tonminerale Illit, Smectit und Kaolinit gerechnet. Außerdem wurden bei der Berechnung von λ_s die im Labor bestimmten Anteile an Karbonat und organischem Material mit den entsprechenden Wärmeleitfähigkeiten miteinbezogen (Tabelle 2-3). Die Wärmeleitfähigkeit des Wassers (λ_w) beträgt z.B. nach *Clauser* (2006) bei 10°C, die im oberflächennahen Grundwasser üblich sind, $0{,}58 \mathrm{Wm^{-1}K^{-1}}$. Unter Laborbedingungen, d. h. 20°C, hat Wasser eine Wärmeleitfähigkeit von $0{,}60 \ \mathrm{Wm^{-1}K^{-1}}$.

2.4.3 Thermal-Response-Test

Nach dem Einbau der EWS in das Bohrloch ZAEB 1 (Tabelle 2-1) wurde mithilfe des mobilen Messwagens vom Bayerischen Zentrum für Angewandte Energieforschung (ZAE) ein TRT durchgeführt. Dazu wurde das Wärmeträgerfluid über einen Zeitraum von 115 Stunden mit einer konstanten Heizleistung erwärmt und durch die beiden U-Rohre gepumpt. Die Temperatur des Wärmeträgerfluids und die an die Kreisläufe angelegte Heizleistung wurden während der Heizphase in 60 s-Intervallen gemessen. Der Versuchsaufbau und die Versuchsdurchführung werden ausführlich in *Zervantonakis & Reuß* (2006) erläutert. Die Auswertung des TRTs erfolgte auf Grundlage der Linienquelllen-Theorie (Gl. 2−7). Die zur Ermittlung der mittleren effektiven Wärmeleitfähigkeit und des mittleren Bohrlochwiderstandes benötigte ungestörte Bodentemperatur wurde an der EWS gemessen.

2.5   Ergebnisse und Diskussion

2.5.1   Laboruntersuchungen

Die Ergebnisse der Laboruntersuchungen sind in Abbildung 2-1 dargestellt. Die mit dem Isomet 2104 gemessenen Wärmeleitfähigkeiten (λ_m) schwanken mit der Änderung der Lithologie. Die niedrigsten Wärmeleitfähigkeiten weisen die trockenen Kiese in den obersten Metern unter GOK mit 0,5 Wm^{-1}K^{-1} auf. In den Schluffen der Oberen Serie steigen die Wärmeleitfähigkeiten auf Werte von 1,2 bis 2,0 Wm^{-1}K^{-1} an. In den grundwasserführenden Kiesen und Sanden der Mittleren Serie werden Werte zwischen 1,7 und 3,3 Wm^{-1}K^{-1} erreicht. In den Schluffen der Mittleren Serie verringert sich λ_m wieder auf 0,8 bis 1,7 Wm^{-1}K^{-1}, während in den sandig-kiesigen Zwischenschichten die höchsten Werte von bis zu 3,5 Wm^{-1}K^{-1} gemessen wurden.

Die Wassergehalte in den Schluffen und Tonen sind mit Werten zwischen 10 und 25 % durchweg vergleichbar und relativ gering. Wassergehalte von über 25 % wurden nur selten gemessen. Aufgrund des Ruhewasserspiegels von 17 m unter GOK kann für die Sand- und Kiesschichten der Mittleren Serie von vollständiger Wassersättigung ausgegangen werden. Eine Bestimmung des natürlichen Wassergehaltes bei gestörter Probennahme war nicht möglich, sodass in diesen Bereichen (27–29 m, 30–52 m, 57–59 m, 67–72 m, 77– 79 m) keine Werte vorliegen (vgl. Abbildung 2-1). Der Karbonatgehalt in den Sanden und Kiesen ist im Durchschnitt gering und liegt zwischen 0 und 10 %. Der Karbonatgehalt der Schluffe und Tone schwankt hingegen sehr stark. Einzelne Bereiche sind fast kalkfrei, während sich in meist dünnen Zwischenschichten erbsengroße Kalkkonkretionen gebildet haben. Diese Schichten zeigen Karbonatgehalte von bis zu 60 %, während Schichten mit fein verteiltem Kalk Gehalte von bis zu 40 % erreichen. Der Anteil an organischem Material ist in den Sanden und Kiesen mit 0 bis 1 % erwartungsgemäß gering. In den Schluffen und Tonen schwankt der Organikgehalt zwischen 3 und 11 %, wobei die meisten Werte im Bereich bis 8 % liegen.

2.5.2   Korrelationen

Um zu ermitteln, wie die verschiedenen Gesteinseigenschaften die Wärmeleitfähigkeit beeinflussen, wurde überprüft, inwieweit die verschiedenen Gesteinsparameter mit der Wärmeleitfähigkeit und untereinander korrelieren. Die berechneten Korrelationskoeffizienten sind in Tabelle 2-4 dargestellt. Bei den Ergebnissen werden die Korrelationen für die rolligen und

bindigen Lockergesteinsproben separat betrachtet. Wasser-, Karbonat- und Organikgehalte wurden wie die Korndichte nach DIN bestimmt. Die Unsicherheit ist wie die veranschlagte 10 %-Ungenauigkeit (Erfahrungswert) bei den XRD-Messungen klein. Die Porosität wurde nur für sechs rollige und sieben bindige Lockergesteinsproben gemessen. Diese geringe Zahl an Messungen erlaubt nur eine ungenaue Bestimmung von Korrelationen, daher wurden die geschätzten Porositäten ergänzt. Die Verlässlichkeit der letzteren Werte hängt stark von der Schätzgenauigkeit ab.

Tabelle 2-4: Korrelationskoeffizienten der im Labor bestimmten bzw. geschätzten Gesteinsparameter. Der obere Wert steht jeweils für die rolligen Lockergesteinsproben, die unteren für die bindigen Lockergesteinsproben (n.b. = nicht bestimmt).

	Wassergehalt	Kalkgehalt	Organikgehalt	Porosität gemessen	Porosität geschätzt	Korndichte	Quarzgehalt (XRD)	Feldspatgehalt (XRD)	Tongehalt (XRD)
Wärmeleitfähigkeit	n.b./ 0,00	0,30/ -0,10	0,70/ -0,70	-0,36/ 0,84	-0,60/ -0,48	0,01/ 0,12	0,27/ 0,73	-0,28/ 0,62	-0,31/ -0,31
Wassergehalt		n.b./ -0,15	n.b./ -0,14	n.b./ 0,55	n.b./ 0,00	n.b./ 0,03	n.b./ 0,08	n.b./ 0,38	n.b./ 0,07
Kalkgehalt			-0,16/ -0,28	0,58/ 0,05	-0,15/ 0,15	0,56/ 0,52	-0,09/ -0,23	-0,43/ -0,26	-0,21/ -0,83
Organikgehalt				0,07/ -0,67	0,82/ 0,38	0,08/ -0,45	-0,36/ -0,68	0,22/ -0,62	0,32/ 0,62
Porosität gemessen					n.b.	0,79/ -0,10	-0,64/ 0,78	-0,15/ 0,41	0,65/ -0,67
Porosität geschätzt						0,13/ -0,09	-0,24/ -0,54	0,33/ -0,38	0,19/ 0,15
Korndichte							-0,35/ 0,17	-0,18/ 0,17	0,18/ -0,60
Quarzgehalt (XRD)								-0,23/ 0,73	-0,94/ -0,34
Feldspatgehalt (XRD)									0,22/ -0,21

Die Korrelationen von Gesteinsparametern zur Wärmeleitfähigkeit für die rolligen Lockergesteinsproben (vorwiegend Kiese und Sande) und die bindigen Lockergesteinsproben

(toniges und schluffiges Material) sind zum Teil sehr unterschiedlich und angesichts der verschiedenen Materialzusammensetzungen auch zu erwarten. Dies zeigt sich auch in den Korrelationen zwischen den untersuchten Gesteinsparametern. So gehen in den ton- und an organischem Material reicheren bindigen Lockergesteinsproben höhere Ton und Organikgehalte einher mit niedrigeren Quarz- und Feldspatgehalten, während die deutlich geringeren Gehalte in den rolligen Lockergesteinsproben auf keine Korrelationen schließen lassen. Die rolligen Lockergesteinsproben werden einheitlich dominiert von quarz- und feldspatreichen Grobkomponenten, und wegen der vergleichsweise homogenen Zusammensetzung zeichnet sich auch die zu erwartende Abhängigkeit der Wärmeleitfähigkeit vom Quarz und Feldspat-Gehalt nicht ab. Zudem deutet sich kein Einfluss des Karbonatgehalts auf die Wärmeleitfähigkeit an. Im Gegensatz besteht eine deutliche Korrelation für die bindigen Lockergesteinsproben sowie eine negative Korrelation zu Ton- und v. a. Organikgehalt. Letztere ist zurückzuführen auf die relativ niedrige Wärmeleitfähigkeit von organischem Material (Tabelle 2-3).

Im Prinzip sollte die Porosität negativ mit der Wärmeleitfähigkeit korrelieren. Dies ist angedeutet mit Werten des Korrelationskoeffizienten zwischen −0,60 bis −0,48 bei den geschätzten Porositäten (Tabelle 2-4). Angesichts der Ungenauigkeit bei Schätzung sowie auch bei der Messung ist dies erwartungsgemäß. Allerdings findet sich eine starke positive Korrelation der gemessenen Porosität mit der Wärmeleitfähigkeit bei den unterschiedlich ausgebildeten bindigen Lockergesteinsproben. Zwar ist die Signifikanz dieser Korrelation beeinträchtigt durch die kleine Anzahl von Messungen, allerdings auch erklärbar. Die gemessene Porosität verringert sich bei den bindigen Lockergesteinsproben mit dem Organikanteil, welcher offensichtlich einen dominanten Einfluss auf die Wärmeleitfähigkeit hat.

2.5.3 Berechnung der Wärmeleitfähigkeit

Über das geometrische Mittel (Gl. 2−7) wurde für jede Probe die Wärmeleitfähigkeit des Feststoffanteils λ_s berechnet. Die ermittelten Werte liegen in einem Bereich zwischen 3,8 und 6,0 $Wm^{-1}K^{-1}$ für Sande und Kiese, bzw. zwischen 2,4 und 4,0 $Wm^{-1}K^{-1}$ für Tone und Schluffe. Die Werte für λ_s stimmen sehr gut mit denen von *Dehner* (2007) durch Ableitung aus dem Quarz- und Tonmineralanteil ermittelten Werten von Lockersedimenten überein. Abweichungen zeigen sich jedoch zu den Werten von *Hwang et al.* (2010), die mit 3,0 $Wm^{-1}K^{-1}$ für Sand und 1,5 $Wm^{-1}K^{-1}$ für Schluff und Ton angegeben werden.

Abbildung 2-2 zeigt die Korrelation der gemessenen Wärmeleitfähigkeiten $\lambda_{m,gemessen}$ und der berechneten Wärmeleitfähigkeiten des Feststoffanteils λ_s , beide Werte jeweils normiert gegen die Wärmeleitfähigkeit von Wasser. Ebenfalls gezeigt wird der Verlauf der vier theoretischen Wärmeleitfähigkeitsmodelle. Für die Darstellung der Kurven wurde eine Porosität von 0,38 gewählt, die dem arithmetischen Mittel der geschätzten Porositäten aller bindigen und rolligen Lockergesteinsproben entspricht. Wie erwartet bilden arithmetisches (und Modell nach de Vries) bzw. harmonisches Mittel die oberen bzw. unteren Einhüllenden. Das geometrische Mittel liegt dazwischen und liefert wie in vergleichbaren Studien die beste Übereinstimmung (*Woodside & Messmer*, 1961; *Brigaud & Vasseur*, 1989; *Troschke & Burkhardt*, 1998; *Markle et al.,* 2006).
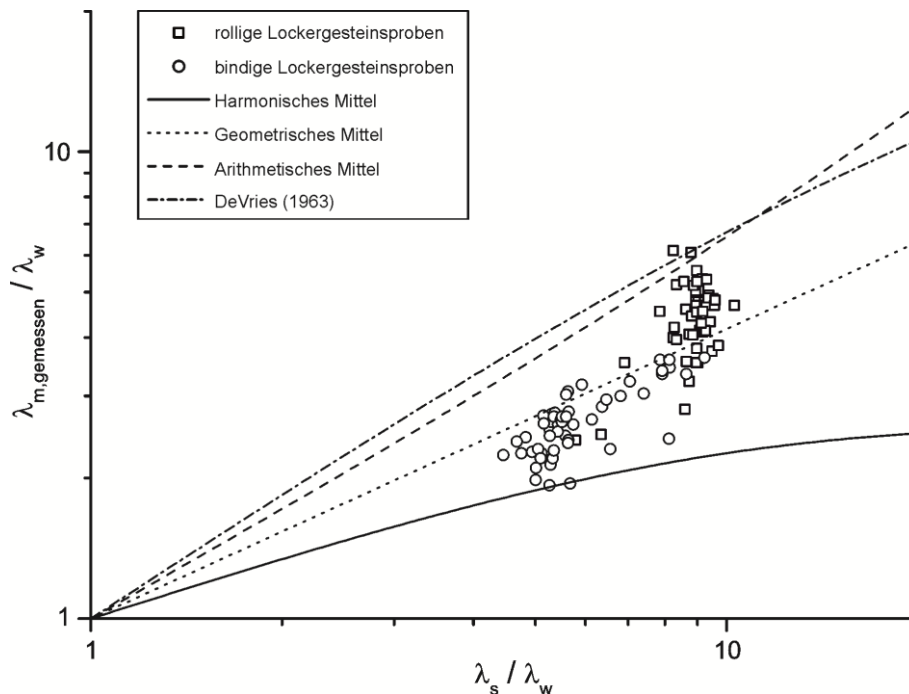

Abbildung 2-2: Lage der gemessenen Werte für bindige und rollige Lockergesteinsproben im Vergleich zu verschiedenen theoretischen Berechnungsmethoden bei einer Porosität von 0,38.

Abbildung 2-3 zeigt einen getrennten Vergleich von den an rolligen bzw. bindigen Lockergesteinsproben gemessenen Wärmeleitfähigkeiten und den mit dem geometrischen Mittel berechneten Wärmeleitfähigkeiten. Zur Einschätzung der Abweichungen sind jeweils die Linien für eine Abweichung von ±20 % des Messwertes dargestellt. Die als Fehlerbalken gezeigten Ungenauigkeiten ergeben sich aus der Abschätzung der Porosität des Materials mit den entsprechenden Schwankungsbereichen nach Tabelle 2-2.
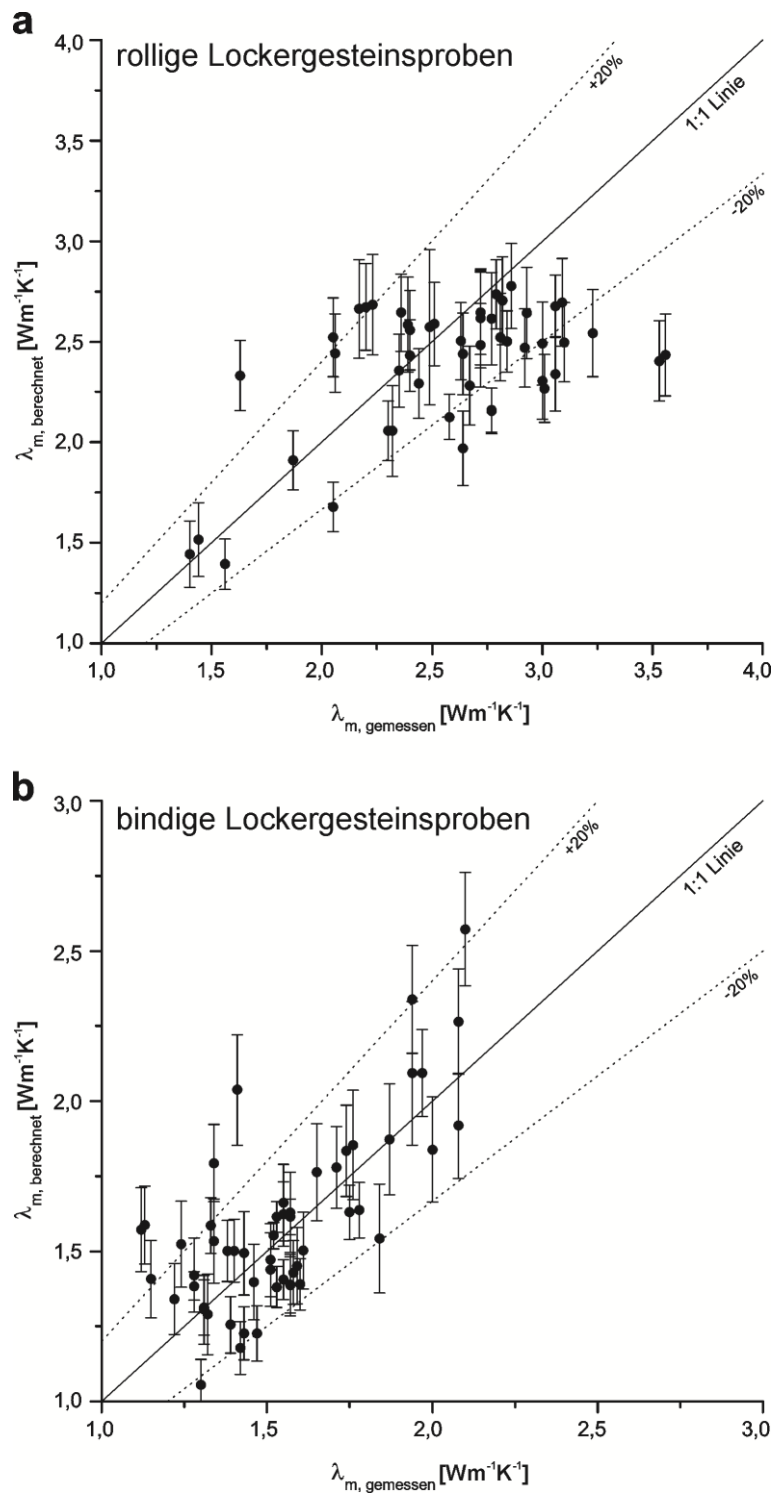
Abbildung 2-3: Vergleich zwischen den mit dem geometrischen Mittel berechneten und den an den rolligen (a) bzw. bindigen Lockergesteinsproben (b) gemessenen Wärmeleitfähigkeiten. Die Fehlerbalken stellen die Unsicherheit dar, die sich durch den Schwankungsbereich der abgeschätzten Porosität ergibt.

Beim Vergleich der Wärmeleitfähigkeiten, λ_m, der rolligen Lockergesteinsproben zeigen sich teilweise große Abweichungen zwischen den gemessenen Werten und den mit dem geometrischen Mittel errechneten Werten. Die mittlere Abweichung beträgt 0,3 $Wm^{-1}K^{-1}$ bzw. 13 % des Messwertes. Einzelne berechnete Werte erreichen immerhin Abweichungen von bis zu 44 % des gemessenen Wertes. Zu hohe berechnete Wärmeleitfähigkeiten ergeben sich vor allem für Proben, die fast ausschließlich aus grobem Material, d. h. mittel- bis grobkörnigem Kies, bestehen. Für diese grobkörnigen Proben wurde eine mineralogische Zusammensetzung angenommen, die von Quarz dominiert wird. Und die sehr gute Wärmeleitfähigkeit von Quarz schlägt sich in der ermittelten Wärmeleitfähigkeit des reinen Feststoffes λ_s nieder. Außerdem leidet wegen der vergleichsweise schlechten Probenoberfläche bei den grobkörnigen Proben die Messgenauigkeit. Durch den ungünstigeren Kontakt der Messsonde mit dem Probenmaterial wird der Einfluss des Wassers auf das Messergebnis größer, was zu niedrigeren Messwerten führt.

Neben den überschätzten finden sich ebenso Proben unterhalb der 20 %-Abweichungslinie, das heißt, bei diesen Proben ist das gemessene λ_m deutlich höher ist als das berechnete λ_m. Diese Proben weisen einen hohen Anteil an feinkörnigem Material auf, der mit niedrigeren Wärmeleitfähigkeiten in die Berechnung von λ_s eingeht. Dies könnte ein Indiz dafür sein, dass der Einfluss der feinkörnigen Bestandteile auf die Wärmeleitfähigkeit eines eher groben Materials mit der hier angewendeten Berechnungsmethode möglicherweise überschätzt wird.

Die Abweichungen zwischen berechneten und gemessenen λ_m der bindigen Lockergesteinsproben sind geringer als die der rolligen Lockergesteinsproben (Abbildung 2-3b). Im Mittel betragen die Abweichungen hier nur 0,18 $Wm^{-1}K^{-1}$ bzw. 11 % des Messwertes. Eine Ursache für die Abweichung bei den bindigen Lockergesteinsproben ist, dass das geometrische Mittel nur ein Zweistoffsystem aus Feststoff und Wasser berücksichtigt. Die bindigen Lockergesteinsproben der hauptsächlich tonigen und schluffigen Schichten waren jedoch bei Messung der Wärmeleitfähigkeit in ihrem natürlichen Zustand nicht vollständig gesättigt. Große Abweichungen vom Mittelwert ergeben sich bei einigen Proben durch zu hohe berechnete Wärmeleitfähigkeiten. Diese Proben verfügen über einen vergleichsweise hohen Anteil an sandigem Material, sodass sich hier wieder der Einfluss der hohen Wärmeleitfähigkeit von reinem Quarz auf die Berechnung mithilfe von λ_s zeigt.

Für 13 Proben wurde die Berechnung der Wärmeleitfähigkeit mit dem geometrischen Mittel auf Grundlage von gemessenen Porositäten und den mithilfe der XRD-Analyse bestimmten mineralogischen Zusammensetzungen durchgeführt. Diese wurden dann zur Validierung mit den (im vorherigen Abschnitt) berechneten Wärmeleitfähigkeiten verglichen, bei denen Porositäten und die mineralogischen Zusammensetzungen abgeschätzt wurden. Für 8 Proben konnten die Wärmeleitfähigkeiten mit Abweichungen $< 0,1$ Wm^{-1}K^{-1} bestätigt werden. Bei den anderen 5 Proben mit Unterschieden von bis zu $0,8$ Wm^{-1}K^{-1} weicht die abgeschätzte Porosität bzw. Mineralogie stark von den gemessenen Werten ab, was durch die sehr heterogene Geologie im Untersuchungsgebiet erklärbar ist. Zudem ist die Bestimmung der Porosität mittels Stechzylinder mit einer gewissen Unsicherheit behaftet, da es z. B. schon während der Probennahme zu einer Beeinflussung der Porosität durch das Einbringen des Stechzylinders in das Probenmaterial kommt.

Die Berechnung der Wärmeleitfähigkeit des porösen Mediums mit dem geometrischen Mittel (Gl. 2−3) wurde für alle Proben mit den im Labor durch XRD-Analyse bestimmten mineralogischen Zusammensetzungen (und den abgeschätzten Porositäten) wiederholt. Die Einbeziehung dieser Daten in die Berechnung führt jedoch beim Vergleich mit den im Labor gemessenen Wärmeleitfähigkeiten zu keiner Verbesserung der Ergebnisse. Bei den bindigen Lockergesteinsproben nimmt die mittlere Abweichung zwischen den berechneten und gemessenen Wärmeleitfähigkeiten um 1 % ab, bei den rolligen Lockergesteinsproben vergrößert sich die Abweichung sogar um 4 %. Bei diesem Vergleich muss berücksichtigt werden, dass die Bestimmung der Mineralogie nur semiquantitativ erfolgte. Da die Abweichungen gering sind, liefert die Abschätzung der mineralogischen Zusammensetzung folglich zufriedenstellende Ergebnisse. Im Vergleich dazu waren die Abweichungen bei der Validierung mit den gemessenen Porositäten deutlich höher. Dies zeigt, dass die Porosität der entscheidende Parameter ist und dass folglich deren Abschätzung zu größeren Abweichungen führen kann.

2.5.4   Abschätzung der Wärmeleitfähigkeit aus Literaturwerten

Zusätzlich zu der Berechnung der Wärmeleitfähigkeit des porösen Mediums mit dem geometrischen Mittel wurde auch noch eine theoretische Abschätzung der Wärmeleitfähigkeit im Untergrund anhand von Literaturwerten durchgeführt. Dazu wurden die Mittelwerte für die angetroffenen Sedimente aus der VDI-Richtlinie 4640 (2010) gewählt und das gewichtete arithmetische Mittel der Wärmeleitfähigkeiten der einzelnen Schichten über die gesamte

Bohrlochlänge gebildet. Aufgrund des Ruhewasserspiegels von 17 m u. GOK wurden zuerst von 0–17 m die trockenen, von 17–80 m die gesättigten Werte verwendet. Auf diese Weise ergibt sich für die gesamte Bohrlochlänge eine mittlere Wärmeleitfähigkeit von 1,6 $Wm^{-1}K^{-1}$. Werden statt der trockenen Werte für den obersten Bereich (0–17 m) ebenfalls die Wärmeleitfähigkeiten für gesättigtes Lockergestein angenommen, ergibt sich eine mittlere Wärmeleitfähigkeit von 1,9 $Wm^{-1}K^{-1}$.

2.5.5 Thermal-Response-Test

In Abbildung 2-4 ist die mittlere Temperatur des in den beiden U-Rohren zirkulierenden Fluids über die logarithmische Zeitdauer des Versuches dargestellt. Zur Ermittlung der effektiven Wärmeleitfähigkeit und des Bohrlochwiderstandes wurde der Temperaturverlauf von 48 Stunden nach Heizbeginn bis zum Heizende nach 115 Stunden betrachtet. Anhand der Steigung in diesem Bereich wurde nach Gleichung 2−7 eine effektive Wärmeleitfähigkeit über die gesamte Bohrlochlänge von 2,4 $Wm^{-1}K^{-1}$ und ein Bohrlochwiderstand von 0,08 mKW^{-1} ermittelt.
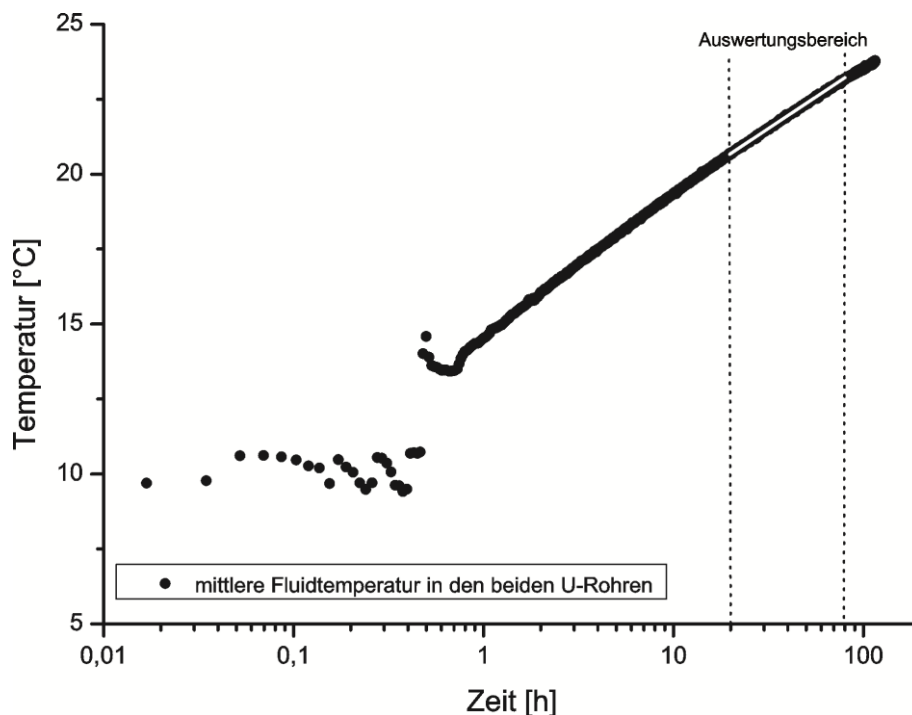

Abbildung 2-4: Verlauf der Fluidtemperatur und Auswertungsbereich des Thermal-Response-Tests.

2.6 Fazit

Eindeutige Korrelationen zwischen der im Labor gemessenen Wärmeleitfähigkeit und bestimmten Gesteinseigenschaften sind an natürlichen, sehr unterschiedlich zusammengesetzten Proben kaum erkennbar. Die einzeln bestimmbaren Einflüsse der Gesteinseigenschaften überlagern sich in den einzelnen Proben zu einer effektiven Wärmeleitfähigkeit. Auch der sonst so groß eingeschätzte Einfluss des Wassergehaltes ist in den Ergebnissen nicht quantitativ sichtbar. Dagegen erwies sich der Gehalt an organischem Material als signifikant. Die negative Korrelation mit der gemessen Wärmeleitfähigkeit von −0,7 und sollte daher bei der Berechnung der Wärmeleitfähigkeit einbezogen werden.

Die Ergebnisse der Bestimmung der Wärmeleitfähigkeit mit den unterschiedlichen Methoden sind in Tabelle 2-5 gegenübergestellt. Die Ergebnisse der Labormessungen, aus der Abschätzung anhand der Literaturwerte und der Berechnung der Wärmeleitfähigkeit (des porösen Mediums mit der Gewichtung der Festphase und des gesättigten Porenraumes über das geometrische Mittel) sind jeweils über die gesamte Bohrlochlänge arithmetisch gemittelt und mit der Mächtigkeit der einzelnen Schichten gewichtet worden, um sie direkt mit den Ergebnissen des TRT vergleichen zu können.

Tabelle 2-5: Übersicht der Ergebnisse der über die gesamte Bohrlochlänge arithmetisch gemittelten Wärmeleitfähigkeit. Die angegebenen Wertebereiche beziehen sich auf die Schwankungsbereiche der VDI 4640 (2010), bzw. die Messgenauigkeit im Labor, die Ungenauigkeiten bei der Berechnung und verschiedene Auswertungsmethoden des TRT.

Verfahren	Wärmeleitfähigkeit [Wm^{-1}K^{-1}] (Mittelwert)
Abschätzung nach VDI 4640 (trockene und gesättigte Bereiche)	1,2 – 2,6 (1,6)
Abschätzung nach VDI 4640 (alle Bereiche gesättigt)	1,4 – 3,0 (1,9)
Labormessungen	1,8 – 2,2 (2,0)
Berechnung der einzelnen Wärmeleitfähigkeiten λ_m nach dem geometrischem Mittel (Gl. 2−3)	2,0 – 2,3 (2,1)
Thermal Response Test	2,3 - 2,4 (2,4)

Die im Vergleich niedrigsten Wärmeleitfähigkeiten ergeben sich durch die Abschätzung mit Literaturwerten aus der *VDI 4640* (2010). Für den wahrscheinlichsten Fall einer Teilsättigung der Lockergesteine im obersten Bereich liegt die mittlere Wärmeleitfähigkeit über die gesamte Bohrlochlänge demnach zwischen 1,6 und 1,9 $Wm^{-1}K^{-1}$. Die Ergebnisse dieser Abschätzung sind damit 0,4–0,1 $Wm^{-1}K^{-1}$ niedriger als die Messergebnisse im Labor und sogar um 0,8–0,5 $Wm^{-1}K^{-1}$ niedriger als die durch den TRT ermittelte Wärmeleitfähigkeit. Die Abschätzung mit den Literaturwerten aus der *VDI 4640* (2010) würde in beiden Fällen zu einer deutlichen Unterschätzung der Wärmeleitfähigkeit im Untergrund führen und als Konsequenz davon z. B. zu einer Überdimensionierung einer EWS-Anlage.

Die Ergebnisse des TRTs stellen in diesem Vergleich die höchsten Werte für die Wärmeleitfähigkeit dar. Dies ist auf einen zusätzlichen konvektiven Anteil des Wärmetransportes in den grundwasserführenden Schichten zurückzuführen, der nur mit dieser Methode erfasst wird. Dazu kommt noch eine gewisse Temperaturabhängigkeit. Beim TRT wird die Wärmeleitfähigkeit bei 25–30°C bestimmt, was dazu führen kann, dass sie unter Umständen um 0,3–0,5 $Wm^{-1}K^{-1}$ größer ist als bei 10°C. Dieser Effekt ist vor allem im ungesättigten Bereich und bei niedrigen Wassergehalten zu erwarten (*Wagner,* 1991).

Die Ergebnisse der Bestimmung der Wärmeleitfähigkeit im Labor ergeben einen Wert, der zwischen diesen beiden eben genannten Methoden liegt. Konvektive Einflüsse werden im Labor nicht berücksichtigt, jedoch gehen die genauen Wassergehalte der einzelnen Schichten in die Berechnung mit ein. Die in dieser Studie ermittelten Abweichungen zwischen Laborergebnissen und dem Ergebnis des TRT befinden sich in der gleichen Größenordnung wie in den Untersuchungen von *Homuth et al.* (2008).

Von den in dieser Studie betrachteten Möglichkeiten zur rechnerischen Bestimmung der Wärmeleitfähigkeit führte die Berechnung der Wärmeleitfähigkeit des porösen Mediums (λ_m) mit der Gewichtung der Festphase und des gesättigten Porenraumes über das geometrische Mittel zur besten Übereinstimmung mit den gemessenen Wärmeleitfähigkeiten. Der gemittelte Gesamtwert der mit dieser Methode berechneten Wärmeleitfähigkeiten, dem die Modellannahme einer zufälligen Verteilung der Komponenten zugrunde liegt, weicht um 0,1 $Wm^{-1}K^{-1}$ von den im Labor gemessenen Werten ab. Dabei muss auch die Genauigkeit der Labormessung von ±10 % berücksichtigt werden. Die Unsicherheiten bei der Berechnung ergeben sich nicht nur durch die Vereinfachungen in den Modellen an sich, sondern vor allem durch die Abschätzung der Porosität (und des Mineralbestandes) des Materials. Durch die Validierung

der Berechnungsmethode mit gemessenen Porositäten und Mineralbeständen konnte gezeigt werden, dass vor allem die Abschätzung der Porosität entscheidend ist und zu großen Abweichungen führen kann. Beim Mineralbestand ist vor allem die Abschätzung des Quarzgehaltes entscheidend, wie auch schon *Dehner* (2007) bei der Beurteilung von Wärmeleitfähigkeiten von Böden bemerkte. Durch die Berechnung der Wärmeleitfähigkeit von 13 Proben, bei denen alle benötigten Parameter im Labor bestimmt wurden, konnte jedoch gezeigt werden, dass auch die Berechnung anhand von abgeschätzten Parametern in der Mehrheit zu guten Ergebnissen führt. Falls jedoch möglichst genaue Werte für die Wärmeleitfähigkeiten benötigt werden, wären Labormessungen der Wärmeleitfähigkeit einer rechnerischen Bestimmung vorzuziehen.

Bei dem Bau von großen EWS-Anlagen oder EWS-Felder ist die Ausführung von umfangreichen Laboranalysen oder von Thermal-Response-Tests zur genauen Bestimmung der Untergrundparameter für eine optimale Auslegung sicherlich sinnvoll. Für die Auslegung kleiner EWS-Anlagen hingegen, z. B. bei Anlagen für Einfamilienhäuser, ist die Durchführung eines Thermal-Response-Tests meist unrentabel. Hier kann mithilfe einer Berechnung der Wärmeleitfähigkeit mit etwas Mehraufwand (z. B. Bestimmung der Porosität, des Karbonatgehaltes und des Anteils an organischem Material) eine deutlich genauere Abschätzung der Untergrundparameter erreicht werden, als beispielsweise mit einer Abschätzung nach der VDI-Richtlinie 4640. Die Wahl des Verfahrens zur Bestimmung der Wärmeleitfähigkeit sollte sich somit immer nach den Anforderungen, der Zielsetzung des Vorhabens und dem vorhandenen Datenmaterial richten.

Danksagung

3 Subsurface urban heat islands in German cities

Abstract

Little is known about the intensity and extension of subsurface urban heat islands (UHI), and the individual role of the driving factors has not been revealed either. In this study, we compare groundwater temperatures in shallow aquifers beneath six German cities of different size (Berlin, Munich, Cologne, Frankfurt, Karlsruhe and Darmstadt). It is revealed that hotspots of up to +20 K often exist, which stem from very local heat sources, such as insufficiently insulated power plants, landfills or open geothermal systems. When visualizing the regional conditions in isotherm maps, mostly a concentric picture is found with the highest temperatures in the city centers. This reflects the long-term accumulation of thermal energy over several centuries and the interplay of various factors, particularly in heat loss from basements, elevated ground surface temperatures (GST) and subsurface infrastructure. As a primary indicator to quantify and compare large-scale UHI intensity the 10–90%-quantile range $UHII_{10-90}$ of the temperature distribution is introduced. The latter reveals, in comparison to annual atmospheric UHI intensities, an even more pronounced heating of the shallow subsurface.

Graphical abstract
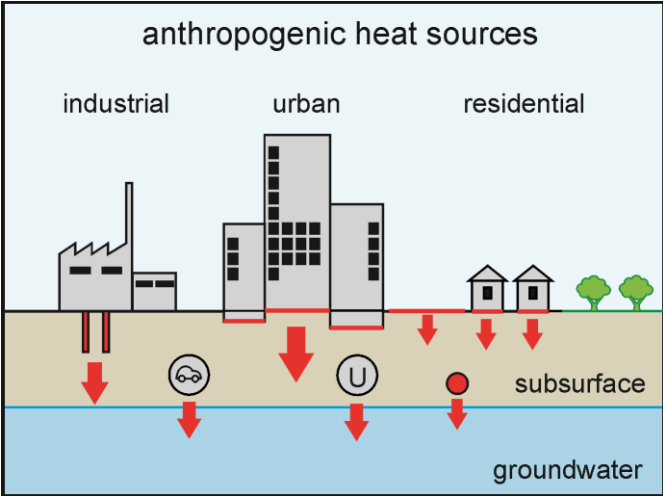
3.1 Introduction

The phenomenon of urban heat islands (UHI) in the atmosphere is widely known and has been a focus of environmental research for several decades (*Landsberg,* 1956; *Kratzer,* 1956). UHI formation is caused by the manifold changes in cities due to urbanization, such as artificial surface cover and anthropogenic heat loss. These factors cause changes in the atmospheric radiation balance and the urban energy balance, which leads to an urban microclimate and more specifically, to the warming of air temperature (*Landsberg,* 1981; *Oke,* 1988). *Oke* (1973) defined the maximum difference in surface air temperature (SAT) between the urban city center and the rural area as the urban heat island intensity (UHII). The latter is the highest in clear and windless summer nights and can reach values of up to 12 K. He also demonstrates a positive correlation between UHII and city population. *Wienert & Kuttler* (2005) suggested a relationship between UHII, the geographical latitude and accordingly, the primary energy use of the city. However, *Landsberg* (1981) pointed out that the UHI effect represents a heterogeneous and site-specific sum of many microclimatic changes. As a consequence, the overall effect can only be inadequately described by a single parameter.

In the subsurface, the temperature (subsurface temperature, SST) is mainly governed by the heat flow from the Earth's interior and the ground surface temperature (GST) (*Huang et al.,* 2009). Variation in GST propagates into the subsurface mainly by thermal diffusion. Especially close to the ground surface, additional local factors may influence the thermal regime, such as advective heat transport from interaction of aquifers with surface water, and any type of direct anthropogenic stimulation (*Molina-Giraldo et al.,* 2011a; *Saar,* 2011).Many studies used vertical borehole temperature profiles to examine palaeoclimate conditions or to back-track recent climate changes (*Birch,* 1948; *Lachenbruch & Marshall*, 1986; *Pollack et al.,* 1998; *Bodri & Cermak*, 1997; *Kohl,* 1998; *Huang et al.,* 2000; *Beltrami et al.,* 2002). *Taniguchi* (1993) analyzed temperature-depth profiles for detecting regional groundwater flow systems. Alterations of surface covers also influence the SST and the measured temperature profiles (*Taylor & Stefan*, 2009). For example, increases in soil temperature of several degrees after deforestation were found by *Taniguchi et al.* (1999a) and *Nitoui & Beltrami* (2005).

In the urban subsurface environment, the temperature regime is more complex than in rural, less disturbed environments. Similar to the UHI in the atmosphere, urbanization leads to a warming of the subsurface environment (*Taniguchi et al.,* 2007), and the observed thermal

conditions are always revealed to be specific. Increased SSTs in fast growing Asian megacities are well documented by numerous studies (e.g. *Taniguchi & Uemura*, 2005; *Taniguchi et al.,* 2009). Others scrutinized the UHI effect in the subsurface of Northern American cities (e.g. *Changnon,* 1999; *Ferguson & Woodbury*, 2007), and elevated SST are reported from several large European cities. *Yalcin & Yetemen* (2009) inspected shallow soil temperatures at different points in time in two districts of Istanbul. It was revealed that temperatures rise by 3.5 K in built-up areas. However, shallow soil temperature varies seasonally following GST oscillation, and thus fixed-time measurements are not representative for an annual average temperature. In London, *Headon et al.* (2009) identified regional temperature differences of up to 5 K. However, this temperature anomaly is apparently triggered by variations in the natural geothermal heat flux. *Zhu et al.* (2010) investigated the spatial distribution of groundwater temperatures below Cologne, Germany, with the highest temperatures under the city center. Similar to the experience from Asian megacities and in North America, intensified vertical heat flux due to urbanization was suspected the main reason.

The factors and processes that cause the subsurface urban warming are not yet comprehensively understood. *Taniguchi et al.* (2007) and *Huang et al.* (2009) explored the relationship between SST and SAT. However, the temperature anomalies in the subsurface cannot be explained only by the increase of urban air temperatures. *Ferguson & Woodbury* (2004) calculated the heat loss from non-insulated buildings in an urban area. This effect is only noticeable within hundred meters from the heated structure. Thus, it cannot fully explain the vast regional increase in SST. In addition, the urban subsurface environment is influenced by a vast amount of other anthropogenic structures, such as subway networks or injections of thermal wastewater, which were not considered in previous studies.

The objective of this study is to evaluate the spatial distribution of groundwater temperatures (GWT) under several German cities, to find commonalities and differences, and to identify the main influencing factors that stimulate warming of urban aquifers. As most investigations of UHIs in the subsurface were conducted in Asian megacities, the question remains if extensive warming of GWT is a phenomenon characteristic mainly for fast growing cities with a large population, or if also smaller cities with nearly constant populations and a different history share similar thermal features. In contrast to related work on borehole climatology that uses subsurface temperature to assess the effects of climate change, this study focuses on the present state and potential sources of subsurface warming in urban areas.

The present study carefully analyzes the GWT beneath six German cities with different population numbers in order to detect the diverse anthropogenic and natural heat sources. While most previous studies focused on individual factors, we consider the interplay of various potential heat sources. For the evaluation of the UHI effect in the subsurface specific city characteristics, such as population and population density are correlated against the UHII and the spatial relationship between GWT and SAT is examined. In the following, first the cities are introduced with special focus on the geological conditions, and the utilized temperature information is shown. Then the thermal subsurface conditions and the dominant urban heat sources are compared for the different cases. This is complemented by contrasting the subsurface conditions with the above ground UHI in two selected cities, Karlsruhe and Berlin.

3.2 Material and methods

3.2.1 Study areas

The locations of the studied German cities are shown in Figure 3-1. In Table 3-1 various data are listed providing an overview on the studied cities and showing available geographical, hydrogeological and statistical information.

Figure 3-1: Geographical locations of the studied German cities.

In order to cover a certain range of different population numbers, the selected cities include both large cities with more than one million inhabitants, as well as smaller cities with a population of less than half a million people (Table 3-1).All cities have a moderate climate and share a similar urban design, with densely built-up city centers, suburban/residential areas

and separated industrial areas. Furthermore, below all studied cities, shallow aquifers are present that are prone to be heated by intensified downward heat fluxes. In the following, the hydrogeological and geological conditions for each city are explained in more detail. Then the findings from case-specific temperature measurements and spatial analyses are reported.

Table 3-1: Characteristics of the studied German cities. The annual mean SAT values are given for the time period 1961-1990. The hydrogeological parameters refer to the topmost aquifer, where the temperature measurements were conducted. v_a is the groundwater flow velocity. The denoted range accounts for the heterogeneity of the aquifer materials. Temperature measurements were preferably done at an equal depth. Due to data availability in some cities, a certain depth interval was chosen.

	Berlin	Munich	Cologne	Frankfurt	Karlsruhe	Darmstadt
Geogr. coordinates[a]	52°31' N 13°24' E	48°08' N 11°34' E	50°56' N 6°57' E	50°07' N 8°41' E	49°00' N 8°24' E	49°52' N 8°39' E
Mean altitude[a] [m asl]	75	518	53	112	115	144
Population[a]	3,442,675	1,330,440	998,105	679,664	291,959	143,332
Pop. density[a] [# km^{-2}]	3861	4282	2463	2737	1683	1174
Total area[a] [km^2]	891.5	310.7	405.2	248.3	173.5	122.1
Annual mean SAT [°C]	8.9	9.2	10.0	10.1	10.7	10.2
Shallow aquifer material	Gravel, sand, silt, clay, till[b]	Gravel, sand[d]	Gravel, sand[e]	Limestone, clay, marl, sand[f]	Sand, gravel[g]	Crystalline rock, sand, gravel[i]
Average v_a [md^{-1}]	0.03-1.4[c]	10-15[d]	ca. 1.0[e]	0.1-1.0[f]	0.5-3.5[h]	8.6×10^{-4}-0.9[h]
Number of observation wells	123	492	52	27	82	16
Investigated area [km^2]	835.9	278.6	119.3	27.2	75.1	25.7
Measurement density [wells km^{-2}]	0.1	1.8	0.4	1.0	1.1	0.6
Measurement depth [m bgl]	20	2-20	15	20	9-12	20-25

[a] *Federal Statistical Office (Destatis)* (2012). [b] *Hannappel & Limberg* (2007). [c]Calculated with values from *SenStadtUm* (2012). [d] *Seiler* (1979) and *Zosseder* (2007). [e] *Zhu et al.* (2010). [f] *Kümmerle & Seidenschwann* (2009). [g] *Geyer & Gwinner* (2011). [h] calculated with values from *Schäfer et al.* (2007) and *Geyer & Gwinner* (2011). [i] *Beier* (2008).

3.2.2   Geology and hydrogeology

3.2.2.1   Berlin

The capital city of Berlin is situated in the Northeast German Basin. The shallow subsurface down to a depth of 250 m is composed of Quaternary and Tertiary glacial and fluvial sediments. The glacial valley with mainly sandy deposits separates the Barnim-Plateau in the North from the Teltow-Plateau, which both are primarily built up of marly till. Due to the heterogeneous character of the sediments, several confined and unconfined aquifers can be found below the city of Berlin. The groundwater level varies between 1 and 10 m below the surface in the glacial valley and up to 40 m below the surface in the plateau areas (*Hannappel & Limberg*, 2007).

3.2.2.2   Munich

The geological and hydrogeological settings of the Munich area are comprehensively described by *Kerl et al.* (2012). Munich is built on Tertiary sedimentary deposits of the Southern German Molasse Basin, which consist of alterations of alluvial sand and silt–clay with varying contents of carbonate. These are overlain by an extensive glacial gravel and cobble plain with a thickness between 2 and 20 m. The plain contains a shallow unconfined porous aquifer with high hydraulic conductivities between 5.0×10^{-4} and 5.0×10^{-1} ms^{-1} (*Seiler,* 1979). Underneath in the tertiary sediments several confined aquifers are present. The groundwater flow direction is generally to the North, with minor variations near to the river Isar. The level of the groundwater decreases from around 18 m in the South to about 1m below the surface in the North (*Dohr & Gruban*, 1999).

3.2.2.3   Cologne

The shallow subsurface in Cologne is composed of Quaternary terrace deposits of predominantly gravel and sand. The main unconfined aquifer in these gravels reaches a depth of 30–70 m and is underlain by an aquitard, which is made of clays and soft coals. Our focus is on the western side of the Rhine River. The groundwater level here is between 10 and 15 m under the surface, and the groundwater flow direction is from Southwest to Northeast, in the direction to the Rhine River (*Zhu et al.,* 2010).

3.2.2.4 Frankfurt

The city of Frankfurt is located in the geological transition zone between the Upper Rhine Valley and the Main–Nidda-depression (*Kümmerle & Seidenschwann*, 2009). The formation of the Upper Rhine Valley caused the Tertiary rocks in this area to break up into a mosaic of tectonic blocks. The Tertiary rocks are dominated by Miocene limestones, marls and clays and reach a thickness of >200 m. In the western part of the city area, these sediments are overlain by Pliocene sand deposits with a varying thickness of up to 60 m. In the whole area, the Tertiary sediments are overlain by Quaternary deposits. Confined aquifers (also artesian confined in the western part of the city) exist in the Miocene limestone layers, and a shallow unconfined aquifer is hosted in the Pliocene and Quaternary sands (*Kümmerle & Seidenschwann*, 2009).

3.2.2.5 Karlsruhe

Karlsruhe is situated in the Upper Rhine Graben, a Cenozoic continental rift valley filled with Tertiary and Quaternary sediments. In the study area, the Quaternary sediments are dominated by sands and gravels with minor contents of silt, clay and stones and reach a thickness of around 150 m (*Geyer & Gwinner*, 2011). Due to sporadic layers with lower permeability, up to three aquifer levels can be separated. The water table in the upper unconfined aquifer ranges between 2 and 10 m below ground. The groundwater flow direction is Northwest to the Rhine River.

3.2.2.6 Darmstadt

The city of Darmstadt is located on the Eastern border fault of the Upper Rhine Graben. The subsurface of the Eastern part is composed of Mesozoic sandstones and Palaeozoic crystalline rocks, which contain fractured rock aquifers. The Western part of the city is underlain by Quaternary fluvial deposits of the Upper Rhine Graben, which reach a thickness of up to 100 m in the Southern part and 30 m in the Northern part. The sand and gravel sediments form up to three aquifers with inconsistent interlayers of silt and clay. The groundwater flow direction in this area is from east to west. The level of the water table ranges from 10 to 30 m below the surface in the entire area (*Beier,* 2008).

3.2.3 Spatial analysis

3.2.3.1 Spatial distribution of groundwater temperatures

For the spatial analysis of groundwater temperatures (GWT), mainly pre-existing data of temperature measurements in observation wells are used. Usually, dense networks of wells are maintained by the German city authorities for monitoring the level of water table and the groundwater quality. This large number of monitoring wells enables a regional evaluation of GWT in each of the selected urban as well as surrounding suburban areas. An overview on the number of measured wells and the depth of measurements in the studied cities is given in Table 3-1.

The temperature measurements in Berlin were conducted by the Senate Department for Urban Development and the Environment in 2010 (*SenStadtUm*, 2012). In the city of Munich, temperature data from a measurement campaign in 2009 was used. Measurements of GWT were carried out 1 m below the water table. Accordingly, the depth below the surface varies between about 2 m in the northern parts and 20 m in the southern parts. Due to the annual variation of SAT, shallow GWT in the upper 15 m of the subsurface usually show similar annual variations depending on the thermal diffusivity of the ground (e.g. *Taylor & Stefan*, 2009). Thus, the arithmetic mean of several measurements at different times during one year was used for the present analysis. *Zhu et al.* (2010) explored the spatial distribution of Cologne's GWT in 2009, and the information of their measurement campaign is adopted for the present study. In Frankfurt, the Hessian State Office for Environment and Geology (HLUG) delivered temperature data from 27 wells from 2009. For the examination of groundwater temperatures in Karlsruhe, we use daily temperature data from data loggers installed in 82 monitoring wells, which are operated by the Public Works Service Karlsruhe. Due to the shallow installation depth (9–12 m) of the data loggers the GWT data is again influenced by the annual variations of air temperatures. The arithmetic mean of the seasonal cycle is therefore taken here as it represents the annual mean GWT. In Darmstadt, the GWT was measured during a study on urban hydrochemistry performed by *Beier* (2008). These measurements were conducted with depths ranging between 5 and 25 m, and so, only 16 wells with a depth of at least 20 m were selected for the present study.

To visualize the GWT spatially, the temperature data is interpolated using kriging in GIS (ESRI® ArcInfo™ 10.0). The method is described in detail by *Kitanidis* (1997). We use

a K-Bessel model for the semi-variogram analysis and optimize the model parameters by cross validation.

3.2.3.2 Urban heat sources

Potential natural and anthropogenic heat sources in the urban subsurface environment are manifold. Previous studies have discussed increased GST and heated basements as potential causes for increased SST (*Taylor & Stefan*, 2009; *Taniguchi et al.,* 2007; *Ferguson & Woodbury*, 2004). However, there are other urban constructions in the subsurface that can act as heat sources, because they are seasonally or permanently warmer than the surrounding subsurface, such as road and subway tunnels, sewage systems, and buried district heating networks. In addition, shallow groundwater is often utilized for cooling in industrial processes and re-injected several degrees warmer into the aquifer (Fig. 2). Likewise, the shallow subsurface in many cities is used thermally by geothermal energy systems, such as ground source heat pump systems (*Blum et al.,* 2011), aquifer thermal energy storage applications or energy piles (*Brandl,* 2006).

In this study, we offer a qualitative analysis of these potential heat sources by comparing the isotherm maps with land-use plans, town plan maps, positions of district heating networks, underground railway systems and locations of thermal wastewater injections.

3.2.3.3 Influencing factors for subsurface urban heat islands

City characteristics, such as population and population density, correlate, to some extent, with local concentration of certain urban heat sources, like basements and sewers. Thus, they could be used as simple surrogates for density of buildings and infrastructures, assuming that the urbanization development in the different cities is similar. A comparable approach was used by *Taniguchi* (2006), who employed the exponential decrease in population density with the distance from the city center as a proxy for the change in air temperature. Population density data is available for the individual districts of the studied cities covering urban, suburban and rural areas. However, industrial areas and inner-city green spaces are disregarded in this data. Nevertheless, we would expect a relation between the city characteristics and the magnitude of subsurface warming. To test this hypothesis, we correlate the spatial distribution of population densities within the studied cities with the spatial distribution of GWT. In addition, we correlate the GWT with the spatial distribution of mean annual SAT in the city of Berlin. SAT are also strongly influenced by urbanization effects and are closely linked to

GST, which are assumed to be a major driver for the warming of GWT (*Taniguchi et al.,* 2007; *Huang et al.,* 2009).

In atmospheric science, the magnitude of the UHI is usually described as a temperature difference between urban and rural areas by the UHI Intensity (UHII) (*Oke,* 1973). In accordance with this atmospheric UHII, a method to quantify the UHII in the subsurface is needed to enable a comparison. For the calculation of the atmospheric UHII most studies use temperature data from single points (e.g. weather stations, meteorological observatories, etc.) (e.g. *Landsberg,* 1956; *Oke,* 1973; *Landsberg,* 1981; *Kim & Baik*, 2004). However, in the subsurface, single point measurements are not very applicable for calculating UHII. GWT and SST measurements at single points can yield extremely high or low temperature values if they are in the vicinity of a local heat source (Figure 3-1) or heat sink (e.g. reinjection of cool water from a groundwater heat pump system). Due to the slow heat conduction in the subsurface compared to heat advection in the air, heat accumulates locally near permanent heat sources or sinks in the subsurface. As a consequence, a high density network of measurement points is required to capture local extremes, but commonly the number of boreholes or observation wells is limited.
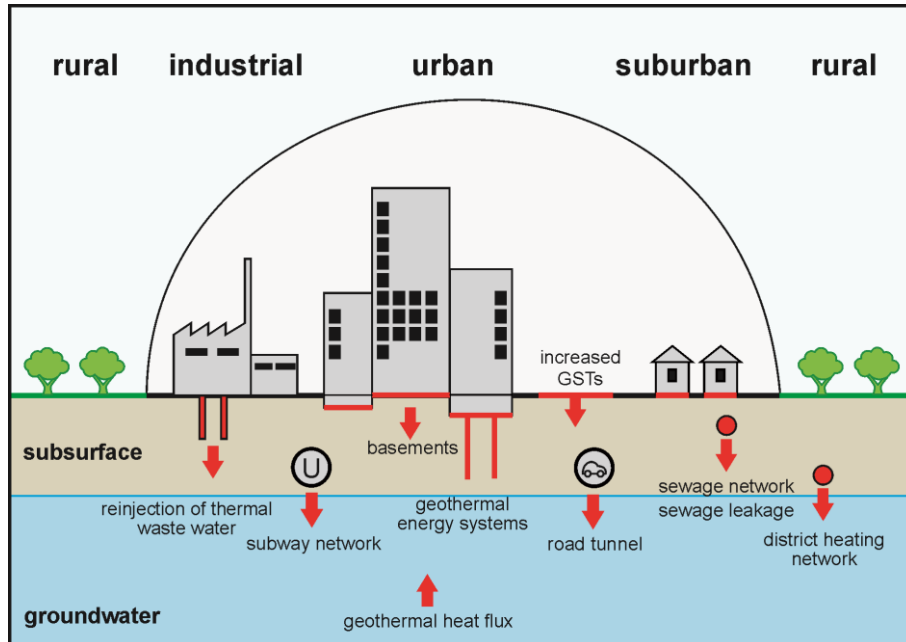

Figure 3-2: Potential anthropogenic and natural heat sources in urban areas.

Since temperature in the ground is more heterogeneous than above ground and balancing heat anomalies from local heat or cold sources is a comparably slow process, the standard indicator of intensity is not expressive for this environment. Values for UHIIs that reflect only extreme local temperatures hardly represent a robust regional parameter. As an alternative to the maximum temperature, we introduce as measure for subsurface UHII, an inner quantile range, $UHII_{10-90}$, of the temperature distribution that cuts the extremes. The cumulative temperature distribution can be plotted as city-specific characteristic curve by pixel-based interpolation between measurement points. We then extract the values of the 10%- and 90%-quantiles and calculate their difference to quantify the UHII in the subsurface. The impact of observed very local heat anomalies is therefore mitigated, while they are still reflected in the cumulative curves. In principle, the $UHII_{100}$ of the subsurface is equivalently determined like the atmospheric UHII or surface urban heat island intensity (SUHII), respectively. Commonly, however, atmospheric UHII or SUHII is not interpolated over the city area. Only few studies provide a 2-dimensional thermal characterization, for instance, based on satellite data (*Schwarz et al.,* 2011; *Peng et al.,* 2012; *Schwarz,* 2012) or model results (*Balázs et al.,* 2009).

3.3 Results and discussion

3.3.1 Spatial distribution of groundwater temperatures

Figure 3-3 shows the results of the GWT measurements as interpolated annual mean isotherm maps for Berlin, Munich, Cologne and Karlsruhe. Due to the low number of sampled wells with no seasonal noise in Frankfurt and Darmstadt, contour maps are considered too speculative. Hence, only single data points are shown. In all six cities, the spatial distribution of the GWT is very variable with a clear warming trend towards the inner cities. In all studied areas, the lowest temperatures of 8–11 °C were measured in the rural parts, mostly under forests or agricultural land. "Cold" locations, for example, are found in the south-eastern part of Berlin and the south of Munich. Apparently, direct anthropogenic impact on the GWT is minimal in these regions, and the observed temperatures are interpreted as a proxy for undisturbed background conditions. In the shallow subsurface in each region these resemble the annual average SAT (Table 3-1).
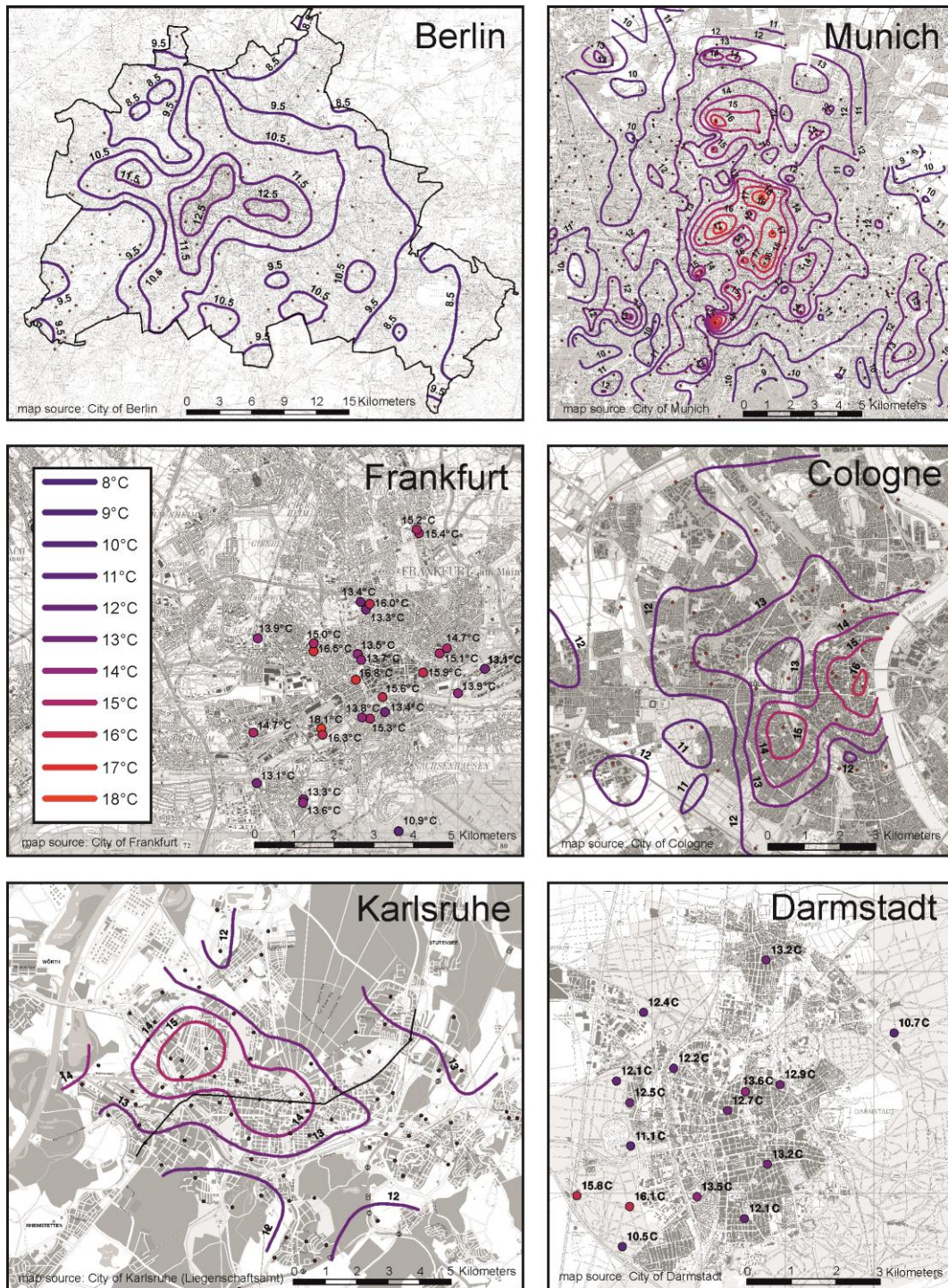
Figure 3-3: Isotherm maps of groundwater temperatures (GWT) in the studied German cities, including locations of observation wells. The measurement depths in the individual cities are listed in Table 3-1. The black line on the map of Karlsruhe indicates the profile section in Figure 3-5.

In suburban and residential areas, the GWT is slightly higher than the background value. The same applies to inner-city green spaces, such as parks or conditions found in airport areas. In almost all cities, the highest GWT of 13–18°C are detected close to the city centers, which are usually the oldest and most densely built-up urban areas. However, the relatively small cities of Karlsruhe and Darmstadt are exceptions. Highest temperatures are found in industrial areas and outside the city, respectively, where known local heat sources are present (Figure 3-3).

In general, the derived annual mean temperature distribution in the urban subsurface turns out to be heterogeneous, strongly depending on the depth of GWT measurements (Table 3-1). In Berlin and Cologne, where GWT measurements were carried out at 15 and 20 m below the surface, respectively, the obtained spatial distribution of GWT is represented by smooth contours. The same applies to Karlsruhe, where daily GWT measurements were used to calculate the annual mean GWT. In contrast, the interpolated Munich isotherm map indicates a more restless pattern. Main reasons here are the spatial and temporal measurement density. The comparable high density of wells (1.8 wells km^{-2}) with often slightly distinct temperature values next to each other strongly influences the visualization and interpolation. Here, especially the shallow GWT measurements in the upper meters (entire range 2–20 m) of the subsurface appear strongly influenced by local heat sources. Aside from this, the annual mean GWT in the shallow subsurface was interpolated from a few measurements during the year, and the non-uniform contours may also be affected by non-resolved seasonal variability.

3.3.2 Urban heat sources

When discussing potential heat sources, which could cause urban temperature anomalies, one must distinguish between natural and anthropogenic temperature variations. Natural causes for GWT fluctuations are, for example, spatial variability in the geothermal heat flux or the existence of local groundwater recharge and discharge zones, as identified in several cities in Japan (*Taniguchi & Uemura*, 2005; *Taniguchi et al.,* 2005). According to the geological and hydrogeological settings, potential variability of the natural background geothermal regime can be neglected in Berlin, Munich, Cologne and Karlsruhe. The cities of Frankfurt and Darmstadt are both partially located on the main border fault of the Upper Rhine Graben. Thus, in both cities spatial differences in the geothermal heat flux and the upwelling of thermal water are likely to influence the spatial distribution of the GWT (*Beier,* 2008; *Seithel,*

2010; *Schmid,* 2010). In Frankfurt, some wells with unusually high GWT correlate with the zone of tectonic disaggregation in vicinity to the main border fault. The identified potential natural and anthropogenic heat sources in all studied cities are depicted in Figure 3-4.
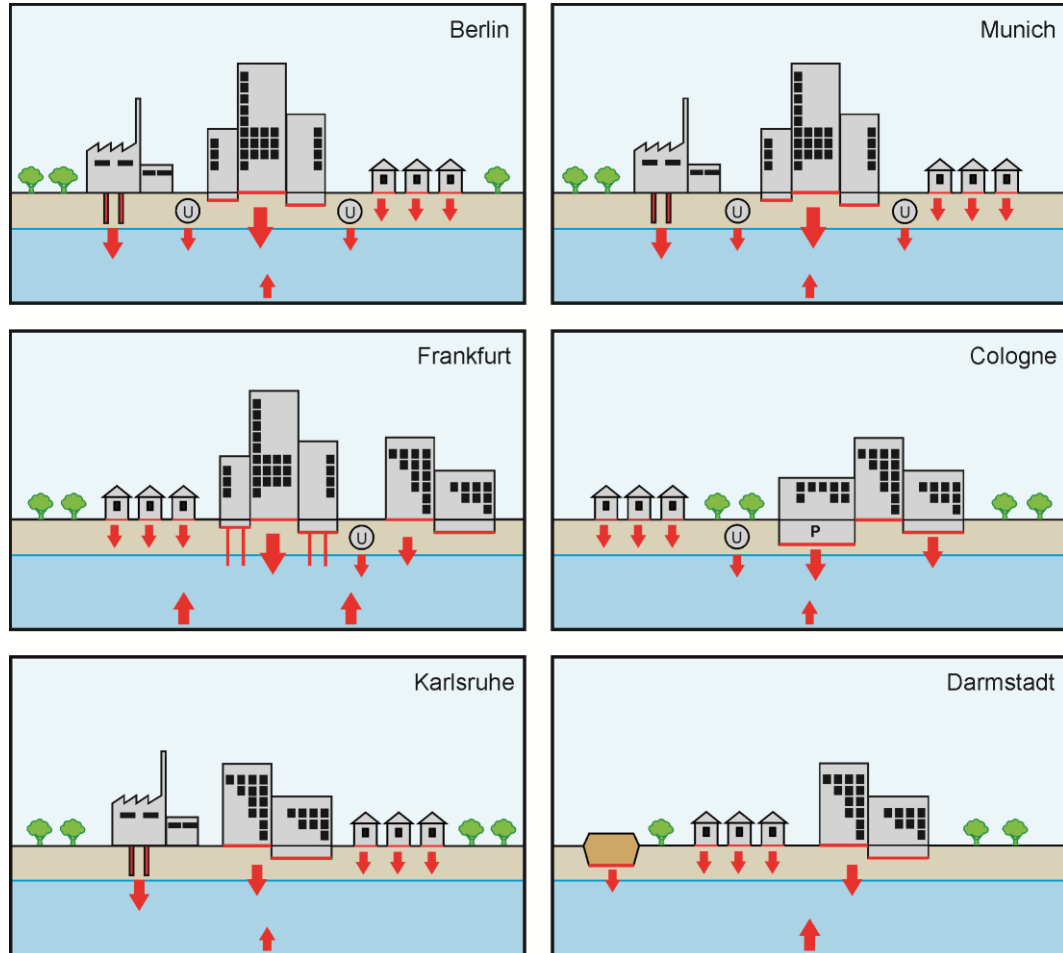

Figure 3-4: Schematic drawing of the identified dominant anthropogenic and natural heat sources in the subsurface of the studied German cities. The thicknesses of the arrows indicate the strength of the heat source.

In all cases, the city center exhibits the absolute (Berlin, Munich, Cologne, Frankfurt) or in some cases a local (Karlsruhe, Darmstadt) GWT maximum. Simultaneously, this is usually the area with the highest density of buildings (and therefore also basements), underground car parks and with the highest percentage of sealed surface cover. *Kottmeier et al.* (2007) showed that there is a direct link between the percentage of sealed surfaces and increasing GST using the example of Berlin. As the density of basements and the percentage of sealed surfaces decrease in suburban and residential areas, so does the GWT. This observation supports the hypothesis that basements and increased GST are dominant heat sources in urban areas. This is

also consistent with findings from related studies by *Ferguson & Woodbury* (2004) and *Taylor & Stefan* (2009).

Some of the local heat anomalies in the cities of Berlin, Munich and Karlsruhe are correlated to industrial areas and especially to combined heat and power stations. In the presence of shallow aquifers, groundwater is often used for cooling purposes and then re-injected into the aquifer at a temperature of up to 20°C, which is the recommended maximum temperature in Germany (*Hähnlein et al.,* 2010). In areas with several reinjections of thermal wastewater, widespread shallow thermally affected zones can develop (e.g. *Lo Russo et al.,* 2012). In the examined cities, installations of geothermal energy systems are also widespread and used for both heating and cooling purposes. Especially in Frankfurt, a great part of the large office buildings in the city center are equipped with energy piles used for cooling (Figure 3-4).

Another potential heat source is the infiltration of warm stream water into urban aquifers as discussed for Switzerland by *Kiefer* (2011) in the area of Zurich, and for the city of Basel by *Epting & Huggenberger* (2012). In the city of Karlsruhe, one shallow observation well next to the Rhine River is clearly influenced by the stream water, as it shows high GWT (Figure 3-3), which follows a seasonal trend. In Munich, infiltration of stream water from the Isar River takes place in some shallow parts of the aquifer. As influences of cold and warm water infiltration throughout the year counteract with each other, only a minor effect on the annual mean GWT can be seen. In the other cities no such effects could be observed, because large-scale infiltrating streams do not exist (Darmstadt, Berlin) and/or because measurements are not in adequate distance of the river.

Another potential heat source in the urban subsurface is the subway system. *Ampofo et al.* (2004) monitored tunnel and station temperatures in London, which were higher than ambient temperatures by several degrees. In addition, they calculated the heat loss from the subway train system in London and concluded that only 70% of the heat is dissipated by the ventilation. The rest is conducted to the subsurface. Four of the studied cities have differently constructed subway systems (Figure 3-4), so it is most likely that some part of the heat in the subsurface of these cities emerges from the subway systems. A considerable influence of the subway system on the GWT was found in Munich by *Dohr* (1989), who measured GWT along the tunnels during the construction works of the subway system. However, due to the coarser distribution of measured wells in this study, we were not able to localize effects of the subway system on GWT.

The same applies to other anthropogenic structures in the subsurface, such as high-voltage cables, district heating networks and sewage systems. Although high-voltage cables and the pipes of the district-heating network are usually insulated, there is still a certain loss of energy in the form of heat from these networks (*Rink*, pers. comm.), which is conducted into the subsurface. The average temperature of the domestic wastewater circulating in the sewage system is likely to be higher than the ambient subsurface temperature. This also stimulates conductive heat loss from the sewage system. *Hötzl & Makurat* (1981) calculated a mixing temperature of wastewater for the entire sewage system, including domestic and industrial wastewater, of 20°C for the city of Karlsruhe. Even if the heat loss from these linear structures might be minor, these heat sources are omnipresent in the urban subsurface and therefore might contribute to the UHI effect. However, their local effect on the GWT is difficult to detect.

A very special anthropogenic heat source, which influences the local GWT, was identified in the city of Darmstadt. The high temperatures in the southwest, outside the city, are measured in wells close to a landfill site (Figure 3-3). Exothermic degradation processes can lead to a warming of landfill bodies of up to 60°C (*Krümpelbeck,* 2000) and thus to a warming of the surrounding subsurface. Another example for a very local, but nevertheless quite significant heat source was found in Frankfurt, where measurements in an observation well showed temperatures of nearly 20°C, which were first thought to be caused by upwelling thermal water. Rapidly decreasing temperatures with increasing depth revealed a different heat source. The observation well is located down gradient to a heated public swimming pool, which was not insulated at the bottom. More common heat sources that cause local GWT to rise extremely are power plants. In the city of Frankfurt, several shallow observation wells revealed GWT > 30 °C in depths between 6 and 20 m. All wells are located in the down-gradient vicinity of a coal-burning power plant.

Finally, we examined the influence of elevated SAT in urban areas on the GWT by comparing both temperatures in Karlsruhe and Berlin. In Karlsruhe, the comparison is made along a cross section through the city (Figure 3-3, Figure 3-5). The SAT was measured on a tram on over 2000 trips along the line in the year 2011 (*Rinke et al.,* 2010). The mean annual SAT in the inner-city center in Karlsruhe is about 1 K higher than in the suburbs and 1.8 K higher than in the rural areas. The maximum annual GWT along this line is at the same location, yet the GWT are continuously 3–4 K higher than the SAT. The dots in Figure 3-5 repre-

sent the wells in the vicinity to the profile section, from which the interpolated GWT was calculated. Despite being measured at similar depths between 9 and 12 m below the surface, they show very dissimilar magnitudes of seasonal temperature variability, which cannot be explained only by the variation of measurement depth. The composition of the sedimentary deposits and the groundwater level also show only minor variations along the profile section. Thus, it can be assumed that local factors and infrastructure in the urban environment additionally influence the local heat flux into the subsurface.
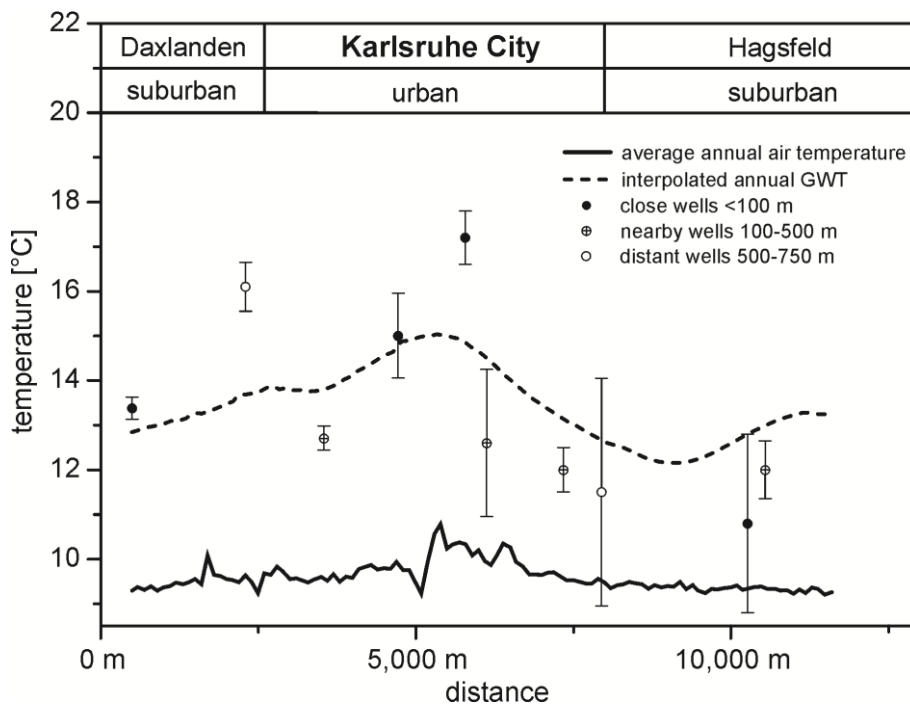

Figure 3-5: Relationship between the mean annual SAT and annual GWT along a profile section through the city center of Karlsruhe and two suburbs. The error bars indicate the annual variation of GWT. The origin of the profile lies in the Southwest of Karlsruhe and the end point in the Northeast of the city (Figure 3-3).

3.3.3 Correlation between influencing factors and subsurface urban heat islands

Spatial correlation of GWT and population density is quantified by correlation coefficients for the studied cities (Table 3-2). When calculated for the whole city area, the coefficients, γ, indicate only small correlations for the larger cities and no correlation for the small city of Karlsruhe. Apparently, population density only is not a good proxy for elevated GWT. Locally specific heat sources dominate the GWT distribution and several elements in the urban environment cannot be captured. Commercial and industrial areas, for instance, only

share naturally low population densities, but often exhibit high GWT stimulated by heat loss from buildings, basements, deep parking lots, focused reinjection of thermal wastewater, etc. Furthermore, population density here is given as average value for city districts, that is, at much less resolution than the interpolated thermal conditions. Local features can therefore hardly be correlated, such as inner-city green spaces with typically low temperature, which are in central districts with high population density.

In a modified correlation analysis, such areas were clipped out of the raster dataset containing the GWT and population density (Table 3-2). The resulting partial correlation coefficients, γ', are considerably higher. Significant correlations between 0.6 and 0.8 can be found in the cities of Berlin, Munich and Cologne. Depending on the city the excluded area accounts for 10–16% of the whole area. However, the correlation analysis is constrained by the relative spatial resolution of the given population density data. This particularly affects the results for smaller cities, such as Karlsruhe, with only a few districts. This is listed in Table 3-2 by the ratio between the individual district areas and the whole city area.

Table 3-2: Pearson's correlation coefficients γ with an uncertainty of 5% between groundwater temperature and population density (spatially defined for the city districts) for the studied German cities.

City	Correlation between GWT and population density			Ratio between district area/ city area
	γ total area	γ' without parks and industrial areas	Excluded area [γ']	
Berlin	0.60 ± 0.005	0.76 ± 0.005	12%	0.01
Munich	0.54 ± 0.01	0.63 ± 0.005	10%	0.01
Cologne	0.61 ± 0.01	0.72 ± 0.005	16%	0.01
Karlsruhe	0.33 ± 0.005	0.52 ± 0.01	14%	0.03

In Berlin spatially resolved SAT data is available from the Urban and Environmental Information System (ISU) of the Senate Department for Urban Development and the Environment (*SenStadtUm*, 2012) as annual mean from 1961 to 1990. For this period, SAT data from multiple observation stations is extrapolated to the whole area of Berlin and compared to local land use in Figure 3-6. In the rural areas, SAT and GWT are comparable. In some rural places, GWT is up to 0.5–1 K higher than SAT due to the difference in thermal diffusivity of air and ground materials, as well as a consequence of meteorological effects (e.g. snow cover and solar irradiation) (e.g. *Putnam & Chapman*, 1996; *Smerdon et al.,* 2006; *Taylor & Stefan*,

2009). Both mean GWT and SAT are the highest in the city center of Berlin, but the maximum GWT is higher than the maximum SAT. The annual SAT covers a range of about 3 K for the area of Berlin; in contrast, the GWT varies by about 4 K. Thus, as observed for Karlsruhe in Figure 3-5, the UHI in the subsurface is more pronounced than the UHI of annual mean SAT in the atmosphere. A spatial comparison of both temperature datasets for the whole Berlin area yields a correlation coefficient of 0.71. This correlation suggests that there is a close link between the SAT and GWT development in urban areas. Similar conclusions were drawn for several large Asian cities such as Tokyo, Osaka, Seoul and Bangkok by *Taniguchi et al.* (2007).
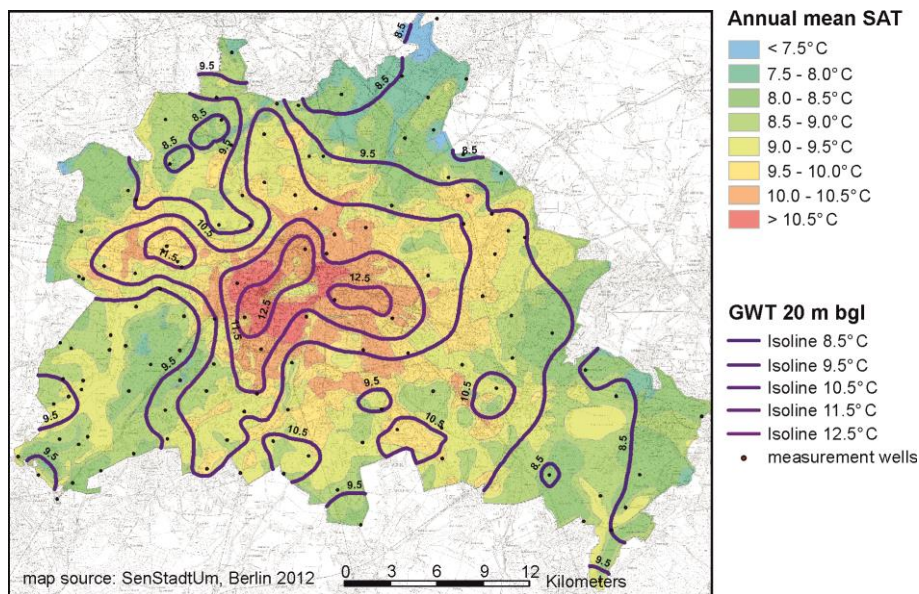

Figure 3-6: Comparison of the annual mean SAT (1961–1990) and the GWT 20 m below surface in Berlin. The method of SAT data acquisition is described in detail by SenStadtUm (2012). Data source for the annual mean SAT is the Urban and Environmental Information System (ISU) of the Senate Department for Urban Development and the Environment, Berlin.

Figure 3-7 shows the cumulative GWT distribution over the investigated area for those four studied cities, where a 2-dimensional interpolation of GWT data was possible (Figure 3-3). The difference between the 90%- and 10%-quantiles yields the following values for the UHII$_{10-90}$: Berlin 2.4 K, Munich, 2.4 K, Cologne 2.1 K and Karlsruhe 1.9 K. Though the number of investigated cities is rather small, a certain tendency in the subsurface UHII is obvious. Elevation of GWT increases with both population and average population density (Table 3-1). Berlin and Munich provide the same subsurface UHII, as Berlin has the larger

population and Munich the higher population density. As discussed above, both parameters have a strong influence on the alteration of GWT.
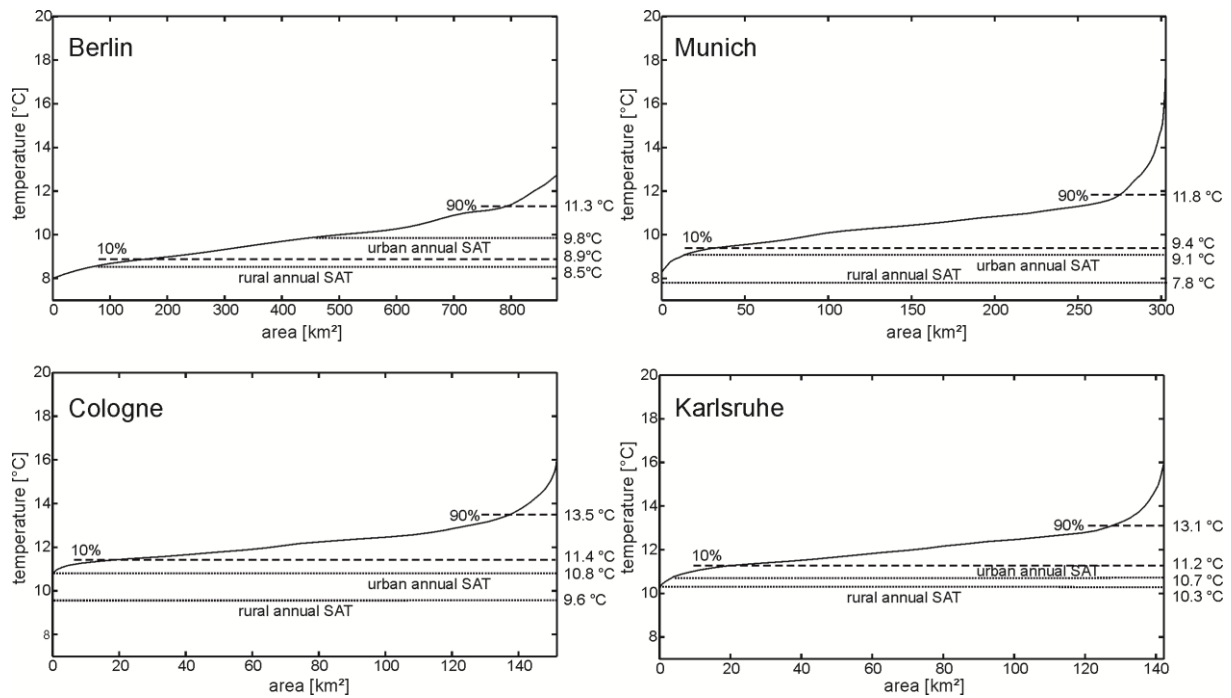

Figure 3-7: Cumulative groundwater temperature curves over the investigated area for four studied cities. The investigated area is delimited by the distribution of the observation wells in Figure 3-3. In each graph, the 10%- and 90%-quantiles for the temperature distribution are displayed as dashed lines. The dotted lines represent the rural and urban mean annual SAT respectively.

Examination of the form of the cumulative temperature curves in Figure 3-7 confirms that the interval between the 90%- and 10%-quantiles demarcates a mostly linear section of the curves. Extremely positive or negative local GWT anomalies in the investigated areas control the neglected marginal upward and downward parts. The UHII$_{10-90}$ accordingly reveals to be an appropriate indicator of regional subsurface UHII. It is less biased by the spatial resolution and accuracy of the measured and interpolated temperatures than that of measured extremes. This becomes obvious by the temperatures peaks (i.e. denoting UHII$_{100}$) of the individual graphs in Figure 3-7. The cumulative GWT curve for Berlin follows a rather constant rise, whereas a sharp peak for high GWT characterizes the conditions of Munich. In Munich, an average number of 1.8 wells km^{-2} was available, in Berlin only 0.1 wells km^{-2} was inspected.

To enable a comparison to the atmospheric UHII values, the annual urban and rural SAT (from meteorological observatories) are also displayed in Figure 3-7. As explained above, comparability between the UHIIs is restricted due to the different calculation procedures. However, comparison shows that GWT are almost always higher than SAT. Atmospheric annual mean UHII from the single SAT values are 0.4–1.8 K and thus substantially smaller than subsurface UHII with 1.9–2.4 K. Both observations are already apparent in Figure 3-5 and Figure 3-6 for the cities Karlsruhe and Berlin.

3.4 Conclusions

We examined the shallow groundwater temperatures (GWT) under six German cities and found pronounced positive temperature anomalies. The regional differences in GWT between urban and rural areas range from 3 to 7 K. Shallow GWT in rural areas correspond to the annual SAT, which causes the GWT in Cologne, Karlsruhe and Darmstadt to be generally higher than in Berlin or Munich. The maximum temperature elevation in large cities, such as Berlin, Munich, and Cologne, is typically close to or in the city center. In Karlsruhe and Darmstadt, the highest GWT were found in industrial areas and close to landfill sites, respectively. The temperature distribution under the urban areas is generally rather heterogeneous. Especially in Munich due to the shallow measurement depth and the high density of observed wells, the isotherm map reveals plenty of local hot spots. Accordingly, the heat input into the urban subsurface is likely to be controlled by many local and site-specific parameters. At the same time, it is difficult to differentiate between the individual heat sources causing the warming of GWT found at local measurement wells. A spatial comparison of SAT and GWT in Karlsruhe and Berlin showed that both parameters are closely linked, and similar processes control the evolution above and belowground surface. As higher GWT occur in more densely built-up areas, one can suspect that buildings/basements and increased GST act as dominant heat sources. These heat sources also affect a large part of the urban area. For the subsurface, additional factors, such as sewage networks, high-voltage cables and district heating networks might also be important. Other heat sources such as reinjections of thermal wastewater affect the GWT only very locally, but often causing local temperature anomalies of high magnitude. In summary, it can be stated that the superposition of various heat sources results in an extensive groundwater temperature increase by several degrees in the long-term.

In order to evaluate the regional magnitude of urban GWT warming, we developed an inner-quantile based method to calculate the subsurface urban heat island intensity, $UHII_{10-90}$. The values of the subsurface UHII cover a range from 1.9 to 2.4 K, with an increasing trend that depends on city population and average population density. In comparison to the atmospheric UHII, warming of the subsurface is more pronounced. This finding is also supported by the spatial comparison of SAT and GWT in Karlsruhe and Berlin. Furthermore, the shown spatial correlation between the GWT and the population density supports the hypothesis of increased GST, buildings/basements and subsurface infrastructure as important urban heat sources. Their individual roles and long-term heat contribution, however, appear to be controlled by many site-specific aspects, and can therefore only be quantified by a more detailed case study.

Acknowledgments

4 Long-term evolution of anthropogenic heat fluxes into a subsurface urban heat island

Abstract

Anthropogenic alterations in urban areas influence the thermal environment causing elevated atmospheric and subsurface temperatures. The subsurface urban heat island effect is observed in several cities. Often shallow urban aquifers exist with thermal anomalies that spread laterally and vertically, resulting in the long-term accumulation of heat. In this study, we develop an analytical heat flux model to investigate possible drivers such as increased ground surface temperatures (GST) at artificial surfaces and heat losses from basements of buildings, sewage systems, subsurface district heating networks, and reinjection of thermal wastewater. By modeling the anthropogenic heat flux into the subsurface of the city of Karlsruhe, Germany, in 1977 and 2011, we evaluate long-term trends in the heat flux processes. It is revealed that elevated GST and heat loss from basements are dominant factors in the heat anomalies. The average total urban heat flux into the shallow aquifer in Karlsruhe was found to be $\sim$759 $\pm$ 89 mWm^{-2} in 1977 and 786 $\pm$ 131 mWm^{-2} in 2011, which represents an annual energy gain of around 1.5×10^{15} J. However, the amount of thermal energy originating from the individual heat flux processes has changed significantly over the past three decades.

Graphical abstract
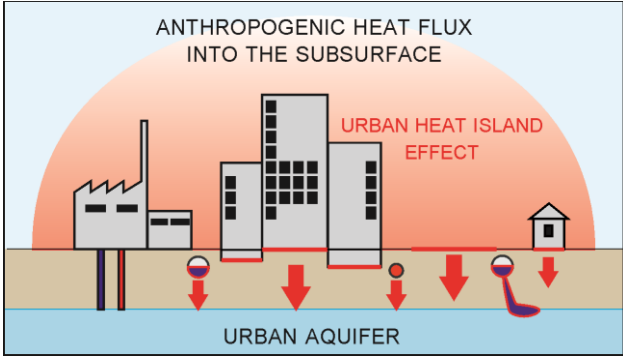
4.1 Introduction

Increasing temperatures due to anthropogenic alteration in urban areas are not solely found in the atmospheric environment [urban heat island effect (UHI)] (*Oke,* 1973; *Landsberg,* 1981; *Arnfield,* 2003; *Schwarz et al.,* 2011; *Peng et al.,* 2012; *Schwarz,* 2012). Also in the subsurface, human activities lead to significant and extensive warming, which causes urban aquifer temperatures to increase by several degrees (*Changnon,* 1999; *Taniguchi et al.,* 2007; *Ferguson & Woodbury*, 2007; *Zhu et al.,* 2010, *Menberg et al.,* 2013b). *Oke* (1988) gives a review of the studies that investigated the diverse processes and factors that lead to atmospheric UHI formation by examination of the urban energy balance. These efforts resulted in the development of various schemes for the quantification of urban heat fluxes into the atmosphere (i.e., upward) such as anthropogenic heat flux (*Ichinose et al.,* 1999; *Flanner,* 2009) and into the subsurface (i.e., downward) such as soil and ground heat flux (*Mirzaei & Haghighat*, 2010; *Roberts et al.,* 2006). The latter is thereby usually incorporated in the urban heat storage term and often calculated as the residual from the radiation balance at the surface (*Roberts et al.,* 2006; *Rigo & Parlow*, 2007). Others developed analytical and numerical solutions to calculate the ground heat flux based on temperature or surface heat flux measurements (*Wang & Bras*, 1999; *Bennett et al.,* 2008; *Wang & Bou-Zeid*, 2012). Average measured and simulated values for monthly ground heat fluxes in urban areas were found to vary between −10 and 20 Wm^{-2}, depending on the location and month of examination (*Wang & Bras*, 1999; *Wang & Bou-Zeid*, 2012).

However, because of the complexity and heterogeneity of the urban environment, studies of ground heat flux yield only data with either spatially (e.g., remote sensed data) (*Rigo & Parlow*, 2007) or temporally high resolution (e.g., time series at single measurement points) (*Herb et al.,* 2008). Another limitation of the commonly used atmospheric models concerning ground heat flux is their lower boundary condition. As discussed, for example, by *Baker & Baker* (2002) and *Kollet et al.* (2009), the assumption of an adiabatic or fixed temperature boundary in the shallow subsurface (<10 m) seems unrealistic and can lead to substantial biases in long-term simulation of subsurface temperature and ground heat flux. *Stevens et al.* (2007) showed that especially subsurface heat storage can be underestimated by up to 75%, if the bottom boundary condition is placed insufficiently deep, leading to significant errors in future climate projections (*MacDougall et al.,* 2008).

The changes in subsurface temperatures due to variations in ground surface temperature (GST) are also used for past climate reconstructions (*Bodri & Cermak*, 1995; *Pollack et al.,* 1998). A common approach is to obtain GST histories and the corresponding ground surface heat flux histories by mathematical inversion of deep borehole temperatures (*Huang et al.,* 2000; *Beltrami*, 2002b). *Beltrami et al.* (2006) derived spatial patterns of heat gain in the subsurface of the Northern Hemisphere with a mean surface heat flux of ~21 mWm^{-2} over the past 200 years based on 588 boreholes. Other studies scrutinized the coupling of surface air temperatures (SATs), GSTs, and shallow subsurface temperatures showing that the temperature offset is mainly influenced by surface cover and climate conditions (*Děděcek et al.,* 2012; *Smerdon et al.,* 2003; *Smerdon et al.,* 2004). However, studies of the evolution of urban subsurface temperature and GST are rare (*Yamano et al.,* 2009). *Taniguchi et al.* (2007) found temperature anomalies in the subsurface of four Asian megacities at depths of up to 140 m that correspond to the historic air temperature increase due to urbanization. Especially in built-up areas, solar irradiation of artificial surfaces leads to heterogeneously increased GST and thus ground heat fluxes (*Kottmeier et al.,* 2007). *Taylor & Stefan* (2009) investigated GSTs of different surface types in Minneapolis-St. Paul and found differences of up to 3 K in the annual mean GST between grass and asphalt cover.

The upper boundary of the urban subsurface is formed by not only open ground covered by different surface materials but also basements of buildings. The heat loss from basements or ground floors of single buildings into the ground has been examined for design and thermal comfort purposes (*Thomas & Rees*, 1999; *Emery et al.,* 2007). Various analytical and numerical methods for predicting the seasonal heat loss for individual buildings with specific geometries and different kinds of insulation exist (*Adjali et al.,* 1998; *Rees et al.,* 2000). The applicability of such models to study processes on the urban scale, however, is limited.

In addition to the heat input from above, there are embedded anthropogenic heat sources that emit heat directly in the urban subsurface, like sewage networks, incompletely insulated district heating pipes, or reinjections of thermal wastewater (*Menberg et al.,* 2013b). However, until now, the question of which heat sources contribute what amounts to subsurface urban warming is unresolved. As pointed out by *Taylor & Stefan* (2009) and *Ferguson & Woodbury* (2004), increased GST and heat loss from basements, respectively, cannot cause such extensive and widespread temperature anomalies like those found under most urban areas.

In this study, we focus on the heat input into shallow urban aquifers caused by various anthropogenic heat sources, which we define as the anthropogenic heat flux into the subsurface (AHFs). The objective of this study is therefore to quantify the contribution of the individual heat processes that cause underground urban warming. A novel approach using an analytical heat flux model is developed for the city of Karlsruhe, Germany. To account for the uncertainty of the various input parameters and to identify the most relevant processes and parameters, we perform a Monte Carlo simulation and sensitivity analysis. Using a data set from 1977 and recent measurements from 2011, the long-term evolution of the subsurface urban heat island in Karlsruhe is comprehensively assessed by analyzing all dominant heat flux processes. The heat fluxes from buildings are spatially resolved for both years to also investigate the spatial temperature development.

4.2 Materials and methods

4.2.1 Study area

As a study site, we chose the city of Karlsruhe because the subsurface temperature distribution was intensively investigated in the past and recently (*Menberg et al.,* 2013b, *Hötzl & Makurat*, 1981; *Makurat,* 1980). The study area is shown in Figure 4-1. It is delimited to the built-up area of Karlsruhe, covering urban, suburban, and industrial compartments, as well as inner city green spaces. The city is located in the upper Rhine Valley in southwest Germany, at approximately 49°00′ N and 8°24′ E, at a mean altitude of 115 m above sea level. The total population amounted to 275,828 inhabitants in 1977 and increased to 294,761 in 2011. The shallow subsurface geology in the study area is mainly composed of sand and gravel with minor contents of silt and clay (*Geyer & Gwinner*, 2011). The uppermost aquifer is unconfined and reaches a thickness of up to 30 m. The water level below the surface varies between 3 and 8 m, and the general groundwater flow direction is northwest to the Rhine River (Figure 4-1).

Water level and shallow vertical groundwater temperature (GWT) profiles in 1977 were measured monthly at 142 observation wells by *Makurat* (1980). For 2011, we use daily values of water level and GWT from data loggers installed in 83 wells, which are operated by the Public Works Service Karlsruhe. Although only 41 of the original wells in 1977 could be used for measurements in 2011, both measurement campaigns yield representative regional GWT distributions because of the homogeneous distribution of the wells within the study area

(Figure 4-1). Because of the fixed position of the data loggers in 2011, GWT in 2011 is only available at a depth of 3−4 m below the water table. The difference in GWT at the groundwater surface and 4 m below the surface in the 142 profiles in 1977 was found to be on average −0.1 ± 0.3 K, which is in the same range as the accuracy of the measurement device in 1977 (*Makurat,* 1980). Thus, in 2011, the variability of GWT over this depth is expected to be minor and the temperatures from 3 to 4 m below the water table are adopted to approximate the GWT at the groundwater surface. The spatial distribution of the annual mean of the groundwater level and the GWT is shown in Figure 1 for 1977 and 2011. Also depicted are the locations of all reinjection wells, where cooling water (i.e., warm water injection) from, for example, industrial processes is discharged into the aquifer, and the total discharged energy.
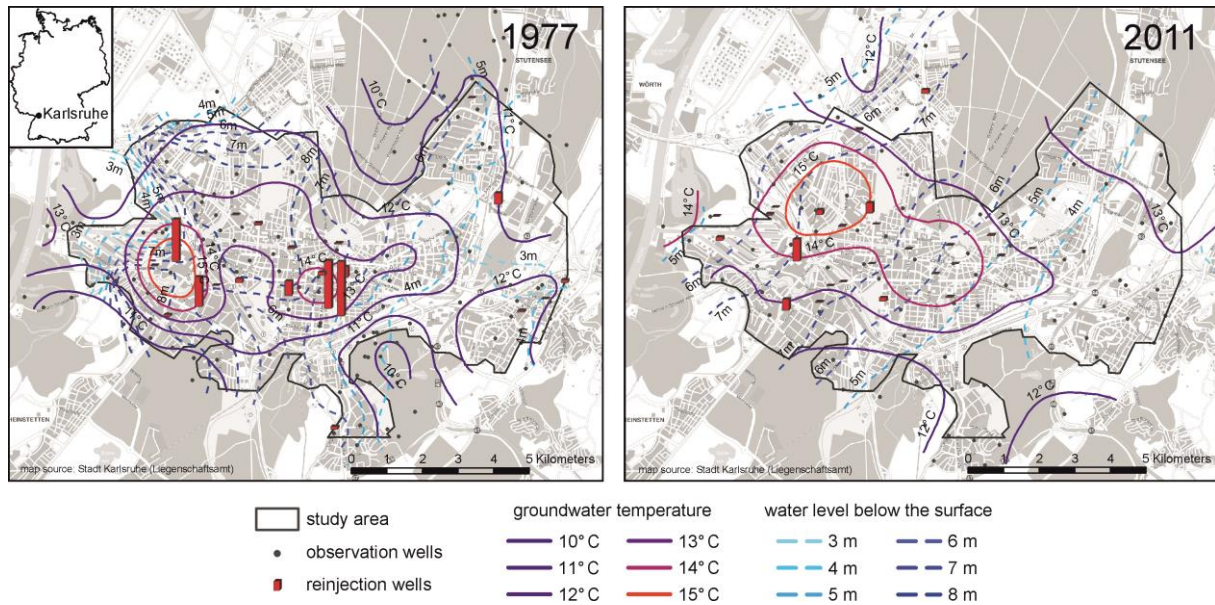
Figure 4-1: Location of the study area with contours of groundwater level and temperature. The groundwater temperature in 1977 was measured at the water surface and in 2011 3−4 m below the water level. The length of the bars indicates the reinjected energy amount per year. The bar in the legend represents ∼0.5 MW. Note that both background images display a map of Karlsruhe in 2010.

In 1977, the highest GWT occurred in industrial areas close to major reinjection sites and in the city center. Compared to those in 1977, background temperatures in 2011 have increased by approximately 1 K, while the maximal GWT is nearly equal at ∼15 °C. However, the area of the thermal anomaly has spread significantly over the past three decades. In some areas, for example, in the northeastern parts, where a large residential area was developed, the GWT increased by even up to 2 K. The long-term development of major climate and ground-

water parameters over the past decades in Karlsruhe is shown in Figure S1 of the Supporting Information. The mean annual SAT at a weather station outside of Karlsruhe was 10.7 °C in 1977 and increased to 11.5 °C in 2011, which is in agreement with the general long-term trend of SAT (*German Weather Service*, 2012) (Figure S 4-1a). This climatic trend is reflected in an increase in GWT in the rural background. The annual precipitation shows a slightly decreasing trend over the past decades (Figure S 4-2b). In contrast, the water level indicates an opposite development of higher water tables. Here, reductions in the size of groundwater withdrawals and the influence of the regional flow system are also important factors.

4.2.2 Heat flux model

To evaluate AHFs, we developed a statistical analytical heat flux model. In this model, vertical heat fluxes from several heat sources through the unsaturated zone to the top of the groundwater body are considered. On the basis of spatial inspection of groundwater temperatures in several cities (*Menberg et al.,* 2013b), six individual heat flux processes q_i (eqs 4−2 - 4−7) are summed up in the annual AHFs analysis (eq.4−1).

$$AHF_s = \sum_{i=1}^{6} q_i$$

(eq.4−1)

All model parameter values are listed in Table 4−1 and illustrated in Figure S 4-2 of the Supporting Information. The ground heat flux in our model is expressed as a heat flux process because of the increased GST and calculated by Fourier's law of heat conduction (eq.4–2) (*Weber,* 2006). We choose the temperature gradient in the unsaturated zone between the ground surface and the water table and apply the heat flux to that part of the study area that is not covered by buildings. The corresponding temperature difference is defined by the local variance between GST and GWT at the groundwater surface.

$$q_1 = \lambda \cdot dT / dz \cdot \left(A - A_b \right) / A$$

(eq. 4−2)

The heat flux from basements of buildings (eq. 4–3) is also calculated based on Fourier's Law and applied to the area covered by buildings. Here, only the heat flux through the basement floor is considered. The heat flux through the basement walls is neglected, because experimental and modeling studies on the heat loss through basements showed that the heat loss through the walls is mainly connected to the atmosphere (*Thomas & Rees*, 1999; *Emery et al.,* 2007). Likewise, the increased heat flux that can be observed at the edges of a basement is primarily upwards directed. Thus, we assume no correction factor for edge effects or build-

ing geometries. The temperature gradient is set between the air temperature inside the basement and the GWT. The thermal conductivity in eq. 4–3 is the integral conductivity of the basement slab and the soil underneath.

$$q_2 = \lambda \cdot (T_b - T_{gw})/(dz - db) \cdot A_b / A \qquad \text{(eq. 4–3)}$$

As Fourier's law only describes conduction, advective heat transport, for example by infiltration, is neglected. Infiltration of surface water in urban areas is assumed to be low because of the high rate of surface sealing (*Liu et al.,* 2011). Thus, vertical advective heat transport in the study area is expected to be rather small. The heat input due to reinjections of thermal waste water is assessed by the energy content of the amount of water and the temperature difference between withdrawal and reinjection:

$$q_3 = c_{pw} \cdot \gamma_w \cdot V_{ri} \cdot (T_{ri} - T_{gw}) / A \qquad \text{(eq. 4–4)}$$

Two heat flux processes are assumed to arise from the sewage system. First, a conductive heat flow from the pipes of the sewage network, which are partly filled with wastewater of a certain temperature and emit heat to some extent upwards as well as downwards:

$$q_4 = \lambda \cdot (T_s - T_{gw})/(dz - ds) \cdot (d_{sd} \cdot \pi \cdot l_{sn}) / A \cdot r_{dhf} \cdot (1 - r_{satm}) \qquad \text{(eq. 4–5)}$$

Additionally, sewage leakage occurs to some degree from all sewage pipes (*Eiswirth,* 2002; *Klinger,* 2007). The energy content of the leaked water is calculated and assumed to partly reach the water table:

$$q_5 = c_{ps} \cdot \gamma_s \cdot V_s \cdot r_l \cdot (T_{ri} - T_{gw}) / A \cdot (1 - r_{latm}) \qquad \text{(eq. 4–6)}$$

As the city of Karlsruhe operates a widespread district heating network, also heat losses from the underground district heating pipes are considered to cause a partly downward directed heat flux:

$$q_6 = P_{ld} \cdot r_{dhf} / A \qquad \text{(eq. 4–7)}$$

The methods for the calculation of the heat fluxes q_3 and q_6 are adopted from *Makurat* (1980). He estimated average heat fluxes in the shallow subsurface mostly based on literature values such as solar irradiation and heat loss from buildings. As a consequence, that approach yields partly unreasonable results when applied for the entire city.

Table 4-1: Assumed parameter range and distribution for the Monte Carlo simulation in 1977 and 2011.

Heat flux process	Parameter	Name	Unit	Year	minimum	mode	maximum	distribution
	λ	Thermal conductivity (unsaturated zone)[a]	$Wm^{-1}K^{-1}$		0.3	1	1.8	triangular
	dT	Temperature difference GST-GWT[b]	K	1977	0	1	5	triangular
				2011	0.8	1.8	5.8	triangular
Increased GSTs	dz	Depth of water table	m					spatial distribution
	A	Study area	km^2		-	61.94	-	constant value
	A_b	Area covered by buildings[c]	Km^2	1977	10.34	10.88	11.43	triangular
				2011	12.37	13.02	13.67	triangular
	T_b	Temperature of basement / ground floor[d]	°C		15	17.5	20	triangular
Buildings	T_{gw}	Groundwater temperature	°C					spatial distribution
	db	Depth of basements	m					spatial distribution
	c_{pw}	Heat capacity of water[e]	$Jkg^{-1}K^{-1}$		-	4,195	-	constant value
	γ_w	Water density[e]	$kg\,m^{-3}$		-	999.8	-	constant value
Reinjection of thermal wastewater	V_{ri}	Volume of reinjected thermal wastewater[f]	m^3a^{-1}	1977	6,408,034	7,209,038	8,010,042	triangular
				2011	3,526,640	3,967,470	4,408,300	triangular
	T_{ri}	Reinjection temperature[f]	°C	1977	20.4	22.7	24.9	triangular
				2011	18	20	22	triangular
	T_s	Sewage temperature[g]	°C		12	18.5	25	triangular
	d_{sd}	Diameter of sewage drains[h]	m		0.1	0.4	2	triangular
	ds	Depth of sewage drains[i]	m		1	2	5	triangular
Sewage network	l_{sn}	Length of sewage network[k]	m	1977	532,000	600,000	665,000	triangular
				2011	770,000	880,000	990,000	triangular
	r_{dhf}	Percentage of downwards directed heat flux	%		25	37.5	50	triangular
	r_{satm}	Percentage of heat flux to atmosphere	%		20	30	40	triangular
	c_{ps}	Heat capacity of wastewater[l]	$Jkg^{-1}K^{-1}$		3,708	4,120	4,532	triangular
	γ_s	Density of wastewater[l]	$kg\,m^{-3}$		990	1,100	1,210	triangular
Sewage leakage	V_s	Annual wastewater volume[g]	m^3a^{-1}	1977	41,259,600	45,844,000	50,428,400	triangular
				2011	33,997,000	35,707,500	37,418,000	triangular
	r_l	Leakage rate[h]	-		0.05	0.15	0.25	triangular
	r_{latm}	Percentage of heat flux to atmosphere	%		20	30	40	triangular
District heating network	P_{ld}	Heat loss from district heating pipes[m]	MW	1977	8.99	9.99	10.99	triangular
				2011	7.99	9.13	10.27	triangular

a: *Menberg et al.* (2013c), *VDI 4640* (2010)
b: *Taylor & Stefan* (2009), *Dědeček et al.* (2012), *German Weather Service* (2012)
c: mode estimated from Google Earth, ± 5%
d: range from *DIN EN ISO 13370* (2008)
e: *Clauser* (2006)
f: 90% of the licensed data: *Makurat* (1980), public works service Karlsruhe, ± 10%
g: *Makurat* (1980), public works service Karlsruhe
h: Data from *Eiswirth et al.* (2002), *Klinger* (2007)
i: *Stadt Karlsruhe* (2010)
k: *Makurat* (1980), *Stadt Karlsruhe* (2010), ± 10%
l: *Makurat (1980)*, ± 10%
m: Data from *Makurat* (1980) and municipal energy supplier Karlsruhe, ± 10%

4.2.3   Monte Carlo simulation

Most of the parameters of the heat flux equations in Table 4−1 cannot be captured with single values for the entire study area, thus parameter ranges are specified. Some parameters, such as groundwater temperature or thermal conductivity of the unsaturated zone, show strong spatial and temporal variability. For other parameters, such as leakage rate or sewage temperature, measured data is not available for the study area, so that the chosen representative literature values carry uncertainty. To consider the entire range of possible input parameters the heat flux is calculated with a Monte Carlo approach with a defined statistical distribution for each parameter. Few parameters can be assessed with a fixed value, such as the size of study area. For the other parameters a triangular distribution was assumed by defining minimum and maximum values, as well as a mode value with the highest probability.

The difference in local GST and GWT, *dT*, is assumed to range between 0 and 5 K. In long-term steady-state examinations mean annual GST and shallow GWT are usually assumed to equal each other (e.g. *Taylor & Stefan*, 2009) with no heat flux occurring into the subsurface. Alteration of the surface cover leads to a change in GST. Changes from vegetated surfaces to bare soil were found to cause an increase in annual mean GST between 0.3-1 K, while concrete and asphalt surfaces show a GST that is 2–5 K higher than at a grass or forest site (*Dědeček et al.,* 2012; *Taylor & Stefan*, 2009). The percentages of different surface types in the study area were estimated based on a land use plan, similar to the approach by *Taylor & Stefan* (2009). According to the land use plan of Karlsruhe, approx. 20% of the study area are covered by buildings and the rest is characterized by different kinds of vegetation (approx. 56%) and artificial surface covers (approx. 24%). Due to this distribution and the fact that the GWT below the urban area is already elevated compared to the undisturbed background the mode value for *dT* is set to 1 K. As the annual mean SAT in 2011 was 0.8 K higher than in 1977 (*German Weather Service*, 2012) this value was added to the triangular distribution, given that GST usually track SAT in long-term trends (*Smerdon et al.,* 2004). For the depth of the water table, the groundwater temperature and the depth of basements, we derived spatially resolved values from an interpolated raster data set in GIS (ESRI® ArcInfo™ 10.0) (Figure 4-1). Thus, the heat flux from buildings can be calculated for each raster pixel by assigning probabilistic values for the parameters that are not spatially known. The number of Monte Carlo iterations is adapted to the number of raster pixels and set to 275,257 runs. A detailed description of the assumed values for the other parameter ranges is given in the Supporting

Information. Finally, a contribution to variance analysis is performed by calculating Spearman's rank correlation coefficients between the total heat flux result and the individual input parameters.

4.3 Results and Discussion

4.3.1 Monte Carlo simulation

The total sum of the median heat fluxes and standard deviations from all considered heat sources is 759 ± 89 mWm^{-2} in 1977 and 786 ± 131 mWm^{-2} in 2011. The results of the Monte Carlo simulation for the individual heat fluxes are displayed in Figure 4-2a. The highest heat fluxes occur from increased GST (1977: 249 ± 245 mWm^{-2}; 2011: 349 ± 280 mWm^{-2}) and from buildings, (1977: 224 ± 440 mWm^{-2}; 2011: 276 ± 481 mWm^{-2}). The rather large standard deviations are resembled by the large ranges covered by the boxplots in Figure 4-2a. They are caused by the wide ranges assessed for the parameters in the heat flux equations (Table 4-1), for details see supporting information), which account for high spatial and temporal variability over the study area. The other simulated processes are of minor relevance, contributing by less than 10% to the total AHF$_s$. The negative heat fluxes from the sewage network can occur when the sewage temperature is lower than the groundwater temperature. Likewise, leakages in sewers can also cause groundwater infiltration into the sewers in places where the pipes are installed below the water table.

In comparison to these determined urban heat fluxes, the natural heat fluxes in the subsurface yield much smaller values. The geothermal heat flux in the area of Karlsruhe is about 80 mWm^{-2} (*Cermak & Rybach*, 1979). A spatial analysis of the ground heat flux in rural areas caused by climate warming yielded values of 25-75 mWm^{-2} for the period 1930-1980 in Middle Europe (*Beltrami et al.,* 2006). These natural background heat fluxes are about ten times lower than the total AHF$_s$, thus, the subsurface heat balance in the urban area in Karlsruhe is obviously dominated by anthropogenic heat sources.
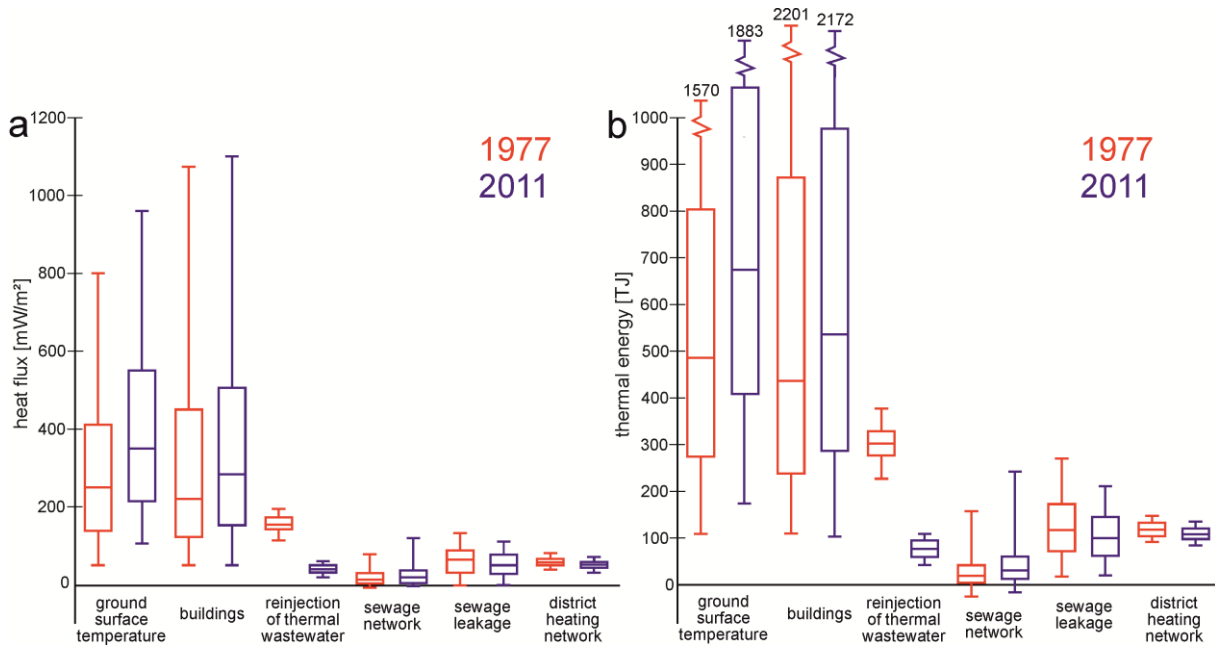
Figure 4-2: Results of the Monte Carlo simulation for 1977 and 2011. a) Boxplots of the individual heat fluxes. b) Thermal energy amount per year for the entire study area caused by the individual heat flux processes (lower end = 5%, upper end = 95% of the entire range).

According to the study of *Flanner* (2009) the atmospheric AHF due to anthropogenic energy use is between 2.5-4.0 Wm^{-2} in southwest Germany, which is about four times higher than the AHF_s calculated in this study. However, the atmospheric AHF value is integrated regionally and contains also rural areas with less anthropogenic heat emissions. Thus, the atmospheric AHF for urban areas alone is likely to be even higher.

Figure 4-2b shows the amount of thermal energy that is discharged into the subsurface by the individual heat flux processes. From this evaluation it becomes obvious that most of the ground heat gain is caused by increased GST (1977: 33%; 2011: 44%). Due to small coverage by buildings in Karlsruhe, influence from buildings is slightly smaller (1977: 30%; 2011: 35%). The spatial distribution of the heat flux from buildings is subsequently discussed. Thermal energy input from reinjections of thermal wastewater (1977: 21%; 2011: 5%), sewage leakage (1977: 8%; 2011: 7%) and from the district heating network (1977: 8%; 2011: 7%) is generally small. However, these processes are constrained to distinct positions, such as reinjection wells or failures in sewage and district heating pipes. Thus, they cause only very local thermal anomalies in the groundwater. Such local heat sources could explain the heterogeneous GWT distribution that is often observed beneath cities (*Taniguchi et al.,* 2007;

Menberg et al., 2013b). In contrast, increased GST as well as buildings influence the subsurface on a larger area and can therefore cause extensive thermal anomalies.

The mean amount of energy discharge accounts for up to $1.48 \times 10^{15} \pm 1.7 \times 10^{14}$ J for 1977 and remains almost equal for 2011 with $1.54 \times 10^{15} \pm 2.6 \times 10^{14}$ J. However, the amount of thermal energy arising from the individual heat flux processes mostly changed within the last three decades. The mean heat input from elevated GST increased by 30% from 4.9×10^{14} J to 6.8×10^{14} J in 2011. This represents a trend that is likely to further continue with future temperature development due to climate change (*IPCC,* 2007).

The heat flux from reinjection of thermal wastewater was relatively high in 1977, but decreased in 2011 due to legal regulations on allowed reinjection temperature and also because of reduction of reinjection volume. Variations in the other heat fluxes are mostly due to changes in specific parameter values (i.e. properties). Heat flux from the sewage network has increased because of the longer sewage network in 2011 that reflects the development of new residential districts in the study area. Despite the longer sewage network, the reduction in wastewater volume leads to a decrease in heat loss by sewage leakage. The trend of decreasing wastewater volume is a prevalent phenomenon in German cities caused by water saving measures. The district heating network in Karlsruhe was likewise expanded to new residential areas; even so the heat loss from the network was reduced by maintenance and insulation actions.

4.3.2 Spatial heat flux from buildings

The heat flux from buildings in Karlsruhe exhibits a considerable spatial heterogeneity (Figure 4-3a, b) with a large range between -100 and >10,000 mWm^{-2}. By comparing spatial heat flux and the contours of water table depth, it becomes obvious that the vertical distance is the dominating factor for the computed temperature gradient.
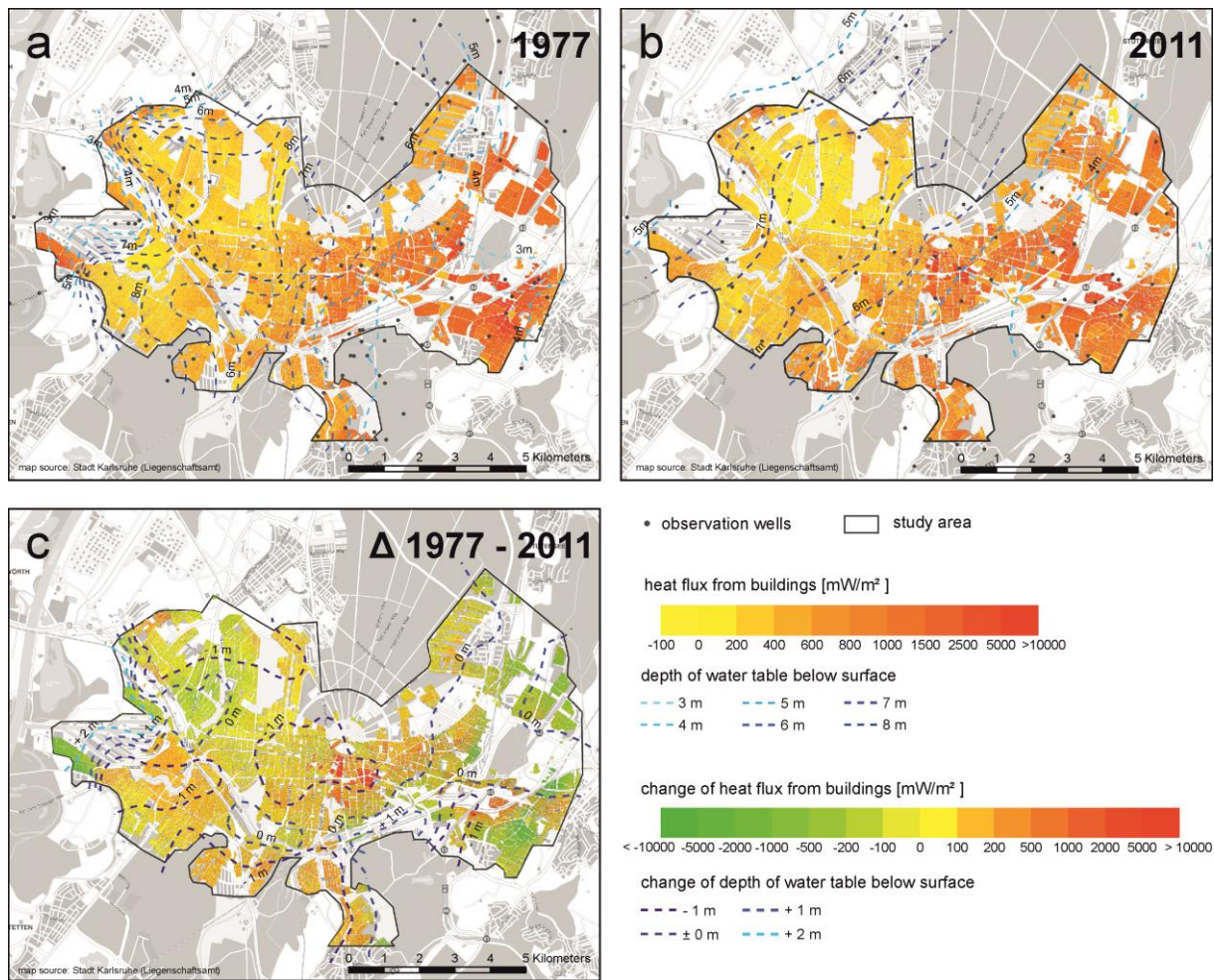
Figure 4-3: Spatial heat flux from buildings in 1977 (a) and 2011 (b). Plot (c) shows the changes in the spatial heat flux from buildings and the change in the depth of the water table from 1977 to 2011.

Furthermore, buildings with deep basements, such as shopping malls and underground parking lots in the city center, cause local hot spots in 2011. This strong dependence of the heat loss from buildings on the existence of shallow groundwater has been previously observed by other studies (*Rees,* 2001; *Ferguson & Woodbury*, 2004). The high heat fluxes in the southeastern part of Karlsruhe are also promoted by the relatively low GWT (Figure 4-1) that result in a high temperature gradient. Although this area is a rather old city district, GWT in 1977 and in 2011 is low, because it is significantly influenced by an inflow of thermally unaffected groundwater from the rural background, which is estimated to be around 520 m³d⁻¹.

Due to the chosen statistical approach, such advective effects are not adequately considered. However, the range of heat flux values obtained are in good agreement with the heat

loss under individual basement in other studies, which reaches 2-28 Wm^{-2} depending on the site parameters, such as depth of water table and the thermal conductivity of the soil (*Kusuda & Bean*, 1984; *Adjali et al.,* 1998; *Thomas & Rees*, 1999; *Ferguson & Woodbury*, 2004). These studies, as well as our model, do not regard thermal insulation of basements. In Germany, ground slab insulation was not considered in construction regulations until the late 1990s (*DIN 4108-2*, 2011). Thus, most buildings in the study area are expected to have no insulation.

Compared to suburban areas (in particular in eastern part of the city), the inner and western city reveals low to moderate heat fluxes, which are not only caused by a deep water table but also by a higher GWT (Figure 4-1). At some locations in the western part, even negative heat fluxes can occur indicating an annual heat input from the ground into the basements, because basements temperatures are probabilistically assigned and therefore can be lower than the annual GWT. Figure 4-3c displays the changes in the heat flux from buildings and the spatial changes of the water table from 1977 to 2011, which are mainly caused by modifications of groundwater pumping (Figure 4-1). Green areas indicating a decrease in heat flux from buildings are mainly situated in the western parts, where water level has decreased by up to 2 m, and in the eastern districts, where the groundwater temperature has increased (Figure 4-1). Rising heat fluxes can be observed in areas with elevated water table that are surrounded by the -1 m-isolines, e.g. in the southwestern part and in some areas in the eastern part. The most significant rise of the heat flux is located in the city center (red pixels), where several deep underground parking garages and basements have been constructed during the last decades. The superposition of these effects of variable depth of water table, groundwater temperature, basement depth and building density leads to a spatially heterogeneous development of heat flux from buildings.

4.3.3 Contribution to variance analysis

The highest Spearman's rank correlation coefficients for the model parameters are shown in Figure 4-4. The other parameters revealed correlation coefficients smaller than 0.02 (Table S 4-1) and have therefore, only minor influence on the model outcome. The significance of the individual correlations was tested by calculating the 95% confidence interval that revealed rather close ranges (Table S 4-1). Parameters contributing to the large heat flux from increased GST and buildings exhibit the highest sensitivities. The changes in the correlation coefficients between 1977 and 2011 are the result of the superposition of several effects. They

are not only linked to changes in the parameter ranges, but also to changes in the relative contribution of the individual heat fluxes to the AHF_s (Figure 4-2a).
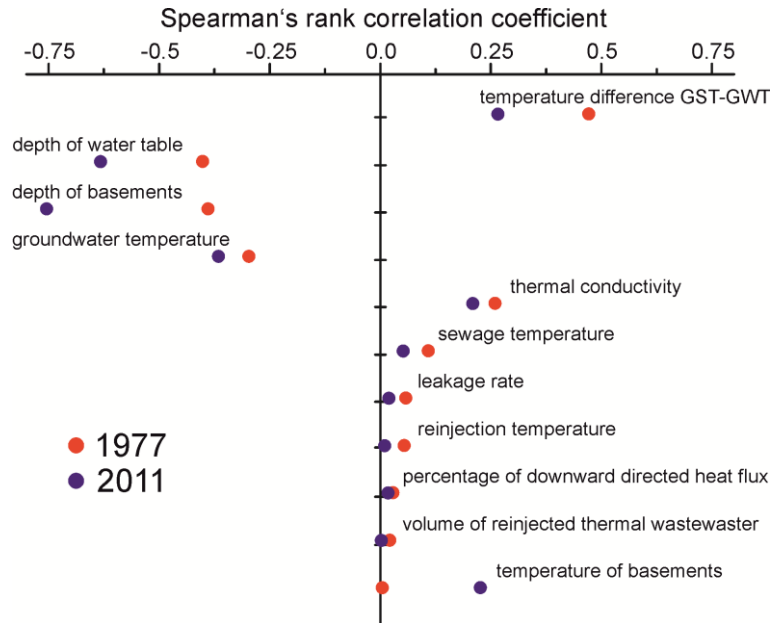

Figure 4-4: Results of the contribution to variance analysis displayed as Spearman's rank correlation coefficients between the heat flux result and the individual parameters. Only parameters with one correlation coefficient > 0.02 are shown here. The results for all parameters and the 95% confidence intervals are listed in Table S 4-1.

It can be stated that the important parameters are either known from spatial measurements, such as depth of water table and groundwater temperature, or can be assumed within a reasonable range, such as thermal conductivity of the subsurface. The annual GST difference represents another major influencing factor. This effect of GST variations on subsurface temperatures in urban areas has also been examined by *Ferguson & Woodbury* (2007), who observed a correlation between GWT and different land use types, which exhibits varying GST. Also changes in land surface cover, such as deforestation or surface sealing, were found to cause strong perturbations of GST and consequently of subsurface temperatures (*Taylor & Stefan*, 2009; *Nitoui & Beltrami*, 2005; *Taniguchi et al.,* 1999b). *Smerdon et al.* (2009) showed that climatic factors, e.g. snow cover, influence the land surface processes and the propagation of temperature signals into the subsurface. Thus the temporal and spatial distribution of the GST in urban areas is expected to be rather heterogeneous. However, measured values of the spatial distribution of GST in urban areas are rare, although they could reduce

the uncertainty of heat flux estimation (Figure 4-2) and consequently improve spatial heat flux analysis.

Although the values obtained by the model in this study apply only for the city of Karlsruhe, the discussed heat flux processes occur in many urban areas (*Menberg et al.,* 2013b). Most cities have a high building density and a high percentage of artificial surface covers. Consequently, the heat fluxes from increased GST and buildings are expected to be the driving forces for subsurface warming in many urban areas. The heat input by the other minor heat sources depends mainly on the local circumstances, such as reinjections of thermal wastewater or district heating networks and on the length and condition of the sewage system. These factors substantially vary in each city, but the assumed parameter ranges in this study are rather large. Thus, it seems unlikely that the relative contribution of the individual components on the AHF_s will change significantly for other cities. Hence, urban areas are prone to exhibit extensive temperature anomalies in shallow aquifers with GWT increased by several degrees (*Menberg et al.,* 2013b). Such significant temperature changes influence chemical and biological properties of groundwater and also affect water quality (*Green et al.,* 2011; *Hähnlein et al.,* 2013). Although most chemical processes are not expected to change significantly below 30°C (*Bonte et al.,* 2011), especially redox reactions are influenced by small temperature variations (*Prommer & Stuyfzand*, 2005; *Jesußek et al.,* 2013). Water temperature also affects diversity of aquifer bacteria and fauna (*Hall et al.,* 2008; *Brielmann et al.,* 2009) that play an important role for water purification and filtration (*Hähnlein et al.,* 2013). On the other hand, elevated GWT enhances the microbiological activity, which can promote remediation of organic contaminations in urban or industrial areas (*Slenders et al.,* 2010).

Acknowledgements

Supporting Information
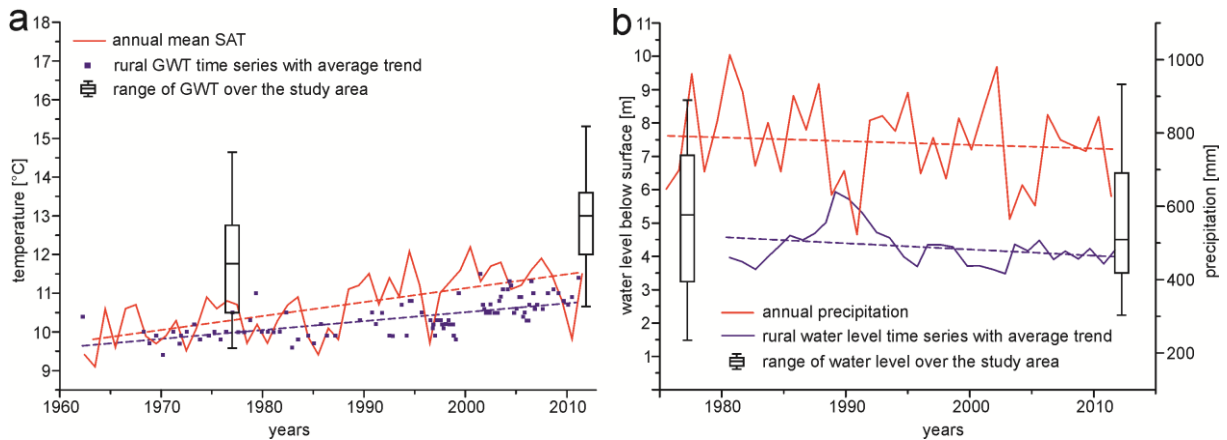
Figure S 4-1: a) Long term development of air and groundwater temperatures in the study area; b) Long term development of water level and precipitation rate in the study area. The boxplots show the spatial distribution of the parameters in the compared years. The background values for GWT and water level were taken from two different wells in a forest outside the city of Karlsruhe.
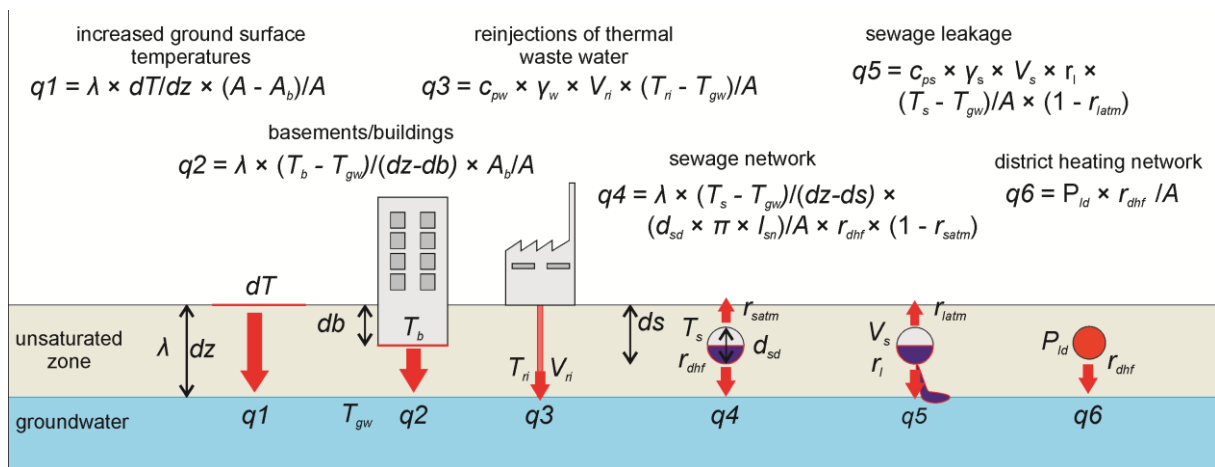
Figure S 4-2: Conceptual sketch of the developed urban heat flux model with heat flux equations and input parameters.

Description of the assumed parameter ranges

In the following paragraphs, the assumptions for the model parameters (Table 4–1) are discussed in detail. For the thermal conductivity, λ, of the unsaturated zone we use literature values (*Menberg et al.,* 2013c; *VDI 4640*, 2010), which correspond to partly saturated sand and gravel deposits typical for the study area (*Geyer & Gwinner*, 2011). Thus, the assumed

range also accounts for changes in the moisture content of the sediments. The lowest λ was set to 0.3 Wm^{-1}K^{-1} for dry gravel; the highest value, 1.8 Wm^{-1}K^{-1}, represents completely saturated sandy material.

The difference in local GST and GWT, *dT*, is assumed to range between 0 and 5 K. In long-term steady-state examinations mean annual GST and shallow GWT are usually assumed to equal each other (e.g. *Taylor & Stefan*, 2009) with no heat flux occurring into the subsurface. Alteration of the surface cover leads to a change in GST. Changes from vegetated surfaces to bare soil were found to cause an increase in annual mean GST between 0.3-1 K, while concrete and asphalt surfaces show a GST that is 2–5 K higher than at a grass or forest site (*Taylor & Stefan*, 2009; *Dědeček et al.,* 2012). The percentages of different surface types in the study area were estimated based on a land use plan, similar to the approach by *Taylor & Stefan*, 2009. According to the land use plan of Karlsruhe, approx. 20% of the study area are covered by buildings and the rest is characterized by different kinds of vegetation (approx. 56%) and artificial surface covers (approx. 24%). Due to this distribution and the fact that the GWT below the urban area is already elevated compared to the undisturbed background the mode value for *dT* is set to 1 K. As the annual mean SAT in 2011 was 0.8 K higher than in 1977 (*German Weather Service*, 2012) this value was added to the triangular distribution, given that GST usually track SAT in long-term trends (*Smerdon et al.,* 2004).

For the groundwater temperature, T_{gw}, and the depth of water table, *dz*, measured data in the study area was interpolated using kriging in GIS (ESRI® ArcInfo™ 10.0) (Figure 4-1). Raster data sets, with a spatial resolution of 15×15 m^2 were created, and the individual pixel values were then used for the Monte Carlo simulation. Likewise, the area covered by buildings, A_b, in 2011 was derived from GIS by evaluating a municipal land-use plan. The actual building density of the individual built-up polygons in GIS was estimated with Google Earth and an uncertainty of ± 5% was assigned. For the year 1977, no detailed land-use plan was available. Instead, the map from 2011 was revised by excluding newly built residential and industrial areas and reducing the overall building density for the remaining built-up polygons by 10% based on statistical data on city development (*Stadt Karlsruhe*, 2013). For each building polygon, a respective basement depth, *db*, was also assigned. The standard basement depth of residential buildings in Germany is approx. 2.5 m (*LGRB*; 1999). Greater depths were assumed for certain areas, for example with underground parking lots or shopping malls, lesser depths or no basements were assigned to industrial areas with large industrial halls. The

relevant distance for the heat flux can then be calculated by subtracting the basement depth from the water table level. For basements with contact to the groundwater, we assume a minimal distance of 0.3 m, which represents the typical thickness of a concrete slab (*Adjali et al.,* 1998). The λ in heat flux q_2 thus, accounts for the subsurface and the slab material. As typical thermal conductivities of different concrete types ranges between 0.45 and 1.8 $Wm^{-1}K^{-1}$ (*DIN EN ISO 10456*, 2010; *DIN V 4108-4*, 2007) and the fraction of the slab to the distance (*dz-db*) is rather small, the same λ as for q_1 is taken for q_2.

For the reinjections of thermal wastewater, data on the reinjected water volume, V_{ri}, and temperature, T_{ri}, was provided by the environmental department of the city of Karlsruhe for 2011. For 1977 this data was taken from the study by *Makurat* (1980). However, both data sets represent mostly licensed values for V_{ri} and T_{ri}, which are usually not confirmed by in situ measurements. Measurements on 8 reinjection sites in 1977 showed that between 80% and 100% of licensed temperature and water amount are actually utilized. Thus, we assume that on average, 90% of the licensed temperature and water amount are utilized, and we account for uncertainty by assigning a range of $\pm$ 10%.

The data to describe the sewage network (*ds*, *ls*, V_s) was provided by the municipal water supplier of Karlsruhe for 2011, and for the year 1977 values were again taken from *Makurat* (1980). The minimum sewage temperature, T_s, is defined by the annual temperature measured at the outlet of the sewers at the treatment plant by the public works service Karlsruhe. The mode and maximum of T_s are based on an estimation of the average domestic waste water temperature by *Makurat* (1980). For the diameter of the sewage pipes, d_{sd}, and the leakage rate, r_l, a range of values from studies in other German cities was applied (*Eiswirth et al.,* 2002; *Klinger,* 2007). The values for the percentage of upward and downward directed heat flux, (r_{satm}, r_{latm}, $r_{dhf)}$ are assumed based on the geometry of the pipes. The heat capacity and density of wastewater are assumed to be slightly higher than of pure water due to solid contents (*Makurat,* 1980).

Contribution to variance analysis

Table S 4-1: Results of the contribution to variance analysis. Spearman's rank correlation coefficients for the total heat flux result and all parameters with the 95% confidence interval determined by bootstrapping.

Parameter	Spearman's rho 1977	95% confidence interval		Spearman's rho 2011	95% confidence interval	
		min	max		min	max
GST difference urban - rural	0.4629	0.4583	0.4687	0.2631	0.2602	0.2663
depth of water table	-0.4050	-0.4100	-0.4001	-0.6271	-0.6293	-0.6250
depth of basements	-0.3523	-0.3575	-0.3461	-0.7464	-0.7480	-0.7450
groundwater temperature	-0.2988	-0.3031	-0.2936	-0.3644	-0.3676	-0.3615
thermal conductivity	0.2578	0.2527	0.2625	0.2085	0.2053	0.2123
sewage temperature	0.1094	0.1048	0.1147	0.0503	0.0469	0.0531
leakage rate	0.0493	0.0440	0.0551	0.0204	0.0168	0.0240
reinjection temperature	0.0412	0.0367	0.0482	0.0087	0.0050	0.0134
percentage of downward directed heat flux	0.0332	0.0260	0.0376	0.0158	0.0131	0.0198
reinjection volume	0.0196	0.0131	0.0256	0.0007	-0.0026	0.0055
diameter of sewage drains	0.0192	0.0133	0.0242	0.0132	0.0087	0.0171
percentage of heat flux to atmosphere (rlatm)	-0.0139	-0.0193	-0.0087	-0.0023	-0.0064	0.0012
heat loss from district heating pipes	0.0105	0.0055	0.0160	0.0061	0.0028	0.0101
depth of sewage drains	-0.0079	-0.0124	-0.0032	0.0007	-0.0042	0.0026
density of waste water	0.0099	0.0019	0.0145	0.0028	0.0000	0.0064
heat capacity of waste water	0.0061	0.0014	0.0107	0.0023	-0.0056	0.0023
sewage volume	0.0117	0.0075	0.0167	0.0013	-0.0021	0.0050
percentage of heat flux to atmosphere (rsatm)	-0.0034	-0.0097	0.0016	-0.0038	-0.0078	-0.0008
area covered by buildings	-0.0015	-0.0055	0.0035	-0.0025	-0.0070	-0.0012
temperature of basements	-0.0048	-0.0103	0.0004	0.1968	0.1924	0.2001
length of sewage network	0.0011	-0.0030	0.0076	0.0029	-0.0003	0.0075

5 Groundwater temperature response to climate regime shifts

Abstract

Climate change is known to have a considerable influence on many components of the hydrological cycle. Yet, the implications for groundwater temperature, as an important driver for groundwater quality, thermal use and storage, are not yet comprehensively understood. Here, we examine the coupling of atmospheric and groundwater warming by statistically analyzing temperature time-series of several decades with regard to abrupt regime shifts in the long-term mean. The observed abrupt increases in shallow groundwater temperatures can be associated with preceding positive shifts in regional surface air temperatures, which are in turn linked to global air temperature changes. The thermal signals from distinct changes in air temperature are damped and delayed by conductive and advective heat transport in the subsurface, causing a more gradual increase in groundwater temperatures. Hence, these signals can have a significant impact on large-scale groundwater temperatures in shallow, economically important aquifers.

5.1 Introduction

Characterizing changes in time-series of various climatic, physical and biological parameters with the concept of abrupt regime shifts has been the focus of numerous studies in the last two decades (e.g. *Trenberth & Hurrell*, 1994; *Hare & Mantua*, 2000; *Overland et al.,* 2008). Generally, a regime is defined as a period with quasi-stable behavior or with a quantifiable quasi-equilibrium state (*deYoung et al.,* 2004). Accordingly, *Bakun* (2004) refers to a climate regime shift (CRS) as a rapid transition between states with differing average climatic characteristics over multi-annual to multi-decadal periods. CRSs were studied intensively in time-series of atmospheric oscillation indices, such as the Pacific Decadal Oscillation (PDO) or Artic Oscillation (AO) (e.g. *Hurrell,* 1995; *Swanson & Tsonis*, 2009). Furthermore, several studies investigated the impact of the late 1980s regime shift in the AO on hydrological systems in Switzerland, such as temperatures of river water and bank infiltration (*Figura et al.,* 2011) and physical lake properties (*North et al., 2013*).

Climate change is expected to have a significant influence on the hydrological cycle (*Bates et al., 2008*). However, most studies focus mainly on the impact on hydrological processes, such as precipitation or river flow, or the availability of water resources (*Arnell,* 1999; *Bates et al., 2008*; *Kundzewicz,* 2008). Equivalent studies on groundwater systems are limited (e.g. *Stoll et al., 2011*; *Kløve et al., 2013*), and the implications of changing climate conditions on groundwater quality are not yet fully understood (*Green et al.,* 2011). Groundwater temperature (GWT) is known to be an important driver for water quality (*Green et al.,* 2011; *Hähnlein et al.,* 2013) and therefore, it is a crucial parameter for groundwater resource quality management (*Figura et al.,* 2011).

Few studies investigated the changes in shallow subsurface temperatures due to variations in surface air temperatures (SAT) or ground surface temperatures (GST) suggesting that the subsurface thermal regime is strongly influenced by atmospheric temperature signals (*Taylor & Stefan*, 2009; *Dĕdeček et al.,* 2013). Yet, GWT are also very sensitive to non-climatic changes, such as land use changes or anthropogenic alterations in the subsurface, so that not all variations in GWT, particularly in urban areas, are related solely to changing air temperatures (*Taylor & Stefan*, 2009; *Menberg et al., 2013a,b*). *Figura et al.* (2011) showed that temperature variations due to CRS in the Artic Oscillation could be detected in Swiss aquifers that are recharged by river water through bank infiltration. However, the question remains if increasing SAT due to recent climate change also have a detectable effect on long-

term development of shallow GWT. It is also unclear as to whether, and how, aquifers, which are not or loosely connected to infiltrating surface water bodies, respond to climate regime shifts.

In this study, we therefore demonstrate the direct influence of atmospheric temperature development on shallow groundwater temperatures at two sites in Germany by analyzing time-series of air and groundwater temperatures with regard to abrupt changes in the long-term annual mean. The magnitudes of the regime shifts and the time lags between the shifts in the chosen time-series are evaluated under consideration of the different thermal processes in the subsurface and the site-specific hydrogeological settings. Furthermore, we compare different spatially averaged temperature time-series from individual weather stations to global mean air temperature change bringing our observations in the context of global climate change.

5.2 Data and methods

5.2.1 Data and site description

For the analysis of shallow GWT, we use time-series from four observation wells in porous and unconfined aquifers in Germany (Table 5-1). Two of the wells are installed in the surrounding area of Cologne outside the small villages Dansweiler and Sinthern in agricultural areas. The other two wells are located in a forest, called Hardtwald, close to the city of Karlsruhe and are therefore named Hardtwald 1 and 2. The proximate surroundings of all four wells have remained steady in the last decades, so that variations in GWT due to land use changes are not likely. Both aquifers are recharged by infiltration of meteoric water through the unsaturated zone. GWT in all wells was measured one to six times per year for a period of at least 32 years (1974-2006) during pumping, so that the temperature can be seen as representative annual means for the upper part of the aquifers. Additional information on the hydrogeological settings of the wells and aquifer parameters are given in the auxiliary material. If two or more GWT measurements were available per year, the arithmetic mean is adopted as annual mean value.

Annual air temperature data is available from weather stations operated by the German Weather Service (DWD) in both Cologne and Karlsruhe. Though located several kilometers from the observation wells, the SAT from these stations is expected to yield a good approximation for the development of SAT at the well sites. For the comparison with air temperatures

on a larger scale, we use time-series of mean air temperature anomalies based on the reference period 1951-1980 from the NASA Goddard Institute for Space Studies (GISS) (*e.g. Hansen et al.,* 2010). Of the spatially averaged temperature data sets available, we evaluate the annual global mean from land-surface air and sea-surface water temperature anomalies and the annual zonal mean for the northern hemisphere between 90°N-24°N based on land-surface air temperature anomalies.

Table 5-1: Location coordinates of the observation wells with basic information about the hydrological setting.

Well	Easting	Northing	Altitude [m asl]	Subsurface material	Depth of water table [m bgl]
Dansweiler	2553462	5646975	88.2	fine to coarse sand, minor contents of gravel and silt[a]	18 ± 2
Sinthern	2555310	5648820	64.4		16 ± 2
Hardtwald 1	3457460	5435140	112.4	gravel and coarse sand with layers of fine sand and silt[b]	7 ± 3
Hardtwald 2	3457500	5435200	112.1		7 ± 3

[a] *Klostermann,* 1992; [b] *HGK,* 2007

5.2.2 Regime shift analysis

To detect possible regime shifts in the temperature time-series, we use the sequential t-test analysis for regime shifts (STARS) (*Rodionov*, 2004, *Rodionov & Overland*, 2005), a method that is commonly used to identify abrupt changes in the long-term mean of environmental time-series (*Marty*, 2008, *Figura et al.*, 2011, *North et al.*, 2013). STARS is a parametric test that can detect multiple regime shifts and needs no a priori assumption for the timing of possible shifts. Identification of a shift is based on the calculation of the Regime Shift Index (RSI), which represents the cumulative sum of the normalized deviations from the mean value of a regime and thus reflects the confidence of a regime shift (*Rodionov*, 2004). For the regime shift analysis, several test parameters can be adjusted to account for specific characteristics, such as the length of the tested time-series. The target significance level in our analysis is set to 0.15, which corresponds to the p-level of false positives. The actual p-value of an identified shift between subsequent regimes is calculated separately with a Student's t-test. The cut-off length of the test corresponds to a low-pass filter, so that regimes with a shorter length are disregarded in the analysis (*Rodionov & Overland*, 2005). Here, we set the cut-off length to 10 years as atmospheric oscillations often occur at decadal intervals

(*Overland et al.*, 2008). Furthermore, the Huber weight parameter (set to 1 in our study) included in the STARS procedure improves the treatment of outliers by weighting them proportionally to their deviation from the mean value (*Overland et al.*, 2008). As pointed out by *Seidel & Lanzante* (2004) atmospheric data tends to be highly temporally auto-correlated, so that especially in short time series spurious regime shifts may be detected due to serial correlation (*Rudnick & Davis*, 2003). Therefore, we apply a prewhitening procedure that removes the red noise component from the temperature time series prior to testing for a regime shift (*Rodionov*, 2006). To investigate the stationarity within detected regimes, the non-parametric Mann-Kendall test for the absence of trend is applied to the temperature data (*von Storch*, 1995).

5.3 Results and Discussion

5.3.1 Regime shifts in air and groundwater temperatures

In all analyzed time-series at least two regime shifts could be detected in the last decades (Figure 5-1). The time-series of global mean temperature change and zonal mean temperature change in 90°N-24°N show significant (STARS, $p < 0.005$) positive shifts in 1977, 1987, 1997 and 1977, 1988 and 1998, respectively (Table 5-2). The observation of shifts in air temperature change in these years is in good agreement with the observation of decadal shift in atmospheric oscillation indices in the late 1970s, late 1980s and late 1990s (*Overland et al.,* 2008). Examining the time-series of local SAT data from Cologne and Karlsruhe, only the CRS in the late 1980s and late 1990s can be found. However, this is not surprising as previous studies observed that the CRS in the late 1970s was most prominent in the North Pacific region (*Hare & Mantua*, 2000; *Overland et al.,* 2008), and less accentuated in Europe. The same applies to the CRS in the late 1990s (*Overland et al.,* 2008; *Swanson & Tsonis*, 2009), which is reflected by the differing RSI values in Figure 5-1.
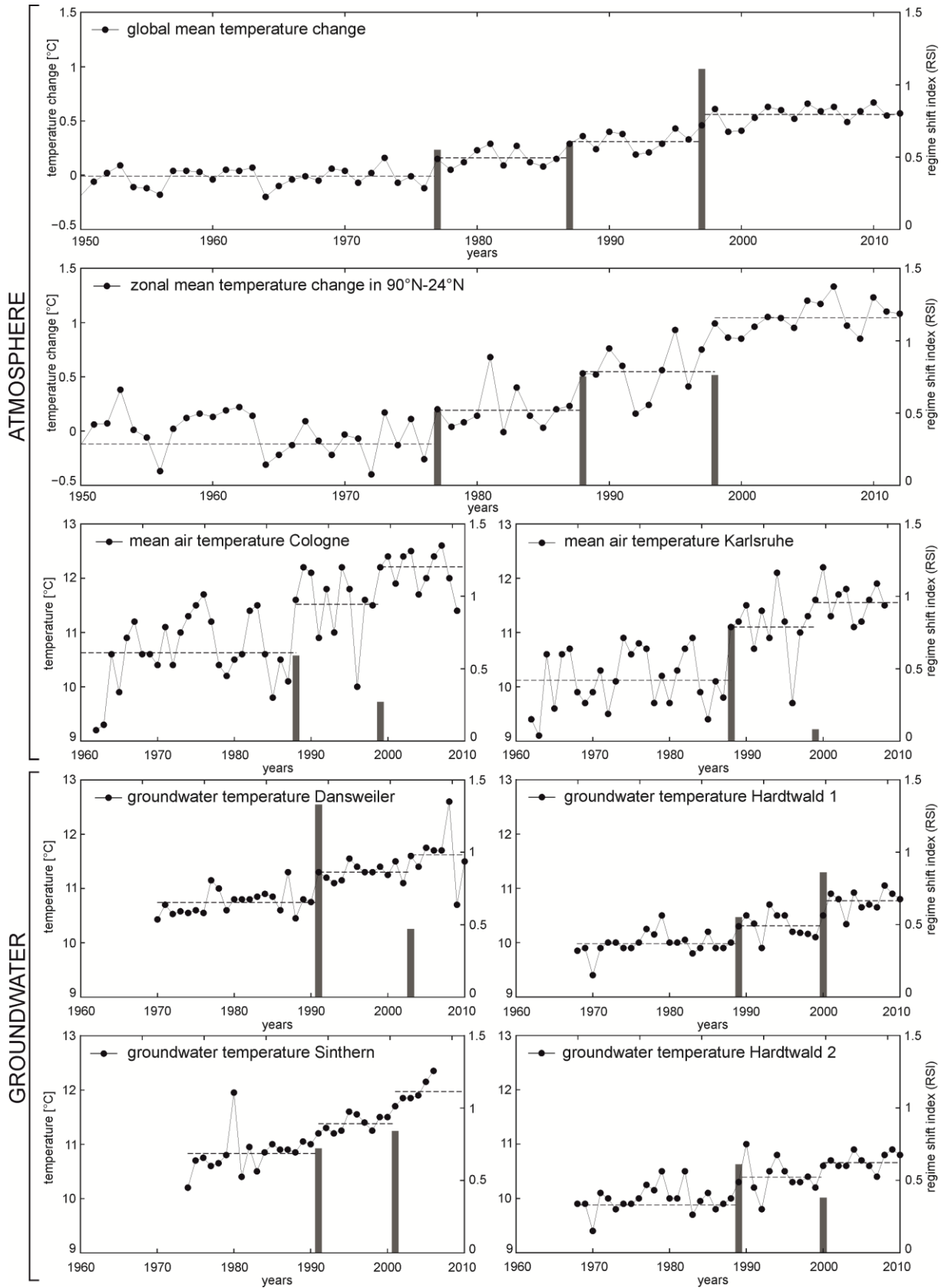
Figure 5-1: Time series of temperature data with long-term means (dashed lines) and observed regime shift with RSI values.

Table 5-2: Time lags and final p-values of the observed regime shifts in air and groundwater temperature. Time lags are given for the regime shifts in GWT in relation to the CRS in local SAT.

Time-series	Regime shift late 1970s		Regime shift late 1980s			Regime shift late 1990s		
	year	p-value	year	Time lag to SAT (years)	p-value	year	Time lag to SAT (years)	p-value
Global mean ΔT	1977	1.8×10^{-5}	1987	–	4.4×10^{-4}	1997	–	1.8×10^{-7}
Zonal mean ΔT	1977	9.1×10^{-4}	1988	–	4.6×10^{-3}	1997	–	5.7×10^{-5}
SAT Cologne	–	–	1988	–	6.7×10^{-4}	1999	–	5.5×10^{-3}
GWT Dansweiler	–	–	1991	+ 3 (±1)	1.1×10^{-9}	2003	+ 4 (±1)	1.0×10^{-1}
GWT Sinthern	–	–	1991	+ 3 (±1)	9.3×10^{-5}	2001	+ 2 (±1)	4.3×10^{-4}
SAT Karlsruhe	–	–	1988	–	3.2×10^{-5}	1999	–	3.8×10^{-2}
GWT Hardtwald 1	–	–	1989	+ 1 (±1)	3.6×10^{-4}	2000	+ 1 (±1)	1.3×10^{-4}
GWT Hardtwald 2	–	–	1989	+ 1 (±1)	9.2×10^{-4}	2000	+ 1 (±1)	1.0×10^{-2}

While the high RSI for the CRS in 1997 in the global mean temperature change indicates a significant shift, the RSIs for the late 1990s CRS in the German SAT time-series are much lower than the RSIs in the late 1980s. *Figura et al.* (2011) correlated the abrupt increase in SAT in Switzerland with a change in the Artic Oscillation (AO) that has a strong influence on air temperatures in Europe. However, no such change in the AO Index can be found in the late 1990s (auxiliary information), suggesting that the CRS in the German SAT is also coupled to the general air temperature increase in the Northern Hemisphere.

In the time-series of GWT of the four wells near Cologne and Karlsruhe two regime shifts were detected, which correspond to the CRS in the atmosphere with a certain time lag (Figure 5-1, Table 5-2). The regime shifts in GWT time-series are all statistically significant ($p <$ 0.01), except for the second regime shift in the late 1990s in Dansweiler. Two prominent out-liers in the third regime of the time series influence the statistical significance for this shift, while the RSI value is calculated under consideration of the outliers according to the Huber weight parameter. Furthermore, the RSI values in Figure 5-1 for the second shifts in Dansweiler and Sinthern are not the final values, as the 10-year cut-off length of the STARS test in the last regime has not yet been reached.

5.3.2   Time lags and magnitude of temperature change

The time lags between the regime shifts in SAT and GWT are listed in Table 5-2. The regime shifts in global mean temperature change and the zonal mean in 90°N-24°N occur simultaneously, except for the regime shift in the late 1980s that has a time lag of one year. However, as annual mean values are used for the analysis, the accuracy of the shift detection is ± 1 year, so that the shifts occur within the uncertainty range. The same applies to the first regime shifts in the local SAT time-series in Cologne and Karlsruhe, while the time lag of 2 years in the second shift is significant. A possible explanation for this variation in the time lags would be that the late 1980s regime shift was very prominent in the Arctic Oscillation that directly influences the European climate (*Figura et al.,* 2011). The late 1990s regime shift however, was more distinct in the North Pacific region (*Overland et al.,* 2008), thus probably causing the delayed shift in the SAT in Germany. Yet, changes in SAT are also expected to be temporally and spatially highly heterogeneous due to the variability of local climate and the complexity of atmospheric circulation systems (*Hansen et al.,* 2010).

The observed regime shifts in GWT lag behind the abrupt increase in local SAT by 1-4 years (Table 5-2). In Karlsruhe the time lag is generally small with one year for all shift events, while the time lags in Cologne vary between 2-4 years. This difference in the time lags reflects the specific hydrogeological site conditions with the unsaturated zone in Cologne with about 17 m being significantly thicker than in Karlsruhe with about 7 m (Table 5-1). Due to the similarity of the thermal properties of the subsurface materials, thermal propagation of the SAT signal into the groundwater takes longer in Cologne than in Karlsruhe. This is based on the assumption that vertical heat transport in the unsaturated zone is usually found to be dominated by conductive heat transport (*Smerdon et al.,* 2004; *Molina-Giraldo et al.*, 2011b; *Dĕdeček et al.,* 2013).

The magnitudes of the temperature increase between two subsequent regimes in the zonal mean SAT change are considerably higher than in the global mean SAT change (Figure 5-2), because the global temperature data set contains ocean temperature measurements, and ocean's temperatures are known to respond more slowly to climatic forcing due to the ocean's large thermal inertia (*Hansen et al.,* 2010). The above mentioned temporal and spatial hetero-geneity of CRS accounts also for the higher increase in SAT in the German time series, which is above the average of the zonal mean in 90°N-24°N. The significant abrupt increase in the

long-term mean of SAT with the late 1980s CRS of close to 1 K was likewise observed in Swiss SAT by *Figura et al.* (2011).
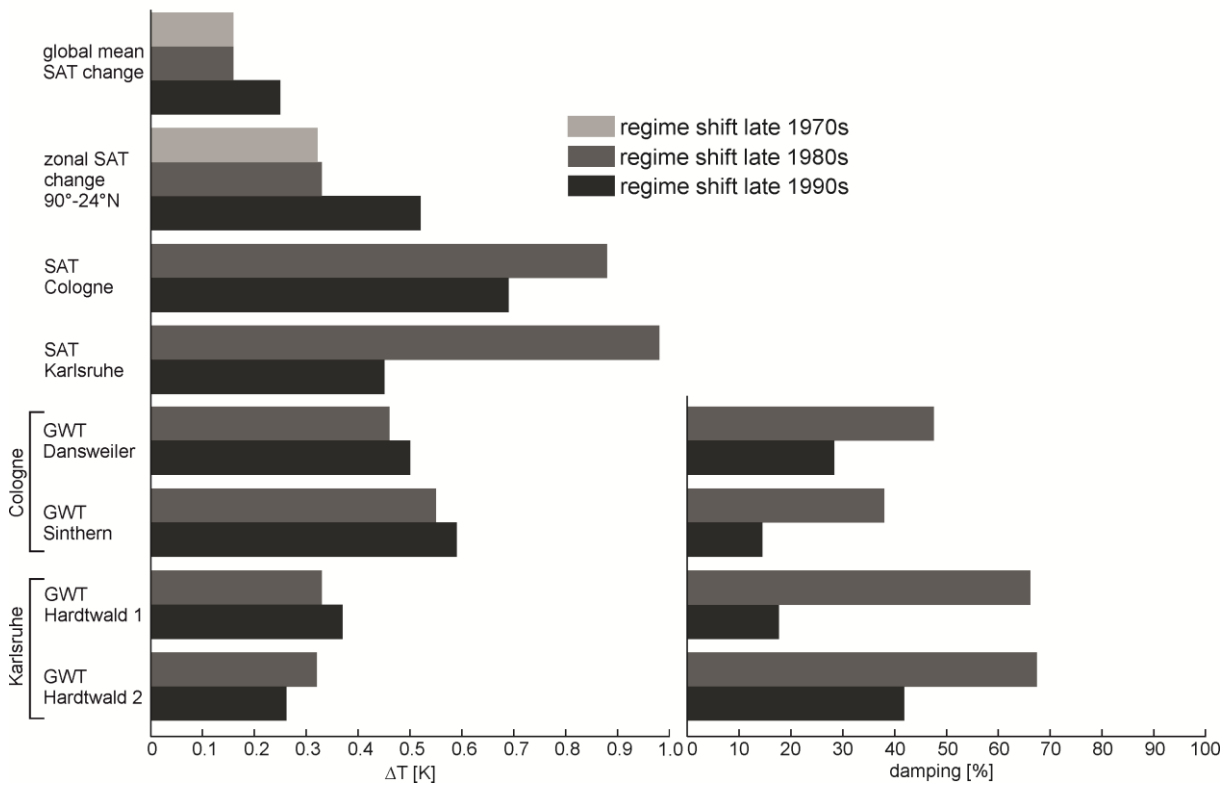

Figure 5-2: Left: Magnitude of regime shift in time-series of atmospheric and groundwater temperatures. Right: relative damping of the regime shift magnitude in groundwater temperatures compared to regional atmospheric regime shift, calculated as 100 minus the ratio of ΔT in GWT to ΔT in SAT in percent.

The magnitudes of the abrupt increases in the long-term means of GWT are lower and damped by up to 70% compared to the shift magnitude in SAT (Figure 5-2). This damping of the amplitude of atmospheric temperature signals is, as the discussed time lags, related to the dominant vertical conductive heat transport in the unsaturated zone (*Smerdon et al.,* 2004; *Dědeček et al.,* 2013). Thus, one would expect that the damping of the temperature shifts is stronger in Cologne than in Karlsruhe. However, the ground heat flux, i.e. the part of the energy budget at the ground surface that propagates from the atmosphere into the subsurface, depends not only on the properties of the subsurface, but also on surface and atmospheric parameters. As the wells near Karlsruhe are located in a forest and the wells near Cologne at a agricultural site, differences in the surface energy balance, such as the dimension of solar irradiation, mainly contribute to the differences in the shift magnitudes. Aside from this, the

temperature signal is further extenuated after propagating down to the groundwater surface, not only by vertical heat transport within the aquifer, but also by horizontal advection and lateral mixing processes caused by fast horizontal groundwater flow and thermal dispersion. Furthermore, due to the pumping of the wells prior to temperature measurements, the extracted water is a blend of groundwater from a certain range of depth (auxiliary material). Thus, the measured values represent averaged temperatures from the well capture zones.

5.3.3   Stationarity within the regimes

In general, the resulting p-values of the Mann-Kendall test in the SAT time-series are with a median value of 0.53, significantly higher than in the GWT time series with a median of 0.20 (auxiliary material), indicating that the SAT time series are generally more stationary. No significant trends could be found within the individual regimes of the examined SAT time-series, suggesting that the temperature increase in the last decades can be attributed completely to the detected CRS. In the GWT time series, a significant trend ($p < 0.05$) with a slope of 0.13°C was detected in the third regime (2001-2006) in the Sinthern well. Also, in the regimes before 1991, the p-values of the time-series in Dansweiler and Sinthern are 0.05 and 0.06, respectively, which are close to the critical p-value of 0.05. For the wells near Karlsruhe no significant trends were found in GWT within the regimes. The more gradual increase in GWT time-series agrees well with the observation described above that, in contrast to the rapid transition in the atmosphere, the temperature signal in the groundwater is damped and delayed by conductive and advective heat transport in the subsurface.

5.4   Conclusions

By applying a regime shift analysis (STARS) to time-series of air and groundwater temperatures, we demonstrated that groundwater temperatures in shallow aquifers show abrupt temperature changes that correspond to positive shifts in local SAT in Germany, which in turn can be traced back to increasing global SAT. This observed direct coupling of atmospheric and groundwater temperature development through the unsaturated zone implies that climate warming will not only affect aquifers recharged by river-bank infiltration (*Figura et al.,* 2011), but also a large number of shallow aquifers on a wide spatial scale. The regime shifts in GWT occur with a certain time lag to the CRS depending on the thermal properties and thickness of the unsaturated zone. The magnitude of the regime shifts in GWT compared to

the shifts in SAT is damped by the thermal propagation of the temperature signal into the subsurface, leading to a more gradual increase in GWT. However, despite the extenuation of the temperature signal by conductive and advective heat transport in the subsurface and the mixing of shallow groundwater during pumping, significant temperature shifts were found in the extracted groundwater. Thus, increasing SATs are prone to have a substantial and swift impact, not only on soil temperatures, but also on large-scale groundwater temperatures in productive and economically important aquifers.

Acknowledgements

Supplementary material

Background information on the hydrogeological site conditions is illustrated in Figure S1 and Table S1. Figures S1 shows schematic cross sections of the two aquifers near Cologne (left) and Karlsruhe (right) showing the approx. depth of the water table below surface level and the depth of the underlying aquitard. The large-scale hydrogeological conditions around the wells in Dansweiler and Sinthern are described by *Klostermann* (1992). For the region around Karlsruhe hydrogeological data is available from *HGK* (2007). Figure S2 also depicts the well constructions with the overall depth and the locations of the filter screens (black areas) that indicate from which depth the pumped water is captured. Furthermore, the distance between the wells pairs is given, as well as the distances to the weather stations, from which the SAT time-series were obtained.
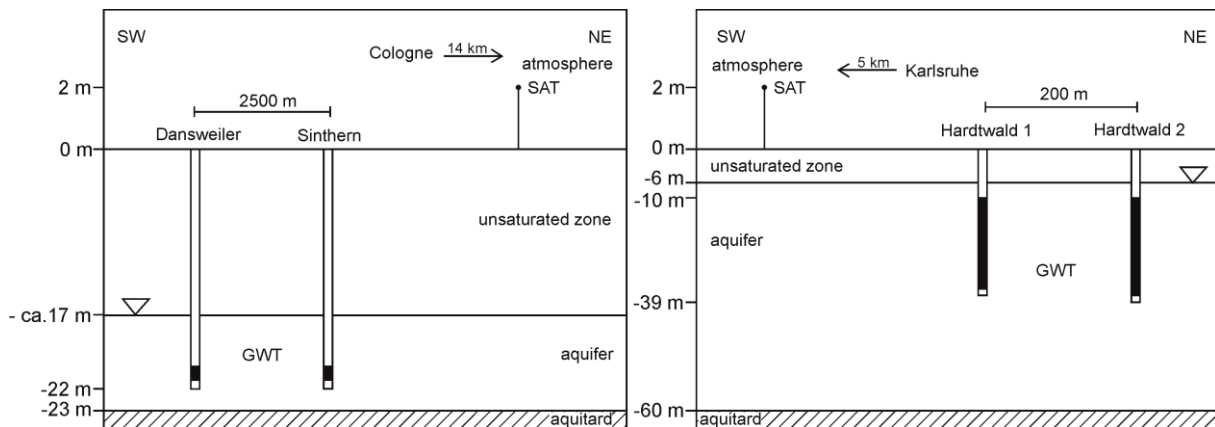
Figure S 5-1: Conceptual sketch of the well settings in the aquifers close to Cologne (left) and Karlsruhe (right). The black zones in the wells indicate the location of the filter screens. Please note the different scales in the subsurface.

Table S1 lists the streams nearest to the four observation wells and the respective perpendicular distance. As the distances cover several kilometers an influence of river water on the groundwater temperature in the wells can be excluded. Regional groundwater flow direction is northwest for the aquifer in Karlsruhe and east for the aquifer close to Cologne, respectively, towards the Rhine River (*Balke*, 1973, *HGK*, 2007). Regionally averaged hydraulic conductivities are in the range of $1.0\text{-}5.0 \times 10^{-4}$ m/s for the aquifer close to Cologne (*Balke*, 1973) and $1.1\text{-}1.4 \times 10^{-3}$ m/s for the aquifer north of Karlsruhe (*Wirsing & Luz*, 2008).

Table S 5-1: Hydraulic and hydrogeological data for the four observation wells.

Well	Nearest stream	Distance to nearest stream	Receiving stream	Groundwater flow direction	Average hydraulic conductivity
Dansweiler	Erft	~ 6 km	Rhine [a]	northeast [a]	$1.0\text{-}5.0 \times 10^{-4}$ ms^{-1} [a]
Sinthern	Erft	~ 9 km	Rhine [a]	northeast [a]	$1.0\text{-}5.0 \times 10^{-4}$ ms^{-1} [a]
Hardtwald 1	Rhine	~ 6 km	Rhine [b]	west [b]	$1.1\text{-}1.4 \times 10^{-3}$ ms^{-1} [c]
Hardtwald 2	Rhine	~ 6 km	Rhine [b]	west [b]	$1.1\text{-}1.4 \times 10^{-3}$ ms^{-1} [c]

[a] *Balke,* 1973. [b] *HGK,* 2007. [c] *Wirsing and Luz,* 2008.

Figure S2 depicts a time-series of annual values of the Arctic Oscillation Index with the identified regimes. The values for the Arctic Oscillation Index were obtained from the website of the US National Weather Service, Climate Prediction Center (http://www.cpc.ncep.noaa.gov/products /precip/CWlink/daily_ao_ index/ao.shtml). The annual mean values were analyzed with STARS (p = 0.15, cut-off-length = 10 years, Huber weight parameter = 1).
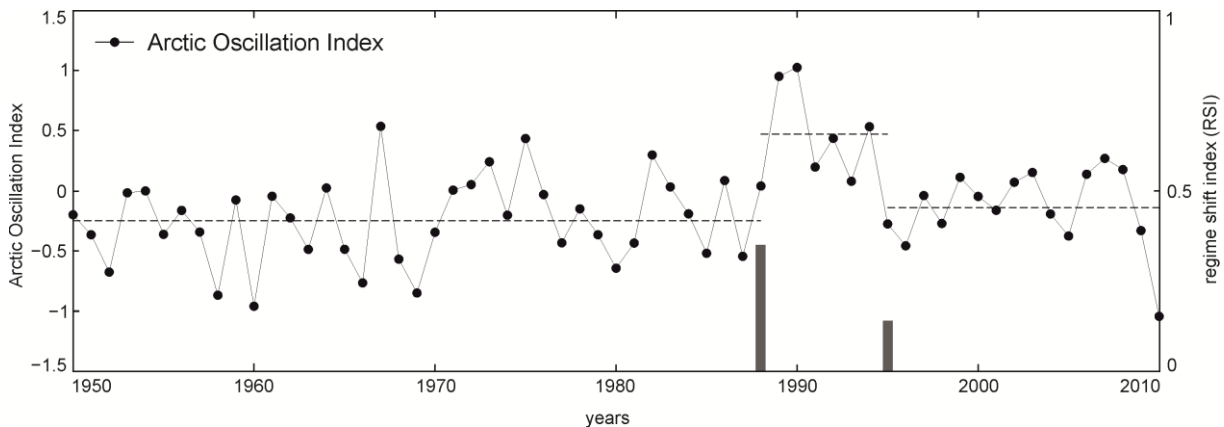
Figure S 5-2: Time series of the Artic Oscillation index with the long-term means for the identified regimes (dashed lines) and RSI values according to STARS.

Table S2 shows the results of the Mann-Kendall-test for the individual regimes in air and groundwater temperature time-series.

Table S 5-2: Results (p-values) from the Mann-Kendall test for all regimes in SAT and GWT time series.

Time-series	Regime I		Regime II		Regime III		Regime IV	
	period	p-value	period	p-value	period	p-value	period	p-value
Global mean ΔT	1950-1976	0.62	1977-1986	1.00	1987-1996	0.72	1997-2012	0.26
Zonal mean ΔT	1950-1976	0.30	1977-1986	0.64	1987-1996	0.47	1997-2012	0.72
SAT Cologne	–	–	1962-1987	0.40	1988-1998	0.89	1999-2011	0.46
SAT Karlsruhe	–	–	1962-1987	0.43	1988-1998	0.31	1999-2009	0.76
GWT Dansweiler	–	–	1970-1990	0.05	1991-2002	0.78	2003-2010	1.00
GWT Sinthern	–	–	1974-1990	0.06	1991-2000	0.18	2001-2006	0.01
GWT Hardtwald 1	–	–	1968-1988	0.22	1989-1999	0.14	2000-2011	0.13
GWT Hardtwald 2	–	–	1968-1988	0.43	1989-1999	0.59	2000-2010	0.31

6 Conclusions

Shallow groundwater temperatures are prone to be influenced by various processes altering the temperature at the ground surface. These temperature variations penetrate through the unsaturated zone mainly by conductive heat transport, which is governed by the temperature gradient and the thermal conductivity of the subsurface material. In the present PhD thesis the influence of diverse ground parameters on the thermal conductivity is examined and different methods for the determination of the thermal conductivity based on theoretical models and laboratory and field tests are compared. Furthermore, a detailed analysis of the spatial distribution of increased groundwater temperatures (GWT) under urban areas is carried out. In contrast to previous studies, a large number of possible anthropogenic heat sources are considered in a quantitative analysis of the governing processes. In addition, alterations of groundwater temperatures in shallow aquifers in rural areas due to climatic changes are examined.

In the study presented in chapter 2, a correlation analysis of the thermal conductivity and several ground parameters from core samples of unconsolidated sedimentary rocks is conducted. The generally low correlation coefficients in this analysis reveal the difficulty to retrace the impact of different soil parameters on the thermal conductivity in natural, heterogeneous rock samples. Beside the porosity, only the content of organic matter is found to have a significant impact on the thermal conductivity, which is therefore included in the calculation of the thermal conductivity of the solid phase.

The best agreement of the applied theoretical models and the thermal conductivity measured in the laboratory is accomplished with the calculation of the geometric mean model. When averaged over the whole borehole length, the difference between the two cumulative thermal conductivities of the laboratory measurements and from the geometric mean model adds up to 0.1 $Wm^{-1}K^{-1}$. Thus, the thermal conductivity of unconsolidated sedimentary rocks can be estimated within a good range with the developed approach under consideration of specific ground parameters, such as carbonate and organic matter content. In contrast, the thermal conductivities estimated based on literature values from the *VDI 4640-1* (2010) yield significantly lower values. The highest thermal conductivity in this study is obtained by the Thermal Response Test, which is 0.4 $Wm^{-1}K^{-1}$ or 16% higher than the cumulative thermal conductivity from the laboratory test. Obviously, advective effects play a role in the ground-

water-bearing layers of the subsurface, which have a tampering influence on the results of the TRT evaluation. Furthermore, the calculation accuracy of the thermal conductivity is lower than the accuracy of the laboratory tests or TRTs, but it nevertheless represents a simple and more accurate method than parameter estimations based on published values.

The detailed analysis of the spatial distribution of shallow groundwater temperatures in several German cities in chapter 3 reveals that extensive positive temperature anomalies exist under all studied cities. While the GWT in rural areas are found to be close to the annual mean air temperatures, GWT beneath the inner cities were up to 3-7 K higher. In general, the spatial distributions of GWT in the urban and suburban areas exhibit rather heterogeneous patterns. Especially in areas with very shallow measurement depths plenty of local hot spots are observed. Thus, the subsurface thermal regime is likely to be governed by diverse local and site-specific factors. The superposition of these effects results in the long-term to the extensive subsurface warming.

Spatial comparisons with the atmospheric urban heat island and the population density, as a surrogate for building and infrastructure density, shows a high correlation between the warming of the subsurface and the mentioned city characteristics. Accordingly, increased ground surface temperatures (GST) and different types of subsurface urban infrastructure, such as basements and sewage systems, might act as important heat sources for the subsurface urban heat island. As local hot spots in the shallow aquifers are frequently observed in industrial areas, it is also shown that reinjections of thermal waste water from industrial processes act as dominant local heat sources.

To estimate the magnitude of regional subsurface warming the developed inner-quantile based $UHII_{10-90}$ proves useful, as it filters extreme local cold and hot spots. The $UHII_{10-90}$ values for the studies cities range around 2 K and show a positive trend with increasing city size, which is also observed for the atmospheric UHII (*Oke,* 1973). However, the magnitude of subsurface warming is found to be more pronounced than in the atmosphere, which is in agreement with the understanding of long-term heat accumulation in the subsurface.

Based on the previously identified heat sources an analytical heat flux model is developed in chapter 4 to quantify the heat input from the individual heat sources into the shallow urban aquifer and evaluated for the city of Karlsruhe for the years 1977 and 2011. It is revealed that the highest heat fluxes occur from increased GST and the basements as anticipated in the previous study presented in chapter 3. Both heat fluxes show an increase within the last

decades due to the proceeding warming of GST due to climatic changes and the growing building density. The other examined heat sources are, when projected to the whole city area, only of minor importance. However, local heat sources, such as reinjections of thermal waste water or sewage leakages, can explain the heterogeneous GWT distribution that was observed under several urban areas in chapter 3. In contrast, the heat fluxes from increased GST and basements occur on large areas and can therefore cause the extensive large-scale thermal anomalies in the subsurface. The spatial evaluation of the heat flux from buildings shows that the heat flux density is highly heterogeneous, which is caused by the spatial variation in GWT and groundwater depth.

These two parameters, along with the basement depth, the magnitude of GST warming and the thermal conductivity are identified as the most sensitive parameters in the heat flux model. The importance of the groundwater and basement depth for the resulting heat flux density agrees with the aforementioned observation that temperatures in the very shallow subsurface are particularly heterogeneous.

The amount of energy released by the individual heat sources changed significantly over the past decades. However, the total mean annual energy input into the shallow aquifer that results from the individual heat sources adds up to 1.5×10^{15} J for both 1977 and 2011. Although the heat flux densities and energy values obtained by the model in this study apply for the city of Karlsruhe, the evaluated processes occur in many urban areas. The main causing features, high building densities and high percentages of artificial surfaces, are typical characteristics that prevail in most cities. Accordingly, heat fluxes due to increased ground surface temperatures and buildings are expected to be the dominant driving forces for subsurface warming in many urbanized areas. However, especially for the spatial analysis of anthropogenic heat fluxes in other cities, it may be important to consider other additional heat sources that are not present in Karlsruhe, such as subway systems or large geothermal energy systems.

Finally, the time-series analysis of groundwater and air temperatures demonstrated that also in rural areas temporal changes of air and ground temperatures can have a significant influence on the development of shallow GWTs. By applying a regime shift analysis, two significant upward shifts were identified in each time-series of long-term annual mean GWTs that were measured in pumping wells. These shifts are clearly linked to corresponding positive shifts in the time-series of local mean air temperatures, which are in turn related to changes in global mean air temperature and changes in large-scale atmospheric oscillation

patterns. While *Figura et al.* (2011) examined the influence on aquifers recharged by bank infiltration, the results in this study demonstrate the direct coupling of air and groundwater temperatures through the unsaturated zone. Although the temperature signal is attenuated by conductive and advective heat transport in the subsurface and the mixing of shallow groundwater during pumping, significant temperature increases are detected in the extracted groundwater. Thus, anthropogenic alterations at and beneath the surface and increasing air temperatures are prone to have a substantial impact on large-scale GWT distribution.

6.1 Perspective

The intense warming of shallow aquifers in urban and rural areas, as observed in this study, has positive as wells as negative implications for groundwater use.

First, the GWT is an important driver for water quality (*Hähnlein et al.*, 2013) and has a significant influence on groundwater ecology, especially on fauna and bacteria diversity that play an important role for water purification and filtration (*Hall et al.*, 2008). Although chemical effects in general are expected to be minor at temperatures below 25°C (*Bonte et al.*, 2013), redox reactions are also influenced by minor temperature changes (*Jesußek et al.*, 2013). For instance, an increase in the precipitation of iron and manganese in combination with an increase of water temperatures was observed in pumping wells in Switzerland during the exceptionally warm summer in 2003 (*Hoehn & Scholtis*, 2011). Thus, increasing GWT due to climatic forcing may have an impact on the drinking water supply from shallow aquifers. As pointed out by *Figura et al.* (2011), increasing water temperatures may necessitate adaption measures for drinking water supply infrastructure and an enhanced groundwater resource quality management. Future studies should therefore further scrutinize the implications of temperature increases for groundwater quality under consideration of the predicted climate warming in the next decades.

On the other hand, the extensive temperature anomalies under urban areas form a vast amount of stored thermal energy that represent attractive energy reservoirs for geothermal usage such as space heating (*Zhu et al.*, 2010). In contrast to the geothermal potential calculated by *Zhu et al.* (2010), which is based on the theoretical heat content in the aquifer that accumulated over a long time, the anthropogenic heat flux into the subsurface calculated in this study corresponds to an annual energy recharge, which represents a sustainable energy source. However, due to the observed spatial heterogeneity of shallow GWT and the heat flux

from buildings, a detailed spatial assessment of the anthropogenic heat input into the subsurface may be beneficial for the development of a regional geothermal usage concept. In particular, the spatial distribution of the GST, which was shown to be a major influencing factor, should be examined in future studies, in order to reduce the uncertainty in the calculated anthropogenic heat input. It may also be important for the evaluation of other cities to consider additional heat sources that were not present in the city of Karlsruhe, such as subway tunnels or interactions with surface water.

The altered subsurface thermal conditions in urban areas may also have implications for the planning and design of geothermal systems, especially with regard to systems with cooling purposes and aquifer thermal energy storage (ATES) systems. Therefore, the aspects of urban subsurface warming presented in this thesis should be incorporated into urban planning. By relating the spatiotemporal heating and cooling demand to the local subsurface thermal conditions, a sustainable usage of the enhanced geothermal resources in urban areas could be facilitated.

7 Acknowledgements

This work was made possible by the help and support of many people. I would like to thank…

… Jun.-Prof. Dr. habil. Philipp Blum for giving me the opportunity to do a PhD, the countless motivating discussions, his excellent supervision and for understanding the need of home office in a long-distance relationship.

… Dr. Peter Bayer for his continuous guidance, the constructive and critical comments on the manuscripts and for always being available for a phone call.

… Prof. Dr. Nico Goldscheider for his uncomplicated willingness to be the co-referent.

… the German Federal Environmental Foundation (DBU) for the economic support and the refreshing workshops.

… Axel Schaffitel, Stephan Jung and Luisa Laier for their excellent works and the enjoyable cooperation.

… Susanne Reimer, Friedhelm Fischer and Annette März (all Stadt Karlsruhe) for providing plenty of data in a very uncomplicated way and for assisting in the field work.

… Ke Zhu for the inspiring discussions about subsurface urban heat islands.

… Valentin Wagner for showing me the marvelous world of MATLAB, his review and the enthusiastic conversations about beaches and pointbreaks.

… Manuela Hübsch for always having an open ear for my issues, for the supply with herbal tea and diverse forms of solid calories and for organizing the opportunities to get rid of them.

… Michael Augenstein for the great time in the office and for standing my tempers in the final phase of the dissertation.

… all other colleagues from the Engineering and the Hydrogeology Group at the AGW for the enjoyable years.

… both my families for always believing in me and for their invaluable support.

… and above all Björn, simply for everything.

8 Declaration of authorship

Study 1

Citation: Menberg, K., Steger, H., Zorn, R., Reuß, M., Pröll, M., Bayer, P., Blum, P. Bestimmung der Wärmeleitfähigkeit im Untergrund durch Labor- und Feldversuche und anhand theoretischer Modelle. Grundwasser 18 (2), 103-116, 2013.

Declaration of authorship: Kathrin Menberg (KM) conducted the sampling and the laboratory experiments in cooperation with Hagen Steger (HS). HS, Roman Zorn and Manfred Reuß were responsible for the planning and installing of the geothermal test site. Markus Pröll planned and evaluated the Thermal Response Tests. KM evaluated the results in consultation with HS, Philipp Blum and Peter Bayer, and wrote the manuscript. The final manuscript was reviewed by all authors.

Study 2

Citation: Menberg, K., Bayer, P., Zosseder, K., Rumohr, S., Blum, P. Subsurface urban heat islands in German cities. Science of the Total Environment 442, 123-133, 2013.

Declaration of authorship: Kathrin Menberg (KM) collected the data in cooperation with Kai Zoßeder and Sven Rumohr. KM evaluated the results in consultation with Peter Bayer and Philipp Blum, and wrote the manuscript. The final manuscript was reviewed by all authors.

Study 3

Citation: Menberg, K., Blum, P., Schaffitel, A. and Bayer, P. Long-Term evolution of anthropogenic heat fluxes into a subsurface urban heat island. Environmental Science and Technology 47, 9747-9755, 2013.

Declaration of authorship: Kathrin Menberg (KM) and Axel Schaffitel developed the analytical heat flux model in consultation with Philipp Blum and Peter Bayer. KM evaluated the results and wrote the manuscript. The final manuscript was reviewed by Philipp Blum and Peter Bayer.

Study 4

Citation: Menberg, K., Blum, P. and Bayer, P. Groundwater temperature response to climate regime shifts, manuscript in preparation.

Declaration of authorship: Kathrin Menberg conducted the statistical analysis, evaluated the results and wrote the manuscript. The final manuscript was reviewed by Peter Bayer and Philipp Blum.

9 References

Adjali, M. H., M. Davies, & J. G. Littler (1998), Earth-contact heat flows: Review and application of design guidance predictions, *Build. Services Eng. Res. Technol.*, *19*(3), 111-121.

Ampofo, F., G. G. Maidment, & J. F. Missenden (2004), Underground railway environment in the UK Part 2: Investigation of heat load, *Appl. Therm. Eng.*, *24*, 633-645.

Anderson, M. P. (2005), Heat as a ground water tracer, *Ground Water*, *43*(6), 951-968.

Arnell, N. W. (1999), Climate change and global water resources, *Global Environ. Change*, *9*, S31-S49.

Arnfield, J. A. (2003), Two decades of urban climate research: a review of turbulence, exchanges of energy and water, and the urban heat island, *Int. J. Climatol.*, *23*, 1-26.

Austin, W. A., C. Yavuzturk, & J. D. Spitler (2000), Development of and In-Situ System for Measuring Ground Thermal Properties, *ASHRAE Transactions*, *106*(1), 365-379

Baker, J. M., & D. G. Baker (2002), Long-term ground heat flux and heat storage at a mid-latitude site, *Climatic Change*, *54*, 295-303.

Bakun, A. (2004), Chapter 25 - regime shifts, in *The Sea*, edited by A. Robinson & K. Brink, Harvard University Press, Cambridge, MA.

Balázs, B., J. Unger, T. Gál, Z. Sümeghy, J. Geiger, & S. Szegedi (2009), Simulation of the mean urban heat island using 2D surface parameters: empirical modelling, verification and extension, *Meteorol. App.*, *16*, 275-287.

Balke, K.-D. (1973), Geothermische und hydrogeologische Untersuchungen in der südlichen Niederrheinischen Bucht, Hannover.

Bates, B., Z. W. Kundzewicz, S. Wu, & J. P. Palutikof (2008), Climate Change and Water, 210 pp, Intergovernmental Panel on Climate Change Secretariat, Geneva.

Beier, M. (2008), Urbane Beeinflussung des Grundwassers: Stoffemissionen und -immissionen am Beispiel Darmstadts, Dissertation, 291 pp, Technische Universität, Darmstadt.

Beltrami, H. (2002a), Paleoclimate: Earth's long-term memory, *Science*, *297*(5579), 206-207.

Beltrami, H. (2002b), Climate from borehole data: Energy fluxes and temperatures since 1500, *Geophys. Res. Lett.*, *29*(23), 26-21.

References

Beltrami, H., & L. Kellman (2003), An examination of short- and long-term air-ground temperature coupling, *Global Planet. Change*, *38*, 291-303.

Beltrami, H., L. Cheng, & J. C. Mareschal (1997), Simultaneous inversion of borehole temperature data for determination of ground surface temperature history, *Geoph. J. Int.*, *129*(2), 311-318.

Beltrami, H., J. E. Smerdon, H. Pollack, & S. Huang (2002), Continental heat gain in the global climate system, *Geophys. Res. Lett.*, *29*(8), 1167.

Beltrami, H., E. Bourlon, L. Kellman, & J. F. Gonzales-Rouco (2006), Spatial patterns of ground heat gain in the Northern Hemisphere, *Geophys. Res. Lett.*, *33*(6), L06717.

Bennett, W. B., J. Wang, & R. L. Bras (2008), Estimation of Global Ground Heat Flux, *J. Hydrometeorol.*, *9*, 744-759.

Birch, F. (1948), The effects of Pleistocene climatic variations upon geothermal gradients, *Am. J. Sci.*, *246*, 729-760.

Blum, P., G. Campillo, & T. Kölbel (2011), Techno-economic and spatial analysis of vertical ground source heat pump systems in Germany, *Energy*, *36*, 3002-3011.

Blum, P., G. Campillo, W. Münch, & T. Kölbel (2010), CO2 savings of ground source heat pump systems – A regional analysis, *Renew. Energ.*, *35*, 122-127.

Bodri, L., & V. Cermak (1995), Climate changes of the last millennium inferred from borehole temperatures: Results from the Czech Republic Part I, *Global Planet. Change*, *11*, 111-125.

Bodri, L., & V. Cermak (1997), Climate change of the last two millennia inferred from borehole temperatures: results from the Czech Republic - Part II, *Global Planet. Change*, *14*, 163-173.

Bonte, M., B. M. van Breukelen, & P. J. Stuyfzand (2013), Temperature-induced impacts on groundwater quality and arsenic mobility in anoxic aquifer sediments used for both drinking water and shallow geothermal energy production, *Water Res.*, *47*(14), 5088-5100.

Bonte, M., P. J. Stuyfzand, A. Hulsmann, & P. van Beelen (2011), Underground thermal energy storage: Environmental risks and policy developments in the Netherlands and European Union, *Ecology and Society*, *16*(1):22.

Brandl, H. (2006), Energy foundations and other thermo-active ground structures, *Géotechnique*, *56*(2), 81-122.

Brielmann, H., C. Griebler, S. I. Schmidt, R. Michel, & T. Lueders (2009), Effects of thermal energy discharge on shallow groundwater ecosystems, *FEMS Microbiology Ecology*, *68*(3), 242-254.

Brigaud, F., & G. Vasseur (1989), Mineralogy, porosity and fluid control on thermal conductivity of sedimentary rocks, *Geophys. J.*, *98*, 525-542.

Campbell, G. S., Jungbauer, J.D. Jr., Bidlake, W.R. and Hungerford, R.D. (1994), Predicting the effect of temperature on soil thermal conductivity, *Soil Sci. Soc. Am. J.*, *158*(5), 307-313.

Carslaw, H. S., & J. C. Jaeger (1959), *Conduction of Heat in Solids (2nd ed.)*, 510 pp., New York, Oxford University Press.

Cermak, V., & L. Rybach (1979), *Terrestrial heat flow in Europe*, Springer Verlag, Heidelberg-Berlin, Germany.

Changnon, S. A. (1999), A rare long record of deep soil temperatures defines temporal temperature changes and an urban heat island, *Climatic Change*, *42*(3), 531-538.

Clauser, C. (2006), *Geothermal Energy*, 115 pp., Springer Verlag, Heidelberg-Berlin.

Davis, M. G., D. S. Chapman, T. M. Van Wagoner, & P. A. Armstrong (2007), Thermal conductivity anisotropy of metasedimentary and igneous rocks, *J. Geophys. Res.*, *112*(5), B05216.

de Marsily, G. (1986), *Quantitative Hydrogeology*, Academic Press, San Diego, California.

de Vries, D. A. (1963), *Thermal properties of soils*, 210-235 pp., North-Holland, Amsterdam.

Dědeček, P., J. Šafanda, & D. Rajver (2012), Detection and quantification of local anthropogenic and regional climatic transient signals in temperature logs from Czechia and Slovenia, *Climatic Change*, *113*(3-4), 787-801.

Dědeček, P., D. Rajver, V. Čermák, J. Šafanda, & M. Krešl (2013), Six years of ground–air temperature tracking at Malence (Slovenia): thermal diffusivity from subsurface temperature data, *J. Geophys. Eng*, *10*(2), 025012.

Dehner, U. (2007), Bestimmung der thermischen Eigenschaften von Böden, *Landesamt für Geologie und Bergbau Rheinland Pfalz, Mainzer geowissenschaftliche Mitteilungen*, *35*, 159-186.

deYoung, B., R. Harris, J. Alheit, G. Beaugrand, N. Mantua, & L. Shannon (2004), Detecting regime shifts in the ocean: Data considerations, *Progr. Oceanogr.*, *60*(2–4), 143-164.

References

DIN 4108-2 (2011), Wärmeschutz und Energie-Einsparung in Gebäuden – Teil 2: Mindestanforderungen an den Wärmeschutz. Deutsches Institut für Normung e.V., Berlin.

DIN V 4108-4 (2007), Wärmeschutz und Energie-Einsparung in Gebäuden – Teil 4: Wärme- und feuchteschutztechnische Bemessungswerte. Deutsches Institut für Normung e.V., Berlin.

DIN 18121-1 (1988), Baugrund, Untersuchung von Bodenproben: Wassergehalt, Teil 1: Bestimmung durch Ofentrocknung. Deutsches Institut für Normung e.V., Berlin.

DIN 18123 (2011), Baugrund, Untersuchung von Bodenproben: Bestimmung der Korngrößenverteilung. Deutsches Institut für Normung e.V., Berlin.

DIN 18124 (2011), Baugrund, Untersuchung von Bodenproben: Bestimmung der Korndichte: Kapillarpyknometer, Weithalspyknometer, Gaspyknometer. Deutsches Institut für Normung e.V., Berlin.

DIN 18128 (2002), Baugrund, Untersuchung von Bodenproben: Bestimmung des Glühverlustes. Deutsches Institut für Normung e.V., Berlin.

DIN 18129 (2011), Baugrund, Untersuchung von Bodenproben: Kalkgehaltsbestimmung. Deutsches Institut für Normung e.V., Berlin.

DIN EN ISO 10456 (2010), Baustoffe und Bauprodukte – Wärme- und feuchtetechnische Eigenschaften. Deutsches Institut für Normung e.V., Berlin.

DIN EN ISO 13370 (2008), Wärmetechnisches Verhalten von Gebäuden – Wärmeübertragung über das Erdreich, Deutsches Institut für Normung e.V., Berlin.

Dohr, F. (1989), Die Grundwassertemperatur im oberflächennahen Grundwasser des Stadtgebiets München, Dissertation, 162 pp, Ludwig-Maximilians-Universität, München.

Dohr, F., & W. Gruban (1999), Grundwasserüberwachungssystem der Landeshauptstadt München, 167 pp, München.

Domenico, P. A., & F. W. Schwartz (1990), *Physical and chemical hydrogeology, second edition*, 2nd ed., 842 pp., John Wiley & Sons, Inc., New York, NY.

Dornstädter, J., P. Heidinger, & B. Heinemann-Glutsch (2008), Erfahrungen aus der Praxis mit dem Enhanced Geothermal Reponse Test (EGRT), paper presented at Der Geothermiekongress 2008 Geothermische Vereinigung - Bundesverband Geothermie e.V., Karlsruhe.

Eiswirth, M. (2002), Bilanzierung der Stoffflüsse im urbanen Wasserkreislauf - Wege zur Nachhaltigkeit urbaner Wasserressourcen, Universität Karlsruhe, Karlsruhe.

Eiswirth, M., I. Held, H. Hötzl, & L. Wolf (2002), Abwasser im urbanen Grundwasserleiter: Stoffeintrag, Umsetzungen und Gefährdungspotential. In Forschergruppe Kanalleckage (2002): Gefährdungspotential von Abwasser aus undichten Kanälen für Boden und Grundwasser.

Eklöf, C., & S. Gehlin (1996), TED - a mobile equipment for thermal response test, MSc Thesis, 62 pp, Lulea.

Emery, A. F., D. R. Heerwagen, C. J. Kippenhan, & D. E. Steele (2007), Measured and Predicted Thermal Performance of a Residential Basement, *HVAC&R Research*, *13*(1), 39-57.

Epting, J., & P. Huggenberger (2012), Thermal management of an urban groundwater body, *Hydrol. Earth Syst. Sci. Dicuss.*, *9*, 7181-7225.

Federal Statistical Office Germany (Statistisches Bundesamt Deutschland). GENESIS Online data base. 2012. Available at https://www.destatis.de. (last accessed 20.07.2012).

Ferguson, G., & A. D. Woodbury (2004), Subsurface heat flow in an urban environment, *J. Geophys. Res.*, *109*(2), B02402.

Ferguson, G., & A. D. Woodbury (2007), Urban heat island in the subsurface, *Geophys Res. Lett.*, *34*(23), L23713.

Figura, S., D. M. Livingstone, E. Hoehn, & R. Kipfer (2011), Regime shift in groundwater temperature triggered by the Arctic Oscillation, *Geophys. Res. Lett.*(38), L23401.

Flanner, M. G. (2009), Integrating anthropogenic heat flux with global climate models, *Geophys. Res. Lett.*, *36*(2), L02801.

Forrer, S., T. Mégel, E. Rohner, & R. Wagner (2008), Mehr Sicherheit bei der Planung von Erdwärmesonden, *bbr - Fachmagazin für Brunnen- und Leitungsbau*, *05/2008*, 42-47.

Gehlin, S., & G. Hellström (2003), Comparison of four models for thermal response test evaluation, *ASHRAE Transactions*, *109*(1), 131-142.

German Weather Service (Deutscher Wetter Dienst). WebWerdis: Weather Request and Distribution System. 2012. Available at http://werdis.dwd.de/werdis. (last accessed 02.08.2012).

Geyer, O. F., & M. P. Gwinner (2011), *Geologie von Baden-Württemberg*, 5 ed., Schweizerbart, Stuttgart.

References

Green, T. R., M. Taniguchi, H. Kooi, J. J. Gurdak, D. M. Allen, K. M. Hiscock, H. Treidel, & A. Aureli (2011), Beneath the surface of global change: Impacts of climate change on groundwater, *J. Hydrol.*, *405*(3-4), 532-560.

Gunawardhana, L. N., & S. Kazama (2012), Using subsurface temperatures to derive the spatial extent of the land use change effect, *J. Hydrol.*, *460-461*, 40-51.

Hähnlein, S., P. Bayer, & P. Blum (2010), International legal status of the use of shallow geothermal energy, *Renew. Sust. Energ. Rev.*, *14*, 2611-2625.

Hähnlein, S., P. Bayer, G. Ferguson, & P. Blum (2013), Sustainability and policy for the thermal use of shallow geothermal energy, *Energy Policy*, *59*, 914-925.

Hall, E. K., C. Neuhauser, & J. B. Cotner (2008), Toward a mechanistic understanding of how natural bacterial communities respond to changes in temperature in aquatic ecosystems, *ISME Journal*, *2*(5), 471-481.

Hannappel, S., & A. Limberg (2007), Determination of the floor distance of shallow groundwater in Berlin, *Brandenburg. geowiss. Beitr.*, *14*(1), 65-74.

Hansen, J., R. Ruedy, M. Sato, & K. Lo (2010), Global surface temperature change, *Rev. Geophys.*, *48*(4), RG4004.

Hare, S. R., & N. J. Mantua (2000), Empirical evidence for North Pacific regime shifts in 1977 and 1989, *Progr. Oceanogr.*, *47*(2–4), 103-145.

Headon, J., D. Banks, A. Waters, & V. K. Robinson (2009), Regional distribution of ground temperature in the Chalk aquifer of London, UK, *Q. J. Eng. Geol. Hydrogeol.*, *42*, 131-323.

Herb, W. R., B. Janke, O. Mohseni, & H. G. Stefan (2008), Ground surface temperature simulation for different land covers, *J. Hydrol.*, *356*, 327-343.

HGK (2007), Hydrogeologische Kartierung und Grundwasserbewirtschaftung im Raum Karlsruhe-Speyer, 90 pp, Umweltministerium Baden-Württemberg and Ministerium für Umwelt, Forsten und Versbraucherschutz Rheinland-Pfalz, Stuttgart, Mainz.

Hoehn, E., & A. Scholtis (2011), Exchange between a river and groundwater, assessed with hydrochemical data, *Hydrol. Earth Syst. Sci.*, *15*(3), 983-988.

Homuth, S., K. Hamm, S. Rumohr, & I. Sass (2008), In-situ-Messungen zur Bestimmung geothermischer Untergrundkennwerte, *Grundwasser*, *13*, 241-251.

Hötzl, H., & A. Makurat (1981), Veränderungen der Grundwassertemperaturen unter dicht bebauten Flächen am Beispiel der Stadt Karlsruhe, *ZDGG*, *132*, 767-777.

Huang, S., H. Pollack, & P. Shen (2000), Temperature trends over the past five centuries reconstructed from borehole temperatures, *Nature*, *403*, 756-758.

Huang, S., M. Taniguchi, M. Yamano, & C. Wang (2009), Detecting urbanization effects on surface and subsurface thermal environment - A case study of Osaka, *Sci. Total Environ.*, *407*, 3142-3152.

Hurrell, J. W. (1995), Decadal Trends in the North Atlantic Oscillation: Regional Temperatures and Precipitation, *Science*, *269*(5224), 676-679.

Hwang, S., R. Ooka, & Y. Nam (2010), Evaluation of estimation method of ground properties for the ground source heat pump system, *Renew. Energ.*, *35*, 2123-2130.

Ichinose, T., K. Shimodozono, & K. Hanaki (1999), Impact of anthropogenic heat on urban climate in Tokyo, *Atmos. Environ. 33*, 3897-3909.

IPCC (2007), Fourth Assessment Report (AR4): Climate Change 2007: Synthesis Report, Contribution of Working Groups I, II and III to the Fourth Assessment Report of the Intergovernmental Panel on Climate Change 109 pp, Intergovernmental Panel on Climate Change Geneva.

Jesußek, A., S. Grandel, & A. Dahmke (2013), Impacts of subsurface heat storage on aquifer hydrogeochemistry, *Environ. Earth Sci.*, *69* (6), 1999-2012.

Johansen, O. (1975), Thermal conductivity of soils, Ph.D. Thesis thesis, Trondheim, Norway.

Kanda, M. (2007), Progress in Urban Meteorology: A Review, *J. Meteorol. Soc. Jpn.*, *85B*, 363-383.

Kerl, M., N. Runge, H. Tauchmann, & N. Goldscheider (2012), Hydrogeologisches Konzeptmodell von München: Grundlage für die thermische Grundwassernutzung (Conceptual hydrogeological model of the City of Munich, Germany, as a basis for geothermal groundwater utilisation), *Grundwasser*, *17*(3), 127-135.

Kiefer, L. (2011), Temperaturtrends im Grundwasser der Umgebung von Zürich., 46 pp, ETH Zurich, Zurich.

Kim, Y.-H., & J.-J. Baik (2004), Daily maximum urban heat island intensity in large cities of Korea, *Theor. App. Climatol.*, *79*, 151-164.

Kitanidis, P. K. (1997), *Introduction to geostatistics — applications to hydrogeology*, 249 pp., Cambridge University Press, Cambridge.

References

Klinger, J. (2007), Beschreibung der Wasser- und Stoffflüsse in einem urbanem Raum unter besonderer Berücksichtigung von Kanalleckagen, Dissertation, 221 pp, Universität Karlsruhe, Karlsruhe.

Klostermann, J. (1992), *Das Quartär der Niederrheinischen Bucht—Ablagerungen der Letzten Eiszeit am Niederrhein*, Geologisches Landesamt Nordrhein-Westfalen, Krefeld.

Kløve, B., et al. Climate change impacts on groundwater and dependent ecosystems, *J. Hydrol., in press,* doi: 10.1016/j.jhydrol.2013.06.037.

Kohl, T. (1998), Palaeoclimatic temperature signals - can they be washed out?, *Tectonophysics*, *291*, 225-234.

Kollet, S. J., I. Cvijanovic, D. Schüttemeyer, R. M. Maxwell, A. F. Moene, & P. Bayer (2009), The influence of rain sensible heat and subsurface energy transport on the energy balance at the land surface, *Vadose Zone J.*, *8*(4), 846-857.

Kottmeier, C., C. Biegert, & U. Corsmeier (2007), Effects of Urban Land Use on Surface Temperature in Berlin: Case Study, *J. Urban Plann. Dev.*, *133*(2), 128-137.

Kratzer, P. (1956), *Das Stadtklima*, Friedrich Vieweg und Sohn, Braunschweig.

Krümpelbeck, I. (2000), Untersuchungen zum langfristigen Verhalten von Siedlungsabfalldeponien, 216 pp, Bergischen Universität - Gesamthochschule Wuppertal, Wuppertal.

Kümmerle, E., & G. Seidenschwann (2009), *Annotations of the geological map of Hesse No.5817 Frankfurt on the Main West* 3rd ed., Wiesbaden

Kundzewicz, Z. W. (2008), Climate change impacts on the hydrological cycle, *Ecohydrology & Hydrobiology*, *8*(2–4), 195-203.

Kusuda, T., & J. W. Bean (1984), Simplified Methods for Determining Seasonal Heat Loss from Uninsulated Slab-on-Grade Floors, *ASHRAE Transactions*, *84*(11), 611-632.

Lachenbruch, A. H., & B. V. Marshall (1986), Changing Climate: Geothermal Evidence from Permafrost in the Alaskan Arctic, *Science*, *234*(4777), 689-696.

Landesamt für Geologie, Rohstoffe und Bergbau Baden-Württemberg (1999). Informationen 11: *Anwendung geowissenschaftlicher Informationssysteme am Landesamt für Geologie, Rohstoffe und Bergbau Baden-Württemberg*. http://www.lgrb.uni-freiburg.de/lgrb/Produkte/schriften/online-publikationen/informationen_11/pdf_pool/info11.pdf (accessed January 18, 2013).

Landsberg, H. (1956), *The climate of towns*, Univ. of Chicago Press, Chicago.

Landsberg, H. E. (1981), *The urban climate*, 275 pp., Academic Press, New York.

Lemcke, K. (1953), *Geologische und sedimentpetrographische Untersuchungen im Westteil der ungefalteten Molasse des süddeutschen Alpenvorlandes* Amt für Bodenforschung, Hannover.

Lesperance, M., J. E. Smerdon, & H. Beltrami (2010), Propagation of linear surface air temperature trends into the terrestrial subsurface, *J. Geophys. Res.*, *115*, D21115.

Liu, C., B. Shi, C. Tang, & L. Gao (2011), A numerical and field investigation of underground temperatures under Urban Heat Island, *Build. Environ.*, *46*(5), 1205-1210.

Lo Russo, S., G. Taddia, & V. Verda (2012), Development of the thermally affected zone (TAZ) around a groundwater heat pump (GWHP) system: A sensitivity analysis, *Geothermics*, *43*, 66-74.

MacDougall, A. H., J. F. González-Rouco, M. B. Stevens, & H. Beltrami (2008), Quantification of subsurface heat storage in a GCM simulation, *Geophys. Res. Lett.*, *35*(13), L13702.

Makurat, A. (1980), Analyse der Temperaturschwankungen des Grundwassers im Stadtgebiet von Karlsruhe, 293 pp, Universität Karlsruhe (TH), Karlsruhe.

Markle, J. M., R. A. Schincariol, J. H. Sass, & J. W. Molson (2006), Characterizing the two-dimensional thermal conductivity distribution in a sand and gravel aquifer, *Soil Sci. Soc. Am. J.*, *70*(4), 1281-1294.

Marty, C. (2008), Regime shift of snow days in Switzerland, *Geophys .Res. Lett.*, *35*(12), L12501.

Menberg, K., P. Blum, A. Schaffitel, & P. Bayer (2013a), Long-term Evolution of Anthropogenic Heat Fluxes into a Subsurface Urban Heat Island, *Environ. Sci. Technol.*, *47*(17), 9747−9755.

Menberg, K., P. Bayer, K. Zosseder, S. Rumohr, & P. Blum (2013b), Subsurface urban heat islands in German cities, *Sci. Total Environ.*, *442*, 123-133.

Menberg, K., H. Steger, R. Zorn, M. Reuss, M. Proell, P. Bayer, & P. Blum (2013c), Bestimmung der Wärmeleitfähigkeit im Untergrund durch Labor- und Feldversuche und anhand theoretischer Modelle [Determination of thermal conductivity in the subsurface using laboratory and field experiments and theoretical models], *Grundwasser*, *18*(2), 103-116.

References

Mirzaei, P. A., & F. Haghighat (2010), Approaches to study Urban Heat Island – Abilities and limitations, *Build. Environ.*, *45*(10), 2192-2201.

Molina-Giraldo, N., P. Bayer, & P. Blum (2011a), Evaluating the influence of thermal dispersion on temperature plumes from geothermal systems using analytical solutions, *Int. J. Therm. Sci.*, *50*, 1223-1231.

Molina-Giraldo, N., P. Bayer, P. Blum, & O. A. Cirpka (2011b), Propagation of seasonal temperature signals into an aquifer upon bank infiltration, *Ground Water*, *49*(4), 491-502.

Nakshabandi, G. A., & H. Kohnke (1965), Thermal conductivity and diffusivity of soils as related to moisture tension and other physical properties, *Agri. Meteorol.*, *2*, 271-279.

Nitoui, D., & H. Beltrami (2005), Subsurface thermal effects of land use changes *J. Geophys. Res.*, *110*, F01005.

North, R. P., D. M. Livingstone, R. E. Hari, O. Köster, P. Niederhauser, & R. Kipfer (2013), The physical impact of the late 1980s climate regime shift on Swiss rivers and lakes, *Inland Waters*, *3*, 341-350.

Oke, T. R. (1973), City size and the urban heat island, *Atmos.Environ.*, *7*(8), 769-779.

Oke, T. R. (1982), The energetic basis of the urban heat island, *Q. J. Roy. Meteor. Soc.*, *108*(455), 1-24.

Oke, T. R. (1988), The urban energy balance, *Progr. Phys. Geogr.*, *12*(4), 471-508.

Overland, J., S. Rodionov, S. Minobe, & N. Bond (2008), North Pacific regime shifts: Definitions, issues and recent transitions, *Progress in Oceanography*, *77*(2–3), 92-102.

Peng, S., S. Piao, P. Ciais, P. Friedlingstein, C. Ottle, F.-M. Bréon, H. Nan, L. Zhou, & R. B. Myneni (2012), Surface Urban Heat Island Across 419 Global Big Cities, *Environ. Sci. Technol.*, *46*(2), 696-703.

Pollack, H., S. Huang, & P. Shen (1998), Climate Change Record in Subsurface Temperatures: A Global Perspective, *Science*, *282*, 279-281.

Popov, Y. A., D. F. C. Pribnow, J. H. Sass, C. F. Williams, & H. Burkhardt (1999), Characterization of rock thermal conductivity by high-resolution optical scanning, *Geothermics*, *28*, 253-276.

Pribnow, D. F. C., & J. H. Sass (1995), Determination of thermal conductivity from deep boreholes, *J. Geophys. Res.*, *100*, 9981-9994.

Prinz, H., & R. Strauß (2006), *Abriss der Ingenieurgeologie*, 671 pp., Elsevier Spektrum akademischer Verlag, München.

Prommer, H., & P. J. Stuyfzand (2005), Identification of Temperature-Dependent Water Quality Changes during a Deep Well Injection Experiment in a Pyritic Aquifer, *Environ. Sci. Technol.*, *39*(7), 2200-2209.

Putnam, S. N., & D. S. Chapman (1996), A geothermal climate change observatory: First year results from Emigrant Pass in northwest Utah, *J. Geophys. Res.*, *101*, 21877-21890.

Rauert, W., M. Wolf, S. M. Weise, G. Andres, & R. Egger (1992), Isotope-hydrogeological case study on the penetration of pollution into the deep Tertiary aquifer in the area of Munich, Germany, *J. Contam. Hydrol.*, *14*, 15-38.

Raymond, J., R. Therrien, L. Gosselin, & R. Lefebvre (2011), Numerical analysis of thermal response tests with a groundwater flow and heat transfer model, *Renew. Energ.*, *36*, 315-324.

Rees, S. W. (2001), The influence of soil moisture content variations on heat losses from earth-contact structures: an initial assessment, *Building and Environment*, *36*, 157-165.

Rees, S. W., M. H. Adjali, Z. Zhou, M. Davies, & H. R. Thomas (2000), Ground heat transfer effects on the thermal performance of earth-contact structures, *Renew. Sust. Energ. Rev.*, *4*(3), 213-265.

Reuß, M., & B. Sanner (2001), Planung und Auslegung von Erdwärmesondenanlagen: Basis einer nachhaltigen Erdwärmenutzung, VDI Richtlinie 4640 und Berechnungsverfahren, *Schweizerischer Ingenieur- und Architektenverein (SIA)*, *Zürich, Schweiz*

Rink M. personal communication 18.08.2011. Municipal energy supplier Karlsruhe (Stadtwerke Karlsruhe GmbH).

Rigo, G., & E. Parlow (2007), Modelling the ground heat flux of an urban area using remote sensing data, *Theor. App. Climatol.*, *90*, 185-199.

Rinke, R., A. Wieser, U. Corsmeier, & C. Kottmeier (2010), Messungen der räumlichen Variabilität der Luftqualität in einem Ballungsraum mittels einer Straßenbahn, paper presented at BWPlus-Statuskolloquium, Karlsruhe.

Roberts, S. M., T. R. Oke, C. S. B. Grimmond, & J. A. Voogt (2006), Comparison of Four Methods to Estimate Urban Heat Storage, *J. App. Meteorol. Climatol.*, *45*, 1766-1781.

Rodionov, S. N. (2004), A sequential algorithm for testing climate regime shifts, *Geophys. Res. Lett.*, *31*(9), L09204.

Rodionov, S. N. (2006), Use of prewhitening in climate regime shift detection, *Geophys. Res. Lett.*, *33*(12), L12707.

References

Rodionov, S. N., & J. E. Overland (2005), Application of a sequential regime shift detection method to the Bering Sea ecosystem, *ICES J. Marine Sci.*, *62*, 328-332.

Rudnick, D. L., & R. E. Davis (2003), Red noise and regime shifts, *Deep Sea Research Part I: Oceanographic Research Papers*, *50*(6), 691-699.

Saar, M. O. (2011), Review: Geothermal heat as a tracer of large-scale groundwater flow and as a means to determine permeability fields, *Hydrogeology Journal*, *19*, 31-52.

Sass, I. & Lehr, C. (2011), Improvements on the thermal response test evaluation applying the cylinder source theory. In Proceedings of the 36th Stanford Geothermal Workshop, Standford.

Sass, J. H., C. Stone, & R. J. Munroe (1984), Thermal conductivity determnations on solid rock - a comparison between a steady-state divided-bar apparatus and a commercial transient line-source device, *J. Volcanol. Geoth. Res.*, *20*, 145-153.

Schäfer, W., F. Wickert, & A. Tiehm (2007), Modellrechnungen zur Quantifizierung von NA-Prozessen für den LCKW-Schadensfall in Karlsruhe-Ost /Killisfeld, *Grundwasser*, *12*, 108-124.

Schmid, F. (2010), Grundwassertemperaturen im Stadtgebiet von Frankfurt am Main, 41 pp, University of Tuebingen, Tübingen.

Schwarz, N. (2012), Comment on "Surface urban heat island across 419 global big cities", *Environ. Sci. Technol.*, *46*(12), 6888.

Schwarz, N., S. Lautenbach, & R. Seppelt (2011), Exploring indicators for quantifying surface urban heat islands of European cities with MODIS land surface temperatures, *Remote Sens. Environ.*, *115*(12), 3175-3186.

Seidel, D. J., & J. R. Lanzante (2004), An assessment of three alternatives to linear trends for characterizing global atmospheric temperature changes, *J. Geophys. Res.*, *109*, D14108.

Seiler, K.-P. (1979), Durchlässigkeiten und Porosität von Lockergesteinen in Oberbayern, *MItt. Ing.- u. Hydrogeol.*, *9*, 105-126.

Seithel, R. (2010), Qualitative Analyse der Untergrundtemperaturverteilung im Raum Frankfurt am Main, 36 pp, Karlsruhe Institute of Technology, Kalrsruhe.

SenStadtUm. Senatsverwaltung für Stadtentwicklung und Umwelt. Environmental Atlas Berlin; 2012. http://www.stadtentwicklung.berlin.de/umwelt/umweltatlas (last accessed 15.07.2012).

Shonder, J. A., & J. E. Beck (2000), Field Test of a new method for determining soil formation thermal conductivty and borehole resistance *ASHRAE Transactions*, 843-850.

Slenders, H. L. A., P. Dols, R. Verburg, & A. J. d. Vries (2010), Sustainable remediation panel: sustainable synergies for the subsurface:combining groundwater energy with remediation., *Remediation Journal*, *20*, 143-153.

Smerdon, J. E., H. Pollack, J. W. Enz, & M. J. Lewis (2003), Conduction-dominated heat transport of the annual temperature signal in soil, *J. Geophys. Res.*, *108*(B9), 2431.

Smerdon, J. E., H. Beltrami, C. Creelman, & M. B. Stevens (2009), Characterizing land surface processes: A quantitative analysis using air-ground thermal orbits, *J. Geophys. Res.*, *114*, D15102.

Smerdon, J. E., H. Pollack, V. Cermak, J. W. Enz, M. Kresl, J. Safanda, & J. F. Wehmiller (2004), Air-ground temperature coupling and subsurface propagation of annual temperature signals, *J. Geophys. Res.*, *109*(21), D21107.

Smerdon, J. E., H. Pollack, V. Cermak, J. W. Enz, M. Kresl, J. Safanda, & J. F. Wehmiller (2006), Daily, seasonal, and annual relationships between air and subsurface temperatures, *J. Geophys. Res.*, *111*, D07101.

Spitler, J. D., C. Yavuzturk, & S. J. Rees (2000), In situ measurement of ground thermal properties, paper presented at Proceedings of Terrastock, Stuttgart, August 28 - September 1.

Stadt Karlsruhe. Tiefbauamt Karlsruhe: *Die Stadtentwässerung in Karlsruhe*. http://www.karlsruhe.de/b3/bauen/tiefbau/entwaesserung/entwaesserungsgebuehr/HF_sec tions/content/ZZk9uVuzOo24XJ/ZZk9uWfqOuhpKP/Tiefbauamt_Broschuere_2010.pdf (accessed March 20, 2013).

Stadt Karlsruhe. Stadtgebiet und Flächennutzung. http://www1.karlsruhe.de/ Stadtentwicklung/siska/sgt/sgt01050.htm. (accessed March 7, 2013).

Stevens, M. B., J. E. Smerdon, J. F. Gonzalez-Rouco, M. Stieglitz, & H. Beltrami (2007), Effects of bottom boundary placement on subsurface heat storage: Implications for climate model simulations, *Geophys .Res. Lett.*, *34*(2), L02702.

Stoll, S., H. J. Hendricks Franssen, R. Barthel, & W. Kinzelbach (2011), What can we learn from long-term groundwater data to improve climate change impact studies?, *Hydrol. Earth Syst. Sci.*, *15*(12), 3861-3875.

References

Swanson, K. L., & A. A. Tsonis (2009), Has the climate recently shifted?, *Geophys. Res. Lett.*, *36*(6), L06711.

Taniguchi, M. (1993), Evaluation of Vertical Groundwater Fluxes andThermal Properties of Aquifers Based on Transient Temperature-Depth Profiles, *Water Resour. Res.*, *29*(7), 2021-2026.

Taniguchi, M. (2006), Anthropogenic effects on subsurface temperature in Bangkok, *Clim. Past Discuss.*, *2*, 831 - 846.

Taniguchi, M., & T. Uemura (2005), Effects of urbanization and groundwater flow on the subsurface temperature in Osaka, Japan, *Phys. Earth Planet. In.*, *152*, 305-313.

Taniguchi, M., D. R. Williamson, & A. J. Peck (1999a), Disturbances of temperature-depth profiles due to surface climate change and subsurface water flow: 2. An effect of step increase in surface temperature caused by forest clearing in southwest Western Australia, *Water Resour. Res.*, *35*(5), 1519-1529.

Taniguchi, M., T. Uemura, & Y. Sakura (2005), Effects of urbanization and groundwater flow on subsurface temperature in three megacities in Japan, *J. Geophys. Eng*, *2*, 320-325.

Taniguchi, M., T. Uemura, & K. Jago-on (2007), Combined Effects of Urbanization and Global Warming on Subsurface Temperature in Four Asian Cities *Vadose Zone J.*, *6*(3), 591-596.

Taniguchi, M., J. Shimada, Y. Fukuda, M. Yamano, S. Onodera, S. Kaneko, & A. Yoshikoshi (2009), Anthropogenic effects on the subsurface thermal and groundwater environments in Osaka, Japan and Bangkok, Thailand, *Sci. Total Environ.*, *407*, 3153-3164.

Taniguchi, M., J. Shimada, T. Tanaka, I. Kayane, Y. Sakura, Y. Shimano, S. Dapaah-Siakwan, & S. Kawashima (1999b), Disturbances of temperature-depth profiles due to surface climate change and subsurface water flow: 1. An effect of linear increase in surface temperature caused by global warming and urbanization in the Tokyo metropolitan area, Japan, *Water Resour. Res.*, *35*(5), 1507-1517.

Taylor, C. A., & H. G. Stefan (2009), Shallow groundwater temperature response to climate change and urbanization, *J. Hydrol.*, *375*, 601-612.

Taylor, R. G., et al. (2013), Ground water and climate change, *Nature Clim. Change*, *3*(4), 322-329.

Thomas, H. R., & S. W. Rees (1999), The thermal performance of ground floor slabs - a full scale in-situ experiment, *Build. Environ.*, *34*, 139-164.

Treidel, H., J. J. Martin-Bordes, & J. J. Gurdak (Eds.) (2012), *Climate Change Effects on Groundwater Resources: A Global Synthesis of Findings and Recommandations* 414 pp., Taylor & Francis publishing, London.

Trenberth, K. E., & J. W. Hurrell (1994), Decadal atmosphere-ocean variations in the Pacific, *Clim. Dynam.*, *9*(6), 303-319.

Troschke, B., & H. Burkhardt (1998), Thermal conductivity models for two-phase systems, *Phys. Chem. Earth*, *23*(3), 351-355.

Turcotte, D. L., & G. Schubert (2002), *Geodynamics*, 2nd ed., Cambridge University Press, Cambridge.

VDI 4640 (2010). Thermische Nutzung des Untergrundes: Grundlagen, Genehmigungen, Umweltaspekte. Verein Deutscher Ingenieure e.V., Düsseldorf.

von Storch, H. (1995), Misuses of statistical analysis in climate research, in *Analysis of Climate Variability Applications of Statistical Techniques.* , edited by H. von Storch & A. Navarra, Springer, New York.

Wagner, B. (1991), Bodenphysikalische, ingenieur- und hydrogeologische Untersuchungen zur Speicherung und zum Entzug von Niedertemperaturwärme in der wassergesättigten Bodenzone mit vertikalen Wärmetauschern. Dissertation, Ludwig-Maximillians Universität, München.

Wagner, V., P. Bayer, M. Kübert, & P. Blum (2011), Numerical sensitivity studies of thermal response tests, *Renew. Energ.*, *41*, 245-253.

Wang, J., & R. L. Bras (1999), Ground heat flux estimated from surface soil temperature, *J. Hydrol.*, *216*, 214-226.

Wang, Z.-H., & E. Bou-Zeid (2012), A novel approach for the estimation of soil ground heat flux, *Agr. Forest Meteorol.*, *154-155*, 214-221.

Weber, S. (2006), Comparison of in-situ measured ground heat fluxes within a heterogeneous urban ballast layer, *Theor.App.Climatol.*, *83*(1-4), 169-179.

Wienert, U., & W. Kuttler (2005), The dependence of the urban heat island intensity on latitude - A statistical approach, *Meteorol. Zeitschrift 14*(5), 677-686.

Wirsing, G., & A. Luz (2008), Hydrogeologischer Bau und Aquifereigenschaften der Lockergesteine im Oberrheingraben (Baden-Württemberg). Freiburg i.Br.

Witte, H. J. L., G. J. van Gelder, & J. D. Spitler (2002), In situ measurement of ground thermal conductivity: the Dutch perspective *ASHRAE Transactions*, *108*(1), 21 pp.

References

Woodside, W., & J. H. Messmer (1961), Thermal Conductivity of Porous Media. I. Unconsolidated Sands, *J. Appl. Phys.*, *32*(9), 1688-1699.

Yalcin, T., & O. Yetemen (2009), Local warming of groundwaters caused by the urban heat island effect in Istanbul, Turkey, *Hydrogeol. J.*, *17*, 1247-1255.

Yamano, M., S. Goto, A. Miyakoshi, H. Hamamoto, R. F. Lubis, V. Monyrath, & M. Taniguchi (2009), Reconstruction of the thermal environment evolution in urban areas from underground temperature distribution, *Sci. Total Environ.*, *407*, 3120-3128.

Zervantonakis, I. & Reuß, M. (2006), Quality requirements of a thermal response test. In: Proceedings of the IEA Conference ECOSTOCK 2006, Richard Stockton, College Pomona, New Jersey, USA.

Zhu, K., P. Blum, G. Ferguson, K.-D. Balke, & P. Bayer (2010), The geothermal potential of urban heat islands, *Environ. Res. Lett.*, *5*(4), 044002.

Zosseder, K. (2007), *Heterogenitäten von PAK-Kontaminationen im Grundwasser*, 236 pp., Bochum.

10 Curriculum Vitae

Personal information

Name	<u>Kathrin</u> Christina Menberg (nee Koch)
Date of birth	28.04.1985
Place of birth	Kassel
Nationality	German

Education

1995 - 2004   A-level, Thomas-Mann-Gymnasium, Stutensee

Academic studies

10/2004 – 03/2010   Karlsruhe Institute of Technology (KIT)

Institute for Applied Geosciences (AGW)

Diploma Degree in Geology (Grade: 1.5)

Diploma-Thesis: "Influence of specific subsurface parameters on the Thermal Response Test (TRT)" (in German).

Professional experience

12/2010-11/2013   PhD student

Scholarship Programme of the German Federal Environmental Foundation (DBU)

Karlsruhe Institute of Technology (KIT)

Institute for Applied Geosciences (AGW)

PhD-Thesis: "Anthropogenic and natural alterations of shallow groundwater temperatures."

Journal publications (peer-reviewed)

Menberg, K., Bayer, P., Zosseder, K., Rumohr, S. & Blum, P.: Subsurface urban heat islands in German cities. Science of the Total Environment 442, 123-133 (2013).

Menberg, K., Steger, H., Zorn, R., Reuss, M., Proell, M., Bayer, P. & Blum, P.: Bestimmung der Wärmeleitfähigkeit im Untergrund durch Labor- und Feldversuche und anhand theoretischer Modelle. Grundwasser 18(2), 103-116 (2013).

Menberg, K., Blum, P., Schaffitel, A. & Bayer, P.: Long Term Evolution of Anthropogenic Heat Fluxes into a Subsurface Urban Heat Island. Environmental Science & Technology 47, 9747-9755 (2013).

Menberg, K., Blum, P. & Bayer, P.: Groundwater temperature response to climate regime shifts. submitted to Environmental Research Letters.

Conference proceedings

Menberg, K., Bayer, P., Blum, P.: Elevated temperatures beneath cities: An enhanced geothermal resource. European Geothermal Congress, Pisa, Italy, June 3-7 2013, 4 pp.

Menberg, K., Bayer, P., Zosseder, K., Rumohr, S., Blum, P.: Urbane Wärmeinseln im Untergrund deutscher Städte. 19. Tagung für Ingenieurgeologie, Munich, Germany, March 13-16 2013, 4 pp.

Menberg, K., Blum, P., Limberg, A., Bayer, P.: Wärmeinseln im Grundwasser unter deutschen Städten. Niedersächsisches Grundwasserkolloquium, Braunschweig, Germany, February 20-21 2013, 9 pp. (Invited Talk).

Conference abstracts

Zhu, K., Bayer, P., Menberg, K., Rumohr, S., Blum, P.: Natural and anthropogenic triggers for subsurface urban heat islands. 8th IAHS International Groundwater Quality Conference, Gainesville, USA, April 21-26 2013.

Menberg, K., Blum, P., Schaffitel, A., Bayer, P.: Long term evolution of the urban heat island beneath the city of Karlsruhe, Germany. European Geosciences Union General Assembly 2013, Vienna, Austria, April 7-12 2013, Geophysical Research Abstracts Vol. 15, EGU2013-6829.

Bayer, P., Menberg, K., Zhu, K., Blum, P.: Investigation of heat flux processes governing the increase of groundwater temperatures beneath cities. Abstract H51J-1486 presented at 2012 Fall Meeting, AGU, San Francisco, USA, December 3-7 2012.

Menberg, K., Schaffitel, A., Blum, P., Bayer, P.: Subsurface urban heat fluxes in German cities. 11th Urban Environmental Symposium, Karlsruhe, Germany, September 17-19 2012.

Menberg, K., Blum, P., Zhu, K., Bayer, P.: Urbane Wärmeinseln im Untergrund deutscher Städte. FH-DGG Tagung 2012, Dresden, Germany, May 16-20 2012, Schriftenreihe der Deutschen Gesellschaft für Geowissenschaften 78 (2012).

Menberg, K., Blum, P., Zhu, K., Bayer, P.: Urban heat islands in the subsurface of German cities. European Geosciences Union General Assembly 2012, Vienna, Austria, April 22-27 2012, Geophysical Research Abstracts Vol. 14, EGU2012-9772.